MEDICAL UNIVERSITY OF VIENNA

Dissecting the molecular pharmacology of targeted protein degradation

Doctoral Thesis at the Medical University of Vienna

for obtaining the academic degree

Doctor of Philosophy

Submitted by

Matthias Brand, MSc

Supervisor:

Georg E Winter, PhD

CeMM Research Center for Molecular Medicine

Lazarettgasse 14, AKH BT 25.3, 1090 Vienna, Austria

Vienna, March 2020

Table of Contents

Declaration i
Acknowledgements ii
Abstract iv
Zusammenfassung vi
List of abbreviations viii
List of figures ix
1. Introduction 1
1.1 The etiology of cancer 1
1.2 State of the art in cancer therapy 2
1.2.1 Traditional chemotherapy 2
1.2.2 Targeted therapies 4
1.3 Mechanisms of resistance to targeted therapies and strategies to overcome them 11
1.3.1 Oncogene reactivation 12
1.3.2 Restoration of the signaling pathway 13
1.3.3 Cell-state transitions 14
1.3.4 Increased drug efflux 14
1.4 Challenges in drug discovery 15
1.5 The ubiquitin-proteasome system (UPS) 16
1.5.1 Ubiquitin 17
1.5.2 The proteasome 19
1.5.3 Determinants of specificity: E3 ubiquitin ligases 20
1.5.4 Cullin-RING ligases (CRLs) 23
1.6 Drugging the UPS 26
1.6.1 Proteasome inhibitors 26
1.6.2 Ubiquitin ligase inhibitors 27
1.6.3 DUB inhibitors 28
1.7 Targeted protein degradation (TPD) 28
1.7.1 Monovalent molecular glue degraders: immunomodulatory drugs and sulfonamides 29
1.7.2 Hetero-bifunctional molecules: PROTACs 31
1.7.3 Features of targeted protein degradation 32
1.8 Aims of this thesis 35

2. Results 36
2.1 Homolog-selective degradation as a strategy to probe the function of CDK6 in AML 36
2.1.1 Prologue 36
2.1.2 PDF of the paper 37
2.2 Identification of genetic determinants of sensitivity to targeted protein degradation 55
2.2.1 Prologue 55
2.2.2 Results 56
2.3 Systematic characterization of genetic resistance mutations to PROTACs 59
2.3.1 Prologue 59
2.3.2 Results 60
3. Discussion 68
3.1 Engineering selectivity into molecular probes via PROTAC conversion 68
3.2 Characterization of the role of CDK6 in acute myeloid leukemia 70
3.3 The CRL machinery is an important mediator of TPD resistance 71
3.4. TPD resistance and possible mechanisms to overcome it 74
3.5 Future directions 77
References 80
Materials and Methods 95
Curriculum Vitae 99
List of Publications 101

Declaration

The majority of the work presented herein has been carried out in the laboratory of Georg Winter at the CeMM Research Center for Molecular Medicine of the Austrian Academy of Sciences in Vienna (Austria). Additional experiments were performed by collaborators in the laboratories of Nathanael Gray and Eric Fischer, both at the Dana Farber Cancer Institute in Boston (United States of America).

Chapter 2.1 was published in **Cell Chemical Biology** and has been reprinted with permission from Elsevier: M Brand, B Jiang, S Bauer, KA Donovan, Y Liang, ES Wang, RP Nowak, JC Yuan, T Zhang, N Kwiatkowski, AC Müller, ES Fischer, NS Gray, GE Winter, **Homolog-Selective Degradation as a Strategy to Probe the Function of CDK6 in AML**, *Cell Chem Biol (2019)*

The data presented in chapter 2.2 was published in the scope of a bigger project in **Molecular Cell**: C Mayor-Ruiz, MG Jaeger, S Bauer, M Brand, C Sin, A Hanzl, AC Mueller, J Menche, GE Winter, **Plasticity of the Cullin-RING Ligase Repertoire Shapes Sensitivity to Ligand-Induced Protein Degradation**, *Molecular Cell* (2019)

The project presented in chapter 2.3 is intended for publication in 2020.

Detailed information on the contribution of the author of this thesis to the projects presented herein can be found in the Prologue to each chapter. All sections of this thesis were written by the author, Matthias Brand, with input from Georg Winter.

Acknowledgements

With this thesis, another chapter in my life comes to an end. A journey that without any doubt has been under many aspects the most challenging in my life, yet the most rewarding at the same time. I wouldn't be here without the support of many people and I am profoundly thankful for every smile, hug or kind word in the past years.

First of all, I would like to sincerely thank Georg Winter for his outstanding supervision. Thanks for having faith in me, for his teachings, for shaping me as a scientist. But most of all, for the example he set by being a hardworking and inspiring leader and always being exceptionally thoughtful and understanding. Through him I have learned what a true Mentor is. Thank you.

Thanks also to the members of my thesis committee, Christoph Bock and Andreas Meyer, for their helpful input and guidance.

Next, I want to thank all members of the Winter lab. It has been a privilege to see us grow and evolve from a tiny group into an exceptional force of great scientists in the course of a few years. While it is hard to say goodbye now, I look forward to seeing what the future holds in store for you! Thanks for inspiring me every day to do better, for all the scientific questions and discussions, while at the same time ensuring that work stays fun through our banter and jokes.

The Winter lab provided fertile soil for me to grow, but the surrounding environment allowed me to really thrive. Thank you to everyone on the 6th floor for an amazing inter-lab collaborative experience! Thank you for the countless discussions, the cozy atmosphere in the office, the constant exchange of expertise. A particular thank you to Alexandra for always being patiently available to help me navigate the world of bioinformatics!

CeMM truly is a special place to do science. I want to thank Giulio, Anita and all of faculty for their vision and commitment. Thanks to Les Macrophages, always remembered as the PhD year with the best dancing skills! Thank you admin team, for your work that makes our life incredibly easier and for always being kind and helpful. But more importantly, a big thank you goes to everyone in the institute for being part of this vision and truly making it live. Many of you will always have a special place in my heart!

Getting through a PhD would not have been possible without an exceptional collection of friends that were constantly by my side throughout the ups and downs of this rollercoaster.

Thank you Ele and Fede, my little piece of home. Whatever I needed, I knew that I always had all your help and support just around the corner.

Physically a bit further, but always just a text or a phone call away, my soulmate Susanna. Thanks for helping me get up every time that science or life pushed me down again.

Thanks to Rico, Ize and Tomislav, for being my safe haven and a catalyst for change. I will deeply miss you, chicos, but no matter how far we'll be apart, you will never get rid of me.

Thanks to all the present and past members of Zozo, my second family. No matter how hard things were in the lab, I was always happy to come back to you. Thank you Brenda and Miguelito for the endless laughs. Thank you Tala, the voice of reason in the house and great chef. Thank you Chris, the absolute best third choice that I ever had in my life. Thank you Juju, my little concentrate of Portuguese temperament, the rock that gave me stability throughout my time here.

Last but not least, a heartfelt thank you to my family, my greatest gift in life. Thanks to the Bundschuh clan, for always being loving and welcoming. Thanks to everyone in my Grande Famiglia for just being amazing and for your endless love. Thank you Opo for being my biggest role model. Thanks to my Brandbros, the best siblings in the world, because even if we're spread all over Europe, every time I talk to you it feels like we never left. Finally, thanks Mum and Dad for always believing in me and supporting me, and for your sacrifices to provide me with the best possible education.

This thesis is for every single one of you.

Abstract

Cancer is a heterogeneous collection of diseases that is responsible for more than 15% of deaths worldwide. Decades of research in cancer genomics, empowered by the advent of accessible sequencing technologies, have led to the identification and characterization of key molecular alterations that sustain cancer pathogenesis. This in turn led to the development of targeted therapies, treatments that selectively affect these molecular drivers of neoplastic transformation. The majority of these drugs are small molecule inhibitors, cell-permeable chemicals that bind to (usually catalytic) pockets on a protein's surface and block the associated function. However, only about 20% of the proteome is estimated to be 'druggable' by this pharmaceutical modality and the design of highly target-selective inhibitors is challenging. Therefore, therapeutic intervention on many high-profile cancer drivers is still out of reach. Additionally, targeted therapies are rarely curative as drug resistance almost inevitably emerges.

In recent years, targeted protein degradation (TPD) has emerged as a novel promising pharmacological paradigm. It is based on the small-molecule mediated induction of molecular proximity between a target protein and an E3 ubiquitin ligase, the specificity-conferring component of the cellular protein degradation machinery. As a result, the target protein is flagged for selective and rapid elimination by the proteasome. The most explored class of small molecule degraders are proteolysis-targeting chimeras (PROTACs), modular heterobifunctional molecules composed of ligands for the target and the E3 ligase connected by a flexible linker. Clinical investigation of the first PROTACs has started in 2019, but due to the novelty of the technology, many aspects of TPD pharmacology are still to be investigated.

In the first chapter of this thesis, we developed BSJ-03-123, a highly selective PROTAC able to discriminate between two closely related protein homologs, CDK4 and CDK6. This molecule utilizes the dual CDK4/6 inhibitor palbociclib as target ligand, yet induces rapid degradation of CDK6, but not CDK4. We showed that BSJ-03-123 binds to both homologs in cells, but only CDK6 stably interacts with the $CRL4^{CRBN}$ E3 ligase upon PROTAC treatment and is consequently degraded. BSJ-03-123 treatment recapitulated the genetic dependency of acute myeloid leukemia on CDK6, while sparing CDK4-dependent cancer cell lines. It further allowed us to characterize the role of CDK6 at the interface of cellular signaling and gene expression via phosphoproteomic and transcriptomic profiling.

In the second part of the thesis, we explored the molecular mechanisms of drug resistance to targeted protein degradation. First, we identified the genetic requirements for degrader efficacy via genome-wide CRISPR/Cas9 screens. Resistance genes comprise components of the hijacked E3 ligase complex, as well as general regulators of its activity, like CAND1 and

the COP9 signalosome. Knockout of the substrate receptor (the E3 ligase subunit engaged by PROTACs) conferred the strongest resistance. To study these components in more detail, we designed a saturating mutagenesis library of the substrate receptors CRBN and VHL and queried it for point mutations that can drive drug resistance. Resistance-conferring mutations cluster around the PROTAC-binding pocket, as well as in proximity of protein-protein contacts between the target and the E3 ligase.

We next characterized genetic mutations in a spontaneous resistance model in the haploid cell line KBM7. In particular, we interrogated 29 putative resistance genes via a hybrid-capture based sequencing pipeline. We found that spontaneous resistance to a CRBN-based PROTAC was mainly driven by mutations in the substrate receptor itself, with a strong predominance of deleterious truncating mutations. In contrast, resistance to a degrader co-opting VHL was rarer and mediated by point mutations in other subunits of the E3 ligase complex as well. These results shed light on mutations of the E3 ligase machinery as an important resistance mechanism specific to targeted protein degradation.

Collectively, the work presented herein showcases the potential of targeted protein degradation as a novel pharmacology, among others thanks to the superior target selectivity that can be achieved by PROTACs compared to small molecule inhibitors. The insights on resistance mechanisms to PROTACs can inform on therapeutic and pharmacologic strategies to limit or overcome resistance to targeted protein degradation and help shape drug discovery efforts in this emerging field.

Zusammenfassung

Krebs ist noch immer die Ursache von mehr als 15% der Tode weltweit. Jahrzehntelange Forschung und die Entwicklung von zugänglichen Sequenziermethoden haben es ermöglicht, Krebs-spezifische molekulare Anomalien zu identifizieren, welche die unkontrollierte Proliferation der Tumorzellen fördern. Dies wiederum führte zur Entwicklung von zielgerichteten molekularen Therapien, also Medikamenten, die selektiv und spezifisch auf diese Regulatoren wirken, um das Krebswachstum zu hemmen. Zum Großteil sind diese Arzneimittel niedermolekulare, zellpermeable chemische Moleküle, die Vertiefungen auf der Oberfläche eines Zielproteins besetzen und die zugehörige (meist enzymatische) Funktion inhibieren. Es wird aber geschätzt, das nur etwa 20% des menschlichen Proteoms solche Vertiefungen aufweist und deshalb durch diese Pharmakologie modulierbar ist. Desweiteren ist die Entwicklung von sehr selektiven Molekülen eine große Herausforderung in der medizinischen Forschung.

In den letzten Jahren wurde gezielter Protein-Abbau (gPA) zu einer vielversprechenden neuen pharmazeutischen Modalität entwickelt. Durch niedermolekulare chemische Wirkstoffe wird ein zu degradierendes Protein in die Nähe einer E3 Ubiquitin Ligase gebracht. Dadurch wird das Protein von der Ligase für den Abbau durch das Proteasom markiert. Besonders PROTACs (kurz für „Proteolysis Targeting Chimera“) wurden intensiv erforscht. PROTACs sind modulare Moleküle, die durch die Verbindung von Liganden für das Targetprotein und die E3 ligase durch einen flexiblen chemischen Linker generiert werden. Die ersten klinischen Studien zu PROTACs haben 2019 begonnen, aber viele Aspekte der neuartigen Pharmakologie von gPA sind noch unerforscht.

Im ersten Teil dieser Dissertation ist die Entwicklung eines hochselektiven PROTACs, BSJ-03-123, beschrieben. Ein dualer Inhibitor gegen die homologen Proteine CDK4 und CDK6 dient hierfür als Baustein zur Definition des Targets. BSJ-03-123 bindet zwar in Zellen an beide Proteine, induziert aber nur den Abbau von CDK6 und nicht CDK4. Nur CDK6 interagiert nämlich aufgrund des Wirkstoffes mit der $CRL4^{CRBN}$ E3 Ligase und wird dadurch ubiquitiniert und degradiert. Dementsprechend rekapitulierte die Behandlung mit BSJ-03-123 die genetische CDK6-Abhängigkeit von akuter myeloischer Leukämie, ist aber auf CDK4-abhängige Zelllinien wirklos. Weiterhin ermöglichte BSJ-03-123 die Charakterisierung der Rolle von CDK6 in der Regulation der zellulären Signaltransduktion und Genexpression durch Phosphoproteomik und Transkriptomik.

Im zweiten Teil untersuchen wir die molekularen Mechanismen der Therapieresistenz zu gPA. Durch genomweite CRISPR/Cas9 Screens konnten wir die genetischen Vorraussetzungen für die Wirksamkeit von PROTACs ermitteln. Resistenzgene umfassen

unter anderem Komponenten der umfunktionierten E3 Ligasen-Komplexe, sowie allgemeine Regulatoren ihrer Aktivität, zum Beispiel CAND1 und das COP9 Signalosom. Knockout der jeweiligen Substratrezeptoren, also der E3-Untereinheiten, an die PROTACs binden, verlieh die stärkste Resistenz. Deshalb mutagenisierten wir die Substratrezeptoren CRBN und VHL, um Punktmutationen zu ermitteln, die Wirkstoffresistenz verleihen. Resistenzmutationen befanden sich hauptsächlich an der Bindungsstelle der PROTACs, sowie an Protein-Protein-Kontaktstellen zwischen der E3 Ligase und dem Target.

Desweiteren charakterisierten wir genetische Mutationen in einem spontanen Resistenzmodell basiert auf der haploiden Zelllinie KBM7. Insbesonders konzentrierten wir uns auf 29 potentielle Resistenzgene, die wir über ein Hybrid Capture-basiertes Verfahren gezielt sequenzierten. Spontane Resistenzmutationen gegen ein CRBN-basiertes PROTAC betrafen hauptsächlich den Substratrezeptoren selbst, vorwiegend durch trunkierende Mutationen. Im Gegensatz kam spontane Resistenz zu einem VHL-basierten PROTAC seltener auf und war durch Punktmutationen verursacht, die zusätzlich zu VHL auch andere Komponenten der E3 Ligase betrafen. Diese Ergebnisse heben Mutationen in der E3 Maschinerie als einen gPA-spezifischen Resistenzmechanismus hervor.

Die hier präsentierten Erkenntnisse unterlegen das Potential von gezieltem Proteinabbau als neues pharmakologisches Paradigma. Dies ist unter anderem der besseren Selektivität zuzuordnen, die durch PROTACs verglichen zu Inhbitoren erzielt werden kann. Die Erkenntnisse zu Resistenzmechanismen gegen PROTACs können zur Entwicklung von therapeutischen und pharmakologischen Strategien dienen, um das Aufkommen von Therapieresistenz zu limitieren oder überwinden, und dadurch die Wirkstoffentwicklung in diesem aufkommenden Forschungsfeld prägen.

List of abbreviations

aa	amino acid
ADCC	Antibody-Dependent Cell-mediated Cytotoxicity
ADME	Absorption, Distribution, Metabolism, Excretion
ALL	Acute Lymphocytic Leukemia
APC	Anaphase-Promoting Complex
BET	Bromodomain Extra-Terminal protein
BTB	Broad complex, Tramtrack, Bric-a-brac
CAND1	Cullin-Associated, NEDD8-Dissociated protein 1
CAR	Chimeric Antigen Receptor
Cas9	CRISPR-associated protein 9
CDK4	Cyclin-Dependent Kinase 4
CDK6	Cyclin-Dependent Kinase 6
CLL	Chronic Lymphocytic Leukemia
CML	Chronic Myeloid Leukemia
COP9	Constitutive Photomorphogenesis 9
CRBN	Cereblon
CRISPR	Clustered Regularly Interspaced Short Palindromic Repeats
CRL	Cullin-RING ligase
CSN	COP9 Signalosome
DCN1	Defective in Cullin Neddylation protein 1
DDB1	DNA-Damage Binding protein 1
DNMT	De Novo MethylTransferase
DUB	Deubiquitinase
E1	Ubiquitin-activating enzyme
E2	Ubiquitin-conjugating enzyme
E3	Ubiquitin ligase
EMT	Epithelial-To-Mesenchymal transition
FDA	Food and Drug Administration
GIST	GastroIntestinal Stromal Tumor
GO	Gene Ontology
HDAC	Histone Deacetylase
HECT	Homologous to E6AP C-Terminus
HER	Human Epidermal growth factor Receptor
IAA	Indole Acetic Acid
IAP	Inhibitor of Apoptosis Protein
IBR	In-Between-RING
IMiD	ImmunoModulatory Drug
MG	Molecular Glue degrader
NAE	NEDD8-Activating Enzyme
NEDD8	Neural precursor cell Expressed, Developmentally Downregulated 8
NSCLC	Non-Small Cell Lung Cancer
PROTAC	PROteolysis TArgeting Chimera
RBR	RING-between-RING
RING	Really Interesting New Gene
SCF	SKP, Cullin, F-box containing complex
SERD	Selective Estrogen Receptor Degrader
SERM	Selective Estrogen Receptor Modulator
sgRNA	single guide RNA
SMI	Small Molecule Inhibitor
SOCS/BC	Suppressor Of Cytokine Signaling/ elongin-BC
SR	Substrate Receptor
STK	Serine/Threonine Kinase
TPD	Targeted Protein degradation
UPS	Ubiquitin-Proteasome System
VHL	Von Hippel-Lindau

List of figures

Figure 1 Comparison of typical survival curves of targeted therapies and immunotherapy..11

Figure 2 Overview of common resistance mechanisms to targeted therapies……12

Figure 3 Schematic representation of the ubiquitination cascade……18

Figure 4 Model of substrate recognition by the proteasome……..20

Figure 5 Schematic depiction of the CRL activation cycle……..26

Figure 7 Overview of the two modalities of targeted protein degradation……29

Figure 8 Comparison of targeted protein degradation to conventional targeted therapies…34

Figure 9 Small molecule degraders utilized in the project……...56

Figure 10 Genome-wide positive selection CRISPR/Cas9 screens……...57

Figure 11 Comparison of dBET6 and ARV-771……....61

Figure 12 Systematic mapping of resistance-conferring point mutations in CRBN and VHL via saturating mutagenesis…….....62

Figure 13 Characterization of spontaneous resistance mutations to dBET6 and ARV-771...65

Figure 14 Mapping of ARV-771 resistance mutations onto the $CRL2^{VHL}$ complex……..…...66

1. Introduction

1.1 The etiology of cancer

Cancer is a major global health problem. It is estimated that cancer accounts for 1 in every 6 deaths, adding up to more than 10 million deaths a year, making it the second leading cause of death after cardiovascular disease (Howlader et al., 2019).

Cancer is an extremely complex collection of diseases, displaying incredible heterogeneity not only between patients, but also within an individual tumor. It arises due to the accumulation of genetic mutations and epigenetic alterations and the resulting deregulation of fundamental cellular pathways controlling cell growth, proliferation, apoptosis and DNA repair. The rewiring of cellular signaling networks allows cancer cells to escape the tightly regulated tissue homeostasis and to proliferate indefinitely.

Despite the heterogeneity, cancer cells share a set of characteristics that are required for malignant transformation, which have been famously termed the “hallmarks of cancer”. These include independence from positive and negative proliferation signals, resisting apoptosis, unlimited proliferative potential, a reprogramming of cellular energy metabolism, the induction of neo-angiogenesis to maintain the supply of oxygen and nutrients, evasion of immune surveillance and the capability to invade and colonize tissues distant from the primary tumor (Hanahan and Weinberg, 2000, 2011). Every cancer has to accumulate these characteristics over time, however how these hallmarks are acquired, both chronologically and mechanistically, is highly variable.

Additionally, a set of equally conserved cancer stress phenotypes have been described. Although they are not required for initiating tumorigenesis, they arise as a consequence of cellular transformation and represent shared oncogenic stresses that malignant cells must tolerate. Among these are oxidative stress, DNA damage and mitotic stress, proteotoxic and metabolic stress (Luo et al., 2009).

Decades of research, aided immensely by the advent of the genomic era, have further refined our understanding of the biology of cancer. Importantly, it has emerged that only a small subset of the mutations present in each tumor are driving the oncogenic process by conferring an advantage to the cells. Most cancers are driven by mutation or altered expression of few driver genes, that represent critical nodes in the regulation of cell proliferation and genome integrity (Martincorena et al., 2017). Prominent examples include the tumor suppressors TP53 and PTEN, signaling pathway hubs such as KRAS, BRAF and PI3KCA, cell cycle regulators like CCND1 and CCNE1, and transcription factors like MYC and ERG (Ampbell et al., 2020).

1.2 State of the art in cancer therapy

The accumulated understanding of cancer pathophysiology is having an important impact on its treatment. One of the major challenges in oncology is achieving a sufficiently large therapeutic window, in which a drug or treatment efficiently kills tumor cells while sparing normal cells, which can be achieved by targeting cellular networks and processes that cancer cells are particularly dependent on. Many anticancer drugs rely on general features described by the hallmarks of cancer, such as the hypersensitivity to DNA damage exploited by most chemotherapeutics, but the resulting therapeutic window is relatively small and heavy side-effects are caused by these treatments (Luo et al., 2009). In contrast, modern targeted therapies aim to selectively target the oncogenic drivers to induce tumor remission, as cancer cells have been shown to be 'addicted' to their driver mutations for sustaining their malignant phenotype (Weinstein, 2002). Cancer cells additionally display a series of so called non-oncogene addictions (or synthetic lethal interactions), which describe increased dependence on certain genes that are themselves not mutated or altered, but rate-limiting for the oncogenic process (Luo et al., 2009).

A more detailed overview of current pharmacological modalities for cancer treatments, as well as a discussion of remaining challenges and unmet needs, is given in this chapter.

1.2.1 Traditional chemotherapy

At the beginning of the 20th century, the only treatment option for cancer patients was the combination of surgery and radiotherapy, which is still the treatment of choice for some solid tumors (Delaney et al., 2005).

A first revolution of cancer therapy happened in the 1940s with the serendipitous discovery of the first genotoxic agents, nitrogen mustards, originally developed for war purposes. They were repurposed for the treatment of hematopoietic cancers, giving birth to the field of chemotherapy. In its original definition, chemotherapy refers to the use of any chemical agent to kill malignant cells or stop their proliferation. In the context of this thesis, it will however be used in a more modern interpretation to describe "classical" chemotherapeutics, drugs that have a general anti-proliferative (or cytotoxic) effect by interfering with cellular processes that are crucial for cell proliferation and survival, distinguishing them from targeted therapies, which aim to selectively block key oncogenes that promote tumor growth.

Cytotoxic drugs block fundamental steps of the cell cycle, such as DNA replication and mitosis. While the high proliferation rate of malignant cells makes them more susceptible to these treatments, creating a therapeutic window for their use in cancer therapy, they affect healthy cells as well. The effects are particularly prominent in tissues with a high cellular

turnover, leading to heavy side effects such as anemia, hair loss, gastro-intestinal disorders, fertility loss and nephrotoxicity.

An overview of the most important classes of chemotherapeutics is given below.

Alkylating agents:

The aforementioned nitrogen mustards are bifunctional alkylating agents, that exert their toxicity by attaching an alkyl group to guanine bases in the DNA and forming inter- and intra-strand crosslinks in the DNA. If not repaired, these lesions prevent DNA replication and ultimately result in cell death, particularly in cells with high proliferation rates (Brookes and Lawley, 1961). The most important nitrogen mustard still in clinical use is cyclophosphamide, utilized across a wide range of indications, including lymphoma, leukemia, breast and ovarian cancer, as well as non-small cell lung carcinoma (NSCLC) (Emadi et al., 2009).

Platinum salts, such as cisplatin, carboplatin and oxaliplatin, similarly display broad antitumor efficacy with comparatively reduced nephrotoxicity, and are widely used as first and second line treatments in various cancers (Dilruba and Kalayda, 2016). Other classes of alkylating agents are nitrosoureas, alkyl sulfates, epoxides and triazene compounds.

Antimetabolites

Conversely, antimetabolites block the synthesis of nitrogenous bases by structurally mimicking the physiological substrates. Nitrogenous bases are crucial building blocks for the synthesis of DNA and RNA nucleotides, which also have an essential role in providing the energy of many enzymatic activities in form of ATP. Inhibition of the purine and pyrimidine synthesis pathways has strong cytotoxic effects via induction of apoptosis or inhibition of cell proliferation. Antimetabolites can be classified into folate analogs (methotrexate), purine analogs (6-mercaptopurine) and pyrimidine analogs (5-fluorouracil). All three classes are still widely used in clinical practice for the treatment of both hematological malignancies and solid tumors (Tiwari, 2012).

Natural compounds

Several chemotherapeutics are bioactive natural compounds isolated from plant extracts. Many of these compounds inhibit cell proliferation by interfering with microtubule dynamics, either by inhibiting their polymerization or by stabilizing them, and consequently blocking mitosis due to defective mitotic spindle assembly. Examples of microtubule-destabilizing agents are Vinca alkaloids, such as vinblastine and vincristine, that were originally extracted from the rosy periwinkle (*Catharantus roseus*). Taxanes (e.g. paclitaxel, docetaxel) are antimitotics extracted from pacific yew that cause stabilization of microtubules. Both classes of drugs are mainly used as second-line therapies in several solid tumors, including breast

cancer, pancreatic adenocarcinoma, NSCLC, gastric and prostatic cancer (Jordan and Wilson, 2004).

Other antimitotics have been discovered to be inhibitors of topoisomerase I (topotecan, irinotecan) and II (etoposide). These enzymes cleave one or both DNA strands to locally unwind DNA, relieving tensional stress caused by supercoiling and releasing intertwined DNA duplexes. Topoisomerase activity is particularly important during DNA duplication and its inhibition causes replication fork arrest and widespread DNA breaks, resulting in generalized toxicity (Delgado et al., 2018).

Doxorubicin and related drugs of the anthracycline family are antibiotics isolated from *Streptomyces peucetius*. The mechanism of action of anthracyclines is more complicated; proposed mechanisms include inhibition of topoisomerase II activity, intercalation of the DNA double strand and generation of radical oxygen species that damage DNA, proteins and cellular membranes. Anthracyclines are routinely used in the treatment of several solid cancers and leukemias, but severe dose-limiting cardiotoxicities are still an unresolved issue (McGowan et al., 2017).

1.2.2 Targeted therapies

The main limitation of antiproliferative agents is their very narrow therapeutic window: since they target fundamental cellular processes, they also affect healthy cells and therefore have strong toxicities that limit their utilization and are heavily debilitating for the patients. A progressive understanding of the molecular mechanisms driving malignant cell growth, which started in the 1980s and was greatly accelerated by the complete mapping of the human genome, allowed instead a more selective approach and started the era of targeted therapies.

Targeted therapies encompass all those treatments that selectively affect specific molecular targets involved in the neoplastic transformation. This includes small molecule drugs obtained by chemical synthesis and biological drugs, mainly recombinant proteins and cellular therapies. Since targeted therapies selectively intervene on key oncogenes driving malignant growth, they affect normal cells to a lesser degree and have minor side effects compared to antiproliferative agents. In addition, their introduction into clinical practice lead to a significant improvement in the progression-free survival and overall mortality of cancer patients.

Biological drugs

Monoclonal antibodies

Seminal work by Köhler and Milstein in the 1970s lay the ground for the large-scale production of monoclonal antibodies specific to selected antigens by the creation of

hybridomas, obtained by fusing murine B cells with human myeloma cells (Köhler and Milstein, 1975). Following further development of the technology, such as genetical engineering to replace murine constant regions of the antibody with the human counterpart, the first monoclonal antibody was approved for clinical use in 1998. 20 years later, monoclonal antibodies have emerged as a major class of therapeutics, as approximately 80 different monoclonal antibodies have been granted regulatory approval (Lu et al., 2020).

Monoclonal antibodies can act through different mechanisms. By binding the extracellular domains of transmembrane proteins, they can block their function through induction of conformational changes, prevention of dimerization with co-receptors or by promoting receptor internalization and degradation, ultimately resulting in inhibition of proliferation or induction of apoptosis. In addition, cells decorated with monoclonal antibodies are prey to cytolysis by effector cells, mainly NKT and T cells, in a process called antibody-dependent cell-mediated cytotoxicity (ADCC). Finally, monoclonal antibodies can act as scavengers to sequester soluble factors (Singh et al., 2018).

The first clinically approved monoclonal antibody is rituximab, which targets the B cell surface marker CD20 and is used for the treatment of refractory non-Hodgkin B cell lymphomas (Coiffier et al., 1998). In the following decades, several more antibodies against surface receptors have been approved for clinical use, most importantly members of the HER (Human Epidermal growth factor Receptor) tyrosine kinase receptor family. These include HER2 antibodies trastuzumab, which is now the gold standard treatment for HER2-positive metastatic breast cancer (Carter et al., 1992), and pertuzumab, which prevents the dimerization of HER2 with other HER members blocking its intracellular signaling (Harbeck et al., 2013). Cetuximab is a monoclonal antibody targeting EGFR (HER1) utilized for the treatment of head and neck cancers and colorectal carcinomas (Fornasier et al., 2018).

Effective monoclonal antibodies targeting soluble factors have similarly impacted clinical practice. For example, bevacizumab binds and sequesters the vascular endothelial growth factor A (VEGF-A) and was the first anti-angiogenic therapy to be developed. It is now widely used for the treatment of a variety of solid tumors (Ferrara et al., 2004).

Checkpoint inhibitors

Cancer cells have the ability to escape the action of the immune system by activating immune checkpoints through overexpression of particular surface antigens. These markers bind receptors on the surface of the T cell (particularly CTLA-4 and PD-1, bound by CD80/86 and PD-L1, respectively) and trigger signaling cascades that result in inactivation of the T cell response (Darvin et al., 2018).

Monoclonal antibodies that prevent this downregulation of the immune response, commonly called checkpoint inhibitors, have revolutionized immunotherapy since their market entry in the 2010s. The first checkpoint inhibitor to be approved was ipilimumab, an antibody targeting the CTLA-4 receptor expressed on the surface of regulatory T cells (Hodi et al., 2010). Another promising therapeutic target is PD-L1: this transmembrane protein is expressed by some tumor types and acts by binding to the receptor PD-1 on T cells, which consequently become unable to recognize and kill cancer cells. Several different monoclonal antibodies interfering with this axis have been recently approved, for example nivolumab and pembrolizumab, which both bind PD-1, and durvalumab and atezolizumab, which target PD-L1 (Darvin et al., 2018).

Since they boost the natural anti-tumor immune response, checkpoint inhibitors are particularly effective in cancers with a high mutational burden, as they are more immunogenic due to the generation of neo-epitopes. Thus, treatment of incurable tumors such as melanoma and NSCLC has been impacted the most by this novel approach.

Cellular therapies

Another promising immunotherapy approach that has gained a lot of attention since the regulatory approval of the first treatments in 2017 is cellular therapy with CAR-T cells (Chimeric-Antigen Receptor). In brief, CAR-T cell therapy consists in T cells extracted from a patient that are genetically engineered to stably express an artificial T cell receptor (hence “chimeric”) with high specificity towards a tumor antigen. Upon the *in vitro* genetic modification, the cells are re-infused into the patient, where they selectively recognize cancer cells and spare normal tissues.

The first CAR-T therapies have been developed for the treatment B-cell malignancies such as acute and chronic lymphoblastic leukemia and different forms of Hodgkin’s lymphoma. The chimeric receptors are targeting CD19, a surface marker expressed on mature B cells, but not on precursor cells, therefore allowing the reconstitution of the B cell compartment after treatment. To date, two CAR-T treatments have received FDA approval, axicabtagene ciloleucel (Yescarta) and tisagenlecleucel (Kymriah), and showed impressive and durable antitumor responses (Lulla et al., 2018).

Small molecule drugs

While the importance of biologicals as oncology treatments has been constantly increasing over the last decade, the majority of the prescribed drugs are small molecule inhibitors (SMIs) (Saravanakumar et al., 2019). SMIs are typically chemicals < 500 Da that can permeate the cellular membrane and reach intracellular targets.

SMIs bind to defined pockets on the surface of disease-causing proteins, mostly enzymes, and inhibit their function. For the most part, this interaction occurs at the enzyme's substrate-binding site and blocks it for interaction with endogenous ligands (competitive/orthosteric inhibition). Alternatively, drug binding to cavities outside of the active site can induce conformational changes of the protein that prevent its catalytic activity (allosteric inhibition). Other less frequent mechanisms of action of small molecules include the ligand-induced disruption or induction of protein-protein interactions(Lampson and Davids, 2017). While the drug's engagement of the target is usually reversible, a subset of SMIs covalently bind to the target and inhibit it permanently.

Tyrosine kinase inhibitors

Due to their central role in the activation of signaling cascades controlling proliferation, differentiation and cell migration, tyrosine kinases are an attractive target for SMIs. In contrast to monoclonal antibodies, which inhibit receptor tyrosine kinase signaling through binding of their extracellular domains, small molecule inhibitors bind the intracellular portion of the receptor, mostly the ATP-binding pocket.

One of the earliest and most striking examples of a successful targeted small molecule inhibitor in cancer therapy is the tyrosine kinase inhibitor imatinib (Druker et al., 1996). Imatinib targets an oncogenic fusion protein containing the catalytic domain of the tyrosine kinase ABL1 (BCR-ABL), a well-characterized driver of a subset of ALL and CML patients, by blocking the ATP-binding pocket. In addition, imatinib also inhibits PDGFR and c-KIT, two important drivers in gastrointestinal stromal tumor (GIST), and was therefore repurposed for adjuvant treatment in this indication (Raut et al., 2018). Since then, several other BCR-ABL inhibitors have been developed to overcome the emergence of resistance observed in many patients, such as dasatinib, nilotinib and ponatinib (Rossari et al., 2018).

The other important target family of tyrosine kinase inhibitors are the HER growth factor receptors that drive activation of the PI3K-AKT and MAPK pathways. The first SMI targeting them was getfitinib, a potent and selective inhibitor of EGFR and HER2 used for the treatment of EGFR-overexpressing malignancies, such as NSCLC and breast cancer (Barker et al., 2001). Other molecules include lapatinib, a dual EGFR/HER2 inhibitor utilized in patients with

advanced metastatic breast cancer (Geyer et al., 2006), and the EGFR-selective erlotinib (Steins et al., 2018).

Tyrosine kinase inhibitors can also have a broader target spectrum. Sunitinib is a multi-targeted anti-angiogenic SMI that inhibits VEGFR, as well as PDGFR, c-KIT and FLT3, and is approved for several indications including GIST and renal cell carcinoma (Ivy et al., 2009). Sorafenib is another promiscuous kinase inhibitor developed against RAF-1 and BRAF, which also has inhibitory activity towards VEGFR and PDGFR (Wilhelm et al., 2008).

Serine/Threonine kinase inhibitors

Serine/Threonine kinases (STKs) have initially received comparably less attention as drug targets, despite their paramount role in intracellular signaling. STKs phosphorylate a vast array of transcription factors, cell cycle regulators and cellular effectors, many of which have been implicated in human cancer (Edelman et al., 1987).

Perhaps the best characterized oncogene of this family is BRAF, which in its constitutively active V600E mutant form is a driver of 40-60% of melanoma and papillary thyroid carcinoma cases and widely found in colorectal cancer and NSCLC (Davies et al., 2002). Selective ATP-competitive BRAF inhibitors such as vemurafenib (Chapman et al., 2011), dabrafenib (Hauschild et al., 2012) and encorafenib (Dummer et al., 2018) efficiently block the RAF-RAS-MAPK pathway, but are of limited use as monotherapy due to the frequent emergence of resistance. BRAF inhibitors are approved for clinical use in metastatic melanoma and several clinical trials exploring efficacy in other indications are ongoing. The same pathway is targeted further downstream by the MEK inhibitors trametinib (Flaherty et al., 2012a) and cobimetinib (Larkin et al., 2014). These molecules allosterically inhibit the kinase activity of MEK1 and MEK2 by binding a site adjacent to the ATP-binding pocket. MEK inhibitors are usually administered in combination with BRAF inhibitors, as this has been shown to delay the emergence of resistance (Flaherty et al., 2012b).

Cyclin-dependent kinases, such as CDK4 and CDK6, are crucial nodes in the regulation of cell cycle. By association with D-type cyclins, they phosphorylate the transcriptional repressor retinoblastoma (Rb) and release its inhibitory effect on transcription factors of the E2F family, ultimately allowing cells to enter S-phase of the cell cycle and divide. Because of their role in regulating proliferation, CDK4/6 and CCND are often dysregulated in human cancers. This prompted the development of potent and selective ATP-competitive inhibitors of this kinase family and led to the approval of palbociclib (Beaver et al., 2015), ribociclib (Hortobagyi et al., 2016) and abemaciclib (Goetz et al., 2017) for the treatment of breast cancer, either as monotherapy or in combination with endocrine therapy.

Another important hub in cancer signaling is the STK mTOR, the catalytic subunit of mTORC1 and mTORC2 complexes, which have fundamental roles in the regulation of cell growth and proliferation. The first mTOR inhibitor is a natural compound isolated from *Streptomyces hygroscopicus*, rapamycin. Originally developed as an antifungal agent, it was found to potently inhibit activation of T and B cells and was approved as an immuno-suppressant in renal transplantation (Kahan, 2015). In addition, rapamycin and related analogs display antiproliferative effects. Thus, everolimus (Motzer et al., 2008) and temsirolimus (Hudes et al., 2007) were approved for the treatment of different tumor forms, including renal cell carcinoma and mantle cell lymphoma. Of note, these mTOR inhibitors act via a peculiar mechanism: they mediate neomorphic protein-protein interactions between mTOR and the intracellular chaperone FKBP12, thereby sterically hindering substrate recruitment to the active site (Yang et al., 2013). This class of drugs that induce the association of proteins are therefore often referred to as ‘molecular glues’.

Epigenetic drugs

An important hallmark of some cancers is reprogramming of gene expression via alteration of epigenetic marks that determine whether a given gene is expressed or not. Three classes of proteins are important for epigenetic gene regulation: ‘writers’, which deposit histone marks such as acetyl or methyl groups on the histone tails, ‘readers’, which recognize the histone marks through specific domains, e.g. bromodomains or chromodomains, and recruit additional cofactors to remodel the chromatin, and ‘erasers’, which catalyze the removal of the histone marks. While the exact mechanisms are not yet understood, it has emerged that some cancers, particularly hematological malignancies, are driven by and therefore highly dependent on aberrant epigenetic regulation (Dawson and Kouzarides, 2012).

Methylation of DNA in or near the promoter of genes is an important mechanism of epigenetic silencing, as it reduces accessibility of DNA to transcription factors. The writer enzymes of this modification are DNA methyltransferases (DNMTs), which are frequently deregulated in cancer and cause the transcriptional repression of tumor suppressor genes (Herman and Baylin, 2003). Two DNMT inhibitors, azacitidine and decitabine, have been approved for patients with AML and myelodysplastic syndrome. They are cytidine analogs that upon incorporation into DNA covalently bind DNMTs and trap them, ultimately leading to their degradation (Estey, 2013).

Histone deacetylases (HDACs) are eraser enzymes that remove acetylation marks from histone tails, leading to compaction of the chromatin and transcriptional silencing of the associated genes. Several non-specific pan-HDAC inhibitors are in clinical use for the treatment of T cell lymphoma and multiple myeloma, including vorinostat (Richon et al., 1998), belinostat and panobinostat (Prince et al., 2009), mostly in combination with other anticancer

agents. These compounds directly interact with the Zn^{2+} ion in the active site of HDACs, which is required for their catalytic activity. More selective drugs targeting specific HDAC subclasses are in clinical evaluation for a diverse spectrum of hematological and solid tumors.

Epigenetic readers are also a promising therapeutic target class for SMIs, but since they are devoid of catalytic activity, drugs targeting them must follow a different logic and prevent protein-protein interactions rather than enzymatic function. The most advanced molecules target acetylation readers of the family of bromodomain extra-terminal (BET) proteins, which comprises four conserved members called BRD2, BRD3, BRD4 and BRDT. BRD4 in particular has been implicated with promoting tumorigenesis by accumulating on super-enhancers and recruiting transcriptional coactivators to drive expression of oncogenes such as MYC, BCL2, KIT and RUNX2 (Delmore et al., 2011). JQ1 is a potent competitive inhibitor of BET proteins that binds to the acetyl-lysine recognizing bromodomains. It showed strong antiproliferative effects in BRD4-dependent leukemia and breast cancer models, but is not explored for clinical use due to its short half-life (Filippakopoulos et al., 2010). Alternative BET inhibitors such as OTX015 and I-BET762 are in early stage clinical evaluation for the treatment of several cancers, mainly hematological malignancies, lung, prostate and breast cancer.

Other inhibitors

Other protein families have been explored for exploitation of cancer vulnerabilities via targeted treatments, for example metabolic enzymes. Isocitrate dehydrogenases of the IDH2 family are mitochondrial proteins with an important role in the citric acid cycle. Mutations in the IDH2 genes found in a subset of AML patients confer neomorphic activity to the enzyme, resulting in the generation of 2-hydroxyglutarate. At high concentrations, this metabolite can competitively inhibit several epigenetic regulators and cause the accumulation of methylation marks on histones and inhibition of cellular differentiation. Enasidenib is a small-molecule inhibitor that selectively recognizes oncogenic IDH2 variants and has been recently approved for treatment of AML (Pollyea et al., 2019).

Another therapeutic approach aims to modulate induction of apoptosis by pharmacological inhibition of the anti-apoptotic oncogene BCL-2 and related family members. Venetoclax is the first apoptosis-targeting small molecule inhibitor to get clinical approval and is utilized for the treatment of CLL. Venetoclax selectively inhibits the protein-protein interaction between BCL-2 and the pro-apoptotic protein BIM, activating the apoptotic cascade (Lampson and Davids, 2017).

Some subtypes of breast cancer are driven by hyperactivation of the estrogen receptor ERα, so pharmacological approaches to inhibit its function have been developed. Tamoxifen and toremifene are Selective Estrogen Receptor Modulators (SERMs), which upon binding to

the ER induce conformational changes leading to receptor dimerization and blockage of downstream gene expression. Conversely, fulvestrant is a Selective Estrogen Receptor Degrader (SERD): upon binding, ER dimerization is inhibited and its translocation to the nucleus reduced, leading to its destabilization and accelerated degradation (El Sayed et al., 2019). A complementary approach instead aims to reduce the levels of circulating estrogens by inhibiting aromatase, the enzyme responsible for its synthesis. Several aromatase inhibitors have been approved for the treatment of breast cancer, including the covalent inhibitor exemestane and the reversible competitive inhibitors anastrozole and letrozole (Wood et al., 2003).

Another class of successful targeted therapy SMIs are molecules blocking protein turnover by inhibition of the proteasome, which are discussed in further detail in chapter 1.6.1.

1.3 Mechanisms of resistance to targeted therapies and strategies to overcome them

The advent of targeted therapies has greatly improved the management of cancer patients, both in terms of overall survival and quality of life, with significant mitigation of side effects compared to conventional chemotherapy. Still, both conventional chemotherapy and targeted therapies are rarely curative: while the majority of the patients experiences an initial phase of dramatic response to the drug, resistance almost inevitably arises a few months later. Clinically, this often translates to a high response rate and prolonged progression-free survival compared to standard of care, but only minor improvements in overall survival, as exemplified by getfitinib-treated EGFR-mutated NSCLC patients (Maemondo et al., 2010) and crizotinib treatment of ALK-positive NSCLC (Shaw et al., 2013).

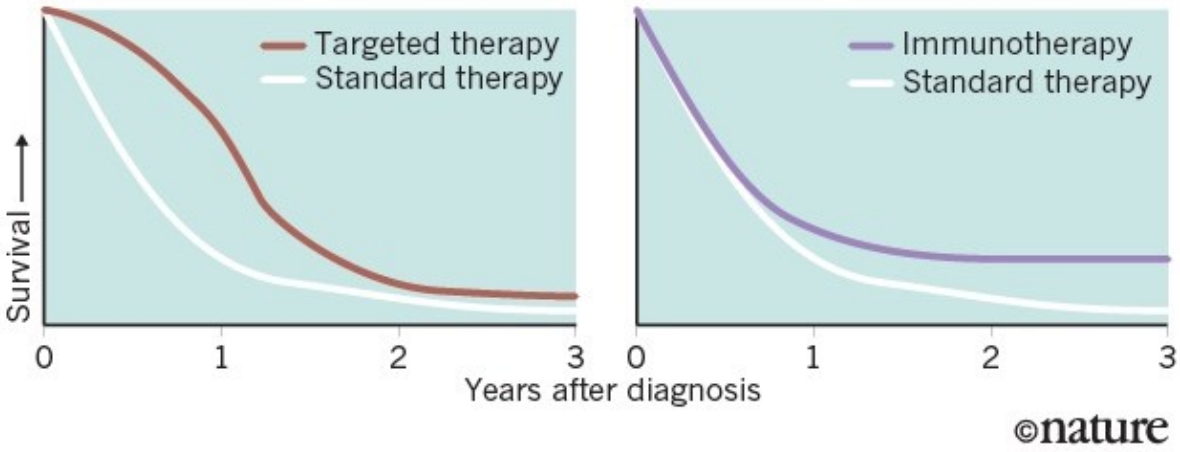

Figure 1 Comparison of typical survival curves of targeted therapies and immunotherapy.
Reprinted with permission from H Ledford, Cocktails for cancer with a measure of immunotherapy, Nature (2016).

Notably, the response to immunotherapy is significantly different: only a fraction of the patients benefit from treatment with immune checkpoint inhibitors, but a subset of the responders achieves durable responses lasting for several years (Hodi et al., 2010) (**Fig 1**).

Extensive efforts to characterize drug-resistant laboratory models and patient samples have yielded an understanding of the basic mechanisms underlying the resistance phenotype, which can in turn be exploited to forestall or circumvent the patients' relapse. Some of the most prominent molecular mechanisms of resistance to targeted therapies, as well as strategies to overcome them, are described in the following (**Fig 2**).

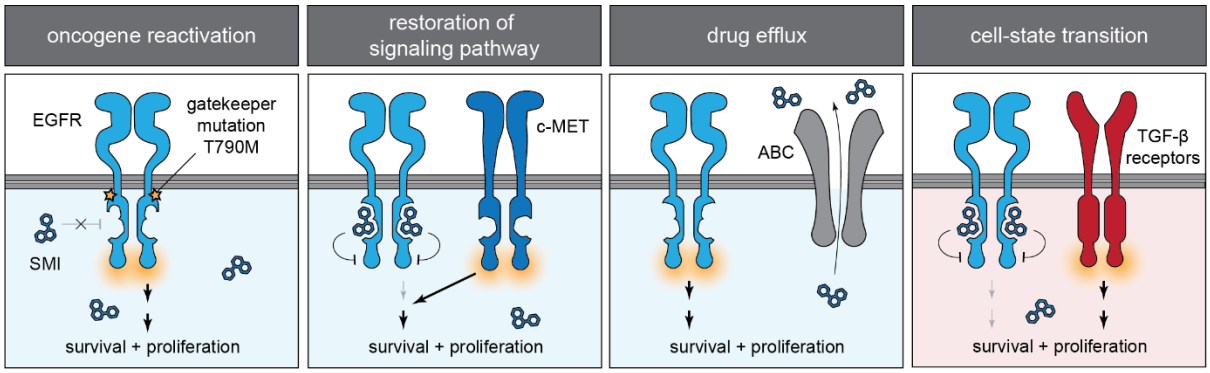

Figure 2 Overview of common resistance mechanisms to targeted therapies, exemplified by a small molecule inhibitor (SMI) targeting EGFR.

1.3.1 Oncogene reactivation

A common cause of clinical failure of targeted therapies is direct restoration of the biological activity of the driver oncogene. For kinase inhibitors, this frequently happens through acquisition of a 'gatekeeper' point mutation in the binding pocket of the target. Gatekeeper mutations abolish the activity of SMIs via different mechanisms, e.g. by sterically hindering drug binding to the target, by inducing allosteric changes that increase kinase activity, or by enhancing ATP binding affinity, which outcompetes drug binding to the receptor. Prominent gatekeeper mutations are the T315I BCR-ABL1 mutant in imatinib- or dasatinib-resistant CML (Soverini et al., 2007) and the T790M mutation in EGFR, which arises in about half of the NSCLC patients treated with erlotinib or getfitinib (Yu et al., 2013).

Importantly, gatekeeper mutations can be overcome by rational design of novel compounds, as exemplified by third generation EGFR inhibitors, like osimertinib and rocitletinib, which show clinical efficacy in patients harboring the T790M mutation (Wang et al., 2016a). Also in this case however, drug resistance arises through acquisition of additional gatekeeper mutations in EGFR, such as C797S, prompting the development of fourth generation allosteric inhibitors (Wang et al., 2016b). This example showcases the importance

of characterizing mutations driving the resistance to targeted therapies and to accordingly expand our arsenal of compounds targeting them.

Point mutations are not the only mechanism to restore oncogene activity and drive drug resistance. Malignant cells can also escape drug action through alternative splicing. This can result in the elimination of the drug-binding domain of the target, as in the case of the antiandrogen enzalutamide (Hu et al., 2009), or generate variants with increased activity, such as the BRAFp61 splice variant that displays enhanced dimerization and signaling, conferring resistance to vemurafenib treatment (Poulikakos et al., 2011).

For SMIs to be clinically effective, target engagement with the inhibitor must be close to saturation ('occupancy-driven' pharmacology, further discussed in chaper 1.7.3). Therefore, a common escape mechanism is the overexpression of the target oncoprotein through genomic amplification or transcriptional overexpression to outcompete the drug (Chen et al., 2004). While this resistance mechanism could in principle be circumvented by increasing the dosage of the drug, this approach is usually limited by the consequent enhancement of off-target toxicities. Therefore, development of more potent inhibitors and/or inhibition of downstream signaling pathways are more promising strategies to contrast target overexpression.

1.3.2 Restoration of the signaling pathway

Oncogenic drivers control signaling networks that result in enhanced proliferation and survival. These signaling cascades are however highly complex and redundant, so activation of a parallel pathway can bypass the requirement for the activity of a specific oncogene. For example, EGFR-mutant NSCLC is driven by the hyperactivation of the PI3K-AKT cascade through dimerization with co-receptors HER2 and HER3. In EGFR-inhibitor resistant cells, this signaling pathway is activated irrespectively of EGFR inhibition status via activation of parallel pathways, e.g. through amplification of the related tyrosine kinase MET (Engelman et al., 2007) or HER2 (Takezawa et al., 2012).

Similarly, oncogenic signaling can be maintained through mutation of an alternative target within the same pathway, thereby uncoupling it from the inhibited driver. This is frequent in vemurafenib-resistant melanoma driven by the V600E BRAF mutant, where MAPK pathway activation is restored through hyperactivation of the upstream regulator RAS (Nazarian et al., 2010) or relief of BRAF autoinhibition via loss of the tumor suppressor NF1 (Nissan et al., 2014).

The emergence of resistance through compensatory signaling can be countered through rational drug combinations targeting multiple nodes of the same pathway or parallel cascades. For example, pharmacological inhibition of MET re-sensitizes cells to EGFR inhibitors (Bean

et al., 2007) and combined BRAF and MEK inhibition improves progression-free survival (Flaherty et al., 2012b). Importantly, sequential treatment is less beneficial than combination therapy, highlighting the importance of predicting resistance pathways to design upfront drug combinations (Kim et al., 2013).

1.3.3 Cell-state transitions

A more complex resistance mechanism is the transformation of the cellular identity to reduce drug sensitivity or eliminate the dependence on the driving oncogene altogether.

For example, multiple carcinomas can undergo epithelial-to-mesenchymal transition (EMT) during chemotherapy or targeted therapy treatment through epigenetic changes. Several drivers of EMT have been identified, such as TGF-β and WNT signaling, and the transcription factors SNAI1, ZEB1 and TWIST1 (Kalluri and Weinberg, 2009). However, efforts to target mesenchymal signaling have so far not been successful.

Another relevant model is the transition of NSCLC into small-cell carcinoma, which occurs in about 5-10% of patients that relapse after EGFR inhibitor treatment. It is driven by concomitant loss of tumor suppressors RB1 and TP53 and consequent disruption of cell cycle regulation and suppression of EGFR expression and dependency (Niederst et al., 2015).

Furthermore, acute and reversible epigenetic changes can occur following drug treatment, resulting in a drug-tolerant ‘persister’ state (Sharma et al., 2010). These persister cells can undergo further evolution and develop acquired resistance through accumulation of genetic resistance mutations. At the same time, the persister state is associated with its own therapeutic vulnerabilities, such as dependence on histone demethylase activity (Sharma et al., 2010), hypersensitivity to BCL2 inhibitors (Hata et al., 2016) or acquired dependency on the lipid hydroperoxidase GPX4 (Hangauer et al., 2017).

A deep understanding of the signaling networks underlying these cell-state transitions will be required in to identify vulnerable nodes and therapeutically exploit them with rational drug combinations.

1.3.4 Increased drug efflux

Limitation of intracellular drug concentrations through increase of drug efflux has been long known to be a major reason for resistance to conventional chemotherapeutics, but is of similar relevance for targeted SMIs.

ABC transporters are a family of 48 genes that evolved to protect tissues from metabolites and exogenous toxins by pumping them out of cells in an ATP-dependent manner. However, they similarly transport a variety of drugs and are therefore important contributors to multi-drug

resistance. Among them, ABCB1, ABCC1 and ABCG2 are of particular relevance due to their cargo spectrum which includes paclitaxel, doxorubicin, anthracyclines and several tyrosine kinase inhibitors (Sharom, 2008).

ABC transporters are often upregulated in malignant cells and directly influence their sensitivity to anticancer drugs (Fojo et al., 1987), making them appealing drug targets. However, efforts to develop inhibitors of ABC transporters (also called chemosensitizers) to tackle multi-drug resistance have so far not shown clinical success due to limitations in their selectivity and toxicity profiles (Hamed et al., 2019).

1.4 Challenges in drug discovery

From decades of experience in the treatment of cancer the realization has emerged that the most promising approach for long term management of the disease lies in the utilization of rational drug combinations that prevent or delay the emergence of resistance. While our mechanistic understanding of the molecular actors driving malignant transformation is quite extensive, intrinsic limitations of current pharmacological strategies are hindering the full exploitation of the insights that have been gained in the past decades.

The biggest limitation is the accessible target space, as a large fraction of the proteome is not amenable to pharmaceutical modulation with existing approaches. Monoclonal antibodies and other biologicals are limited to targets exposed on the cellular surface or soluble factors, as they are unable to permeate the cell membrane due to their considerable size. For the same reason, they are not orally bioavailable and have instead to be administered via intravenous infusion or injection. Conversely, SMIs require ligandable functional pockets on the surface of the target protein and the majority of the proteome is devoid of them and therefore deemed ‘undruggable’. According to current estimates, less than 20% of the proteome is accessible for pharmacological intervention via conventional SMIs, excluding whole protein classes and high-interest cancer targets, such as transcription factors, MYC, KRAS, β-catenin and many more (Hopkins and Groom, 2002).

Biologicals face additional logistical challenges. Because of their peptidic nature, they have to be manufactured in living cells, which is a lot more costly than the chemical synthesis of SMIs, and shipped and stocked at controlled temperatures, raising the cost even further. A single treatment round with biological drugs can therefore cost several hundred thousand dollars, straining the resources of healthcare systems in the Western world and making them inaccessible for developing countries.

Conversely, a further limitation of SMIs is that they only block the specific (mostly enzymatic) activity of the pocket that they bind and are thus unable to affect scaffolding or

non-catalytic functions of the target protein. While scaffolding functions are well established for some enzymes, such as tyrosine kinase receptors, there is mounting evidence that they might be more common for other kinases and enzymes as well (Kung and Jura, 2016). Targeting these non-catalytic functions of proteins with SMIs is however out of reach with the current state of the art in drug development.

Due to their functional role, the ligandable pockets are usually highly conserved, making the design of truly selective molecules virtually impossible by current means (Fabbro, 2015). In some cases, the concomitant targeting of multiple related proteins is of therapeutic advantage or can aid repurposing of a drug to a different indication. At the same time however, off-target toxicities of the molecules are the major cause for side effects of targeted therapies and a serious consideration in the design of drug combinations (Liu and Kurzrock, 2014).

In recent years, targeted protein degradation (TPD) emerged as a novel paradigm in pharmacology emerged and rapidly generated a lot of interest in the field, as it promises to overcome several of these limitations. It is an approach that redirects proteins of interest to the cellular waste disposal machinery via small molecules, resulting in their selective, rapid and complete elimination.

In the subsequent chapters, the fundamental principles of the ubiquitin-proteasome system are briefly illustrated. Furthermore, the mechanistic basis of targeted protein degradation, as well as its development and the state of the art are detailed in the following.

1.5 The ubiquitin-proteasome system (UPS)

Protein levels in cells are tightly regulated: since cellular proteins are undergoing continuous turnover, their abundance is determined by the balance of the rate of synthesis and degradation. Protein half-lives can vary greatly, from the range of minutes to days, with important functional implications. For example, short-lived proteins are enriched for regulatory molecules such as transcription factors, providing the cell with the plasticity required to quickly adapt to changing environmental conditions. Other proteins are rapidly degraded in response to specific stimuli, allowing relatively fast responses and the orchestration of complex cellular processes, such as progression through cell cycle. Finally, it is important for cells to recognize and clear damaged and misfolded proteins rapidly to prevent their aggregation and cytotoxic consequences.

Therefore, cells heavily depend on an efficient protein waste disposal machinery. A major requirement of such a system is to contain the proteolytic activity of its effectors in order to prevent uncontrolled degradation of cellular contents. Cells have evolved two distinct mechanisms to accomplish this: (i) lysosomes are membrane-bound vesicles, which spatially

segregate proteases and hydrolytic enzymes at their inside. They are mainly responsible for the degradation of extracellular and transmembrane proteins during endocytosis, as well as organelles and cellular protein aggregates in physiological conditions and in response to nutrient deprivation. (ii) the ubiquitin-proteasome system, which is described in more detail below.

1.5.1 Ubiquitin

Under normal conditions, the predominant protein degradation machinery is the proteasome, a large multi-subunit protease complex which in eukaryotic cells is located in the nucleoplasm and the cytoplasm (Brooks et al., 2000).

Proteins to be degraded are selectively directed to the proteasome by attachment of a “molecular flag” called ubiquitin. Ubiquitin is a small protein of 76 aa (8.5 kDa) with a tightly packed globular conformation mediated by hydrogen bonds (Vijay-Kumar et al., 1987). Important features include its seven lysine residues (K6, K11, K27, K29, K33, K48, and K63), and the C-terminal di-glycine peptide. Ubiquitin is ubiquitously expressed across eukaryotes (but not in prokaryotes) and highly conserved, with 96% sequence identity shared between humans and yeast, and ubiquitin from different species are functionally interchangeable without affecting the cellular phenotype. Humans, as most eukaryotes, have multiple genes encoding for ubiquitin precursors, either fused to ribosomal proteins (UBA52 and RPS27A) or as polyubiquitin chains with 3 or 9 monomer repeats with head-to-tail linkage (UBB and UBC).

Ubiquitin is appended to target proteins via a multi-step process called ubiquitination, which requires sequential action of three enzyme families. First, an E1 ubiquitin-activating enzyme forms an energy-rich thiol ester bond between a cysteine residue in its active site and the C-terminal tail of ubiquitin in an ATP-dependent manner. Ubiquitin is then transferred to an E2 ubiquitin-conjugating enzyme via a thioester-exchange reaction. Finally, an E3 ubiquitin ligase simultaneously binds the E2 enzyme and the target protein and catalyzes the transfer of the activated ubiquitin to the substrate (**Fig 3**). Ubiquitin covalently binds the target protein via formation of an isopeptide bond between the C-terminus of ubiquitin (G76) and the ε-amino group of (generally) a lysine side chain on the target (Pickart, 2001). Another family of enzymes called deubiquitinases (DUBs) can remove or edit ubiquitin marks from proteins by cleavage of the isopeptide bond, allowing dynamic and fine-tuned regulation of the response (Komander et al., 2009).

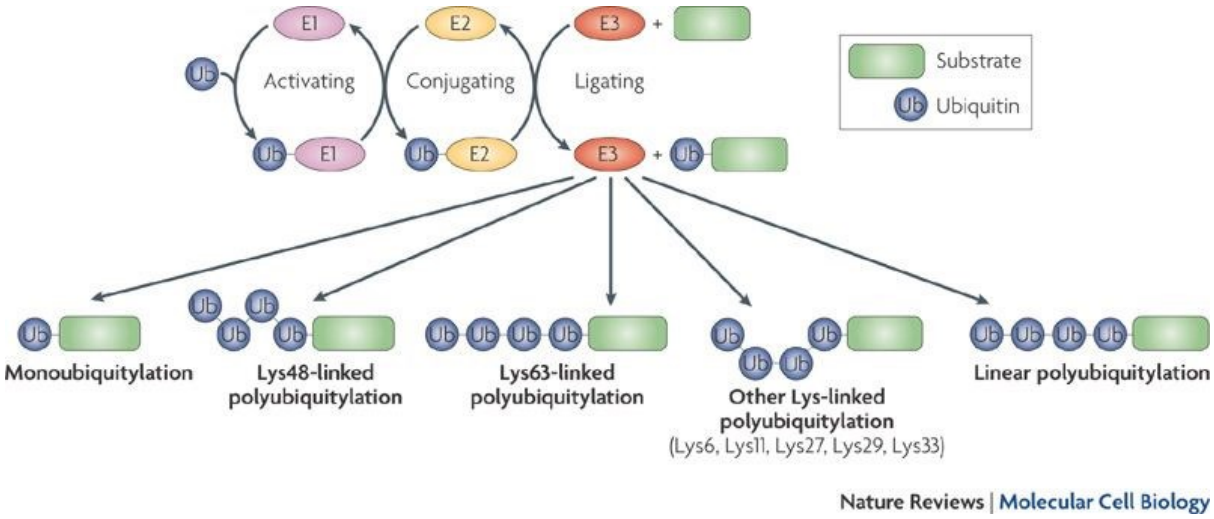

Figure 3 Schematic representation of the ubiquitination cascade, which requires the concerted action of an E1 ubiquitin-activating enzyme, an E2 ubiquitin-conjugating enzyme and an E3 ubiquitin-ligating enzyme.
Reprinted with permission from I Dikic, S Wakatsuki and KJ Walters, Ubiquitin-binding domains – from structures to functions, Nat Rev Mol Cell Biol (2009).

As many other post-translational modifications, ubiquitination can come in different patterns that often lead to distinct fates of the modified protein, giving rise to what has been termed the "ubiquitin code". In its simplest form, a single ubiquitin monomer is attached to one (monoubiquitination) or multiple lysine residues of the target protein (multi-monoubiquitination), thereby affecting its activity, subcellular localization or protein-protein interactions (Hicke, 2001).

However, ubiquitin can itself be target of ubiquitination at its N-terminus (M1) or one of its seven lysine residues, giving rise to a wide array of different conformations by elongation of polymeric chains of different length and linkage. In the case of homotypic chains, all ubiquitin monomers are linked through the same residues. A further level of complexity is added in heterotypic chains, which are composed by ubiquitin monomers connected via different linkages, and can be of two types: in mixed chains, each ubiquitin molecule is modified by only one other, whereas branched chains are formed when a single monomer is modified by two or more ubiquitin molecules (Komander and Rape, 2012; Yau and Rape, 2016).

Based on the chain topology, ubiquitination can elicit a variety of effects on the modified protein. The prototypical example are K48-linked ubiquitin chains, the most abundant linkage in cells across organisms, which are considered the major signal for degradation by the 26S proteasome (Chau et al., 1989). In addition, ubiquitination can signal for proteasome-independent degradation of for example plasma membrane proteins via endocytosis and targeting to the lysosomal compartment. This effect is mainly mediated by monoubiquitylation and K63-linked chains (Mukhopadhyay and Riezman, 2007).

Although outside of the scope of this thesis, several proteolysis-independent consequences of ubiquitination have been described, such as favoring assembly or disruption of macromolecular complexes. Ubiquitination was therefore established as a crucial component in the regulation of several signaling cascades, including activation of the NF-κB and WNT pathways, the DNA damage response and mitochondrial clearance (Komander and Rape, 2012; Mukhopadhyay and Riezman, 2007).

Of note, this chapter presents a very simplified view of the ubiquitin code. Further levels of complexity are added by the fact that ubiquitin itself can again be target of post-translational modifications, such as phosphorylation at S65, affecting its structure and binding to interaction partners (Swaney et al., 2015). Additionally, the human genome encodes for at least 8 further ubiquitin-like proteins (UBLs), such as ISG15, NEDD8 and SUMO, that can covalently modify proteins through an analogous cascade of dedicated E1-E2-E3 enzymes (Cappadocia and Lima, 2018). UBLs can even form heterotypic chains in combination with ubiquitin (Uzunova et al., 2007), thereby dramatically expanding the combinatorial signaling potential of the ubiquitin code.

1.5.2 The proteasome

The proteasome is a 2.5 MDa multi-subunit complex with three major components: the 20S core, which adopts a hollow barrel-like conformation with proteolytically active subunits facing the interior of the complex, and two 19S regulatory particles that assemble on each end of the core and regulate substrate access (Baumeister et al., 1998).

The 20S core is composed of four axially stacked ring structures, namely two external α-rings and two internal β-rings, each formed by 7 structurally related subunits. The α-rings interact with the 19S regulatory particles and together regulate substrate access to the inner chamber; they further facilitate entry of large proteins to the catalytic core by unfolding and linearizing them. The catalytic sites responsible for protein cleavage are contributed by three β-subunits on each β-ring and face the interior of the barrel structure, thereby spatially restricting the proteolytic activity. These sites have been named after their substrate specificity, so caspase-like (β1), trypsin-like (β2) and chymotrypsin-like (β5) (Löwe et al., 1995). Due to the concerted action of the catalytic sites, substrate proteins are hydrolyzed to single amino acids or small polypeptides upon passing through the proteasome.

Poly-ubiquitinated proteins are recognized and bound by receptors associated with the 19S, such as Rpn10 (Elsasser et al., 2004) and Rpn13 (Husnjak et al., 2008). The ubiquitin chain is then cleaved off by Rpn11 in an ATP-dependent manner and released, allowing the ubiquitin monomers to be recycled and the client protein to be pulled through the proteasome core for hydrolysis (Verma et al., 2002). The minimal requirement for efficient substrate

recognition by the proteasome is generally a ubiquitin chain of at least 4 monomers, as determined first by biochemical assays (Thrower, 2000) and later explained by structural studies, as this is the minimal length required to bridge the gap between Rpn10/13 and Rpn11 (Lander et al., 2012) (**Fig 4**). More recent studies however suggest that ubiquitin density, rather than chain length, might be the determining factor, since cooperative binding of multiple mono-or di-ubiquitinated lysine residues provides a stronger degradation signal than the conventional K48-tetraubiquitin chain (Lu et al., 2015).

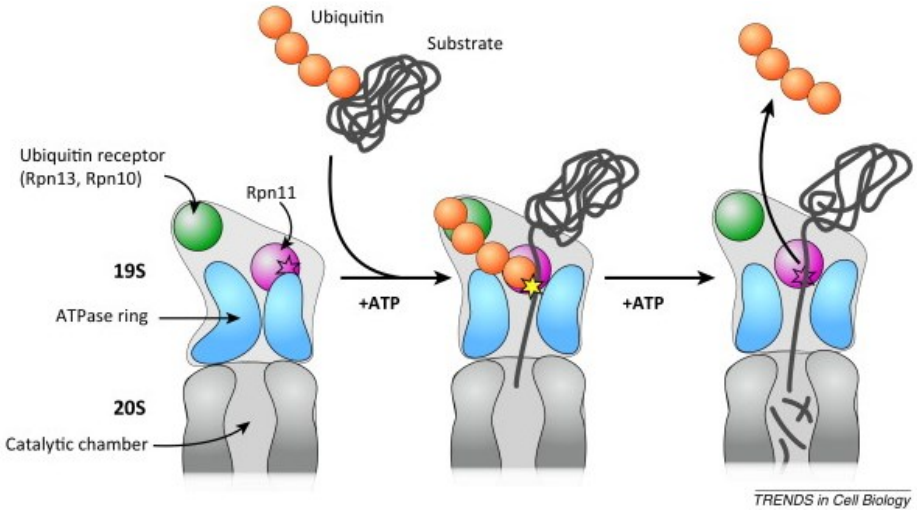

Figure 4 Model of substrate recognition by the proteasome. Binding of a ubiquitinated substrate causes conformational changes in the 19S subunit, permitting access of the polypeptide to the proteasome core, and cleavage of the ubiquitin chain by Rpn11.
Reprinted with permission from G Kleiger, T Mayor, Perilous journey: a tour of the ubiquitin-proteasome system, Trends in Cell Biology (2014).

Other atypical linkage topologies have also been associated with recognition of the modified protein by the proteasome. Homotypic K11 chains and branched K11/K48 chains are deposited among others by the anaphase promoting complex to induce degradation of critical regulators (e.g. cyclins and spindle assembly factors) during progression of the cell cycle (Jin et al., 2008; Meyer and Rape, 2014; Song and Rape, 2010). Studies conducted in yeast have further implied K29-linked chains in proteasomal degradation (Johnson et al., 1995).

1.5.3 Determinants of specificity: E3 ubiquitin ligases

As noted above, ubiquitination is a complex cascade with an important role in cellular homeostasis and signaling. As such, a crucial requirement for the system is the ability to determine with high selectivity which proteins are to be modified and eventually degraded. Because the human genome encodes for two E1 enzymes, approximately 40 E2s and more than 600 E3 ligases (Li et al., 2008), it quickly became clear that the latter are the main component in determining the specificity of the ubiquitination cascade. E3 ligases are a

heterogeneous enzyme class and can be broadly classified into families, HECT, RING and RBR, based on the molecular mechanism of ubiquitin transfer and the presence of characteristic protein domains.

HECT E3 ubiquitin ligases

The 28 members of the HECT (Homologous to E6AP C-Terminus) family of ubiquitin ligases are characterized by a conserved C-terminal catalytic domain of approximately 350 aa. The HECT domain has a bi-lobar structure: the bulky N-terminal lobe is responsible for the binding of the E2 enzyme, whereas the carboxy-terminal lobe contains the catalytic cysteine. The two lobes are connected by a flexible hinge region, allowing adaptation of the HECT domain conformation to facilitate the ubiquitin transfer (Huang et al., 1999).

Ubiquitination by HECT ligases is a two-step process: first, the activated ubiquitin moiety is transferred from the E2 to the catalytic cysteine in a transthiolation reaction, and only subsequently it is handed over from the E3-ubiquitin intermediate to the substrate protein (Weber et al., 2019).

While catalysis of the reaction is mediated by the conserved HECT domain, target specificity of this E3 family is mostly determined by the more diverse N-termini. Based on the domain organization in their N-terminal extensions, HECT E3s can be further categorized into subfamilies. The NEDD4 family comprises 9 members and is characterized by the presence of an N-terminal lipid-binding C2 domain and two to four tryptophane-tryptophane (WW) motifs responsible for substrate recognition (Ingham et al., 2004). The 6 members of the HERC family share one or more RCC1-like domains (RLD), which can in some cases also function as a guanine nucleotide exchange factor for the regulation of small GTPases (Sánchez-Tena et al., 2016). The remaining 13 HECT E3 ligases don’t share common domains and are therefore classified as ‘other’ HECTs.

A distinctive feature of HECT E3 ligases is the ability to catalyze formation of ubiquitin chains of defined linkage irrespectively of the paired E2 enzyme. For example, E6AP synthesized K48-linked ubiquitin chains, whereas NEDD4 HECTs primarily form K63 bonds (Kim and Huibregtse, 2009).

Furthermore, HECT E3 activity is precisely regulated: the enzyme is kept in a catalytically inactive conformation by intramolecular interactions between the N-terminal domains and the HECT domain (Wiesner et al., 2007). Intermolecular interactions can similarly modulate the enzymatic function of the ligases: in the case of HUWE1, homo-dimerization occurring at the HECT domain inhibits its catalytic activity (Sander et al., 2017), while E6AP is on the contrary only active in a homo-trimeric form (Ronchi et al., 2014). The switch between conformations

is often mediated by post-translational modifications, allowing for rapid and precise control of E3 activity.

RING-Between-RING E3 ubiquitin ligases

The RING-Between-RING (RBR) ligase family comprises 14 members in humans. In analogy to HECT ligases, ubiquitination by RBRs involves the formation of a covalent E3-ubiquitin thioester intermediate before the final transfer to the substrate (Marín et al., 2004).

RBRs are characterized by two RING (Really Interesting New Gene) domains separated by an IBR (In-between-RING) domain. Each of the three domains coordinates two Zn^{2+} ions, but they differ in their structure and function. RING1 adopts a cross-brace fold like canonical RINGs (see below) and recruits the ubiquitin-loaded E2. The fold of RING2 is contrarily to the name similar to the IBR domain. RING2 possesses a catalytic cysteine that serves as the active site for formation of the ubiquitin thioester intermediate (Wenzel et al., 2011). The precise function of the highly variable IBR domain is instead not yet fully understood (Duda et al., 2013).

RBRs contain additional domains that are specific to individual members. These are often involved in autoinhibition by masking of the catalytic Cys residue. Several mechanisms of release of the inhibitory contacts have been described, including the phosphorylation of the RBR Parkin by the kinase PINK1 (Pickrell and Youle, 2015), conformational changes induced by protein-protein interactions (Stieglitz et al., 2012) or recruitment to multi-component E3 ligase complexes (Scott et al., 2016).

RING E3 ubiquitin ligases

The by far largest family of E3 ligases, comprising more than 90% of all predicted human E3 ligases, is characterized by the presence of a RING or U-box domain. RING domains contain 8 cysteine and histidine residues in a conformation of C3H2C3 or C4HC3, which fold in a cross-braced arrangement to coordinate two Zn^{2+} ions and form the binding surface for an E2 enzyme (Barlow et al., 1994). The related U-box domain adopts a very similar conformation, but does not require the zinc ions and is instead stabilized by non-covalent interactions between conserved residues (Aravind and Koonin, 2000).

In contrast to ligases of the HECT and RBR families, RING E3s function as allosteric activators of the E2 and as scaffolds to bring them in proximity of the target protein; as such, they mediate direct transfer of ubiquitin from the E2 to the target, without formation of a covalent intermediate (Zheng and Shabek, 2017). Therefore, for this family of E3 ligases the type of ubiquitin chain linkage is generally determined by the E2 enzyme, so a single E3 can employ different E2s to initiate and extend chains of different topology (Stewart et al., 2016).

RING ligases can act either as monomers or associate into homo- or heterodimers via interaction of the RING domains, with other domains contributing additional contacts. While homodimers generally bind an E2 on each subunit, heterodimers often involve an inactive RING partner which is thought to allosterically activate the E2-bound partner (Budhidarmo et al., 2012).

Additionally, RING ligases can act as large multi-subunit complexes, such as the anaphase-promoting complex (APC/C, composed of at least 11 subunits) that triggers cell cycle entry into anaphase by tagging specific regulators for degradation (Castro et al., 2005). Another class of RING ligase complexes that are of fundamental importance for the regulation of a plethora of cellular processes due to their modular nature are Cullin-RING ligases, described in more detail below.

1.5.4 Cullin-RING ligases (CRLs)

Cullin-RING ligases are the largest family of E3 ligases and are estimated to ubiquitinate ca. 20% of all proteins degraded by the UPS (Soucy et al., 2009), regulating a variety of cellular processes, including proliferation, signal transduction and development. CRLs are big, multi-subunit ubiquitin ligase complexes found throughout eukaryotes. Owing to their modular assembly and the great diversity of subunits, hundreds of different CRL complexes can be present in a cell at a given time. Although the heterogeneity of CRL composition and function is astounding, a few general regulatory principles have emerged that apply to the majority of CRLs.

The structural core of a CRL is formed by a protein of the Cullin family, which in human has seven members (CUL1, 2, 3, 4A, 4B, 5, 7). Cullins share a globular C-terminal cullin-homology domain and a curved rigid stalk at the N-terminus that is formed by repeats of a five-helix bundle (Zheng et al., 2002b). The globular domain binds RBX1 (also known as ROC1 or HRT1), a protein containing a RING-H2 domain, which in turn recruits the E2 to the complex and activates it (Kamura et al., 1999).

Through adaptor proteins binding its N-terminus, each Cullin can assemble with a repertoire of specificity-conferring subunits, which are called substrate receptors (SRs), giving rise to numerous complexes that share the catalytic core, but display different substrate specificity. CUL1 CRLs dock SRs containing F-box domains via the adaptor SKP1 (Chang et al., 1996) and are therefore often referred to as SCF ubiquitin ligases (for SKP, Cullin, F-Box containing complex). CUL7 similarly utilizes SKP1 as adaptor protein, but so far only FBX29 has been shown to associate with it. CUL2 and CUL5 share the adaptor proteins Elongin B and C (ELOB/C) which recruit SRs that contain SOCS/BC (Suppressor Of Cytokine Signaling/elongin-BC) domains. SRs involved in CUL4A and CUL4B ubiquitin ligases bind to

the adaptor DDB1 (DNA-Damage-Binding protein 1), but do not share an obvious structural motif (Wertz et al., 2004). For CUL3 CRLs, the adaptor and substrate receptor functions are merged into a single protein, characterized by the presence of a BTB domain (Broad complex, Tramtrack, Bric-a-brac) located at the N-terminus and a protein interaction domain for substrate binding at the C-terminus (Xu et al., 2003).

Regulation of CRL composition and activity

Neddylation

The assembly and catalytic activity of CRLs is subject to several layers of regulatory controls. An important step for CRL activation is modification by NEDD8 (Neural precursor cell expressed, developmentally down-regulated 8), a protein that is highly conserved across eukaryotic species. NEDD8 is a ubiquitin-like protein that shares ~60% sequence identity with human ubiquitin. As such, it is similarly covalently attached to substrate proteins via a cascade of specific E1-E2-E3 enzymes, in a process commonly referred to as neddylation.

The E1 ligase specific for NEDD8 is NAE (NEDD8-activating enzyme), a dimer composed of APP-BP1 and UBA3 which utilizes ATP to activate NEDD8. NEDD8 is then passed on via a transthiolation reaction to one of two E2 enzymes, UBE2F or UBE2M (or UBC12). Finally, an E3 ligase catalyzes the transfer of NEDD8 to the target protein. The best characterized NEDD8 E3s are RBX2, which interacts with UBE2F to neddylate CUL5, and RBX1, responsible for the neddylation of all other Cullins via interaction with UBE2M (Soucy et al., 2010). Neddylation is facilitated by interaction with DCN1 (Defective in Cullin neddylation protein 1), a co-E3 that promotes the catalytically competent orientation of the Cullin-E2-E3 complex (Kurz et al., 2005).

All Cullins can be modified by NEDD8, which is covalently attached to a conserved Lys residue in the Cullin-homology domain, usually in form of a mono-neddylation (Osaka, 2000). Neddylation functions as a molecular switch that activates CRL ubiquitin ligase activity through different effects (Podust et al., 2000; Read et al., 2000). In vitro experiments indicate that recruitment of loaded E2 to the complex and is enhanced by Cullin neddylation (Kawakami et al., 2001). Structural studies further indicated that neddylation induces striking conformational changes, which on one hand reduce the gap between the CRL substrate and the E2 (Saha and Deshaies, 2008), on the other increase the flexibility of RBX1, facilitating ubiquitin transfer (Duda et al., 2008). Underscoring the importance of neddylation in regulation of CRL activity, cellular treatment with the NAE inhibitor MLN4924 results in accumulation of CRL substrates (Soucy et al., 2009).

Neddylation is a reversible modification. NEDD8 can be detached from Cullins by the COP9 signalosome (CSN), a protein complex of 8 subunits, through the isopeptidase activity of the catalytic subunit CSN5 (Lyapina et al., 2001). Importantly, CSN activity is sterically inhibited by CRL substrate binding, so a CRL is most efficiently inactivated in absence of its substrates (Fischer et al., 2011).

SR exchange

Another crucial regulator of CRL activity is CAND1 (Cullin-associated NEDD8-dissociated protein 1) (Zheng et al., 2002a). First discovered as an interactor of the SCF complex, it has since then been reported to bind all Cullins. As the name suggests, CAND1 binds Cullin backbones only in their deneddylated form, so when substrate levels of the CRL are low. CAND1 binding induces release of the bound substrate receptor, accelerating the spontaneously slow dissociation by a million-fold (Pierce et al., 2013). The ejected SR is rapidly replaced by another one from the free cellular pool, which in turn displaces CAND1 from the CRL complex. Supporting the role of CAND1 as a global substrate receptor exchange factor, CAND1 depletion has dramatic effect on the cellular CRL repertoire (Pierce et al., 2013).

As an additional layer of regulation, target recognition by SRs is often regulated at a post-translational level. For example, proteins targeted to SCF complexes are frequently phosphorylated (Lanker et al., 1996), the $CRL2^{VHL}$ complex binds and degrades the hypoxia sensor HIF1α only upon proline hydroxylation under normoxic conditions (Ivan et al., 2001), and methylation-dependent substrate recognition has been suggested for the $CRL4^{DCAF1}$ ligase (Lee et al., 2012).

CRL plasticity

Taken together, the insights emerged in the last two decades reveal CRLs as a highly dynamic system that can rapidly adapt its composition to changes in cellular state. The plasticity is conferred by a cycle of CRL activation (**Fig 5**): a subpool of CAND1-bound Cullins is available for SR association. Upon binding, the complex is stabilized and activated by modification of the Cullin backbone with NEDD8. After depletion of the substrate, neddylation can be reversed by activity of the CSN, resulting in inactivation of the CRL. The deneddylated Cullin backbone is furthermore accessible for CAND1 binding, which displaces the bound substrate receptor and replenishes the pool of unloaded CRL complexes.

Importantly, this model also explains an apparent paradox that had been puzzling researchers: both CAND1 and the CSN have been described as inhibitors of CRL function in vitro, yet they are required for sustained CRL activity in vivo (Cope and Deshaies, 2003; Zheng et al., 2002a). It is now understood that their activity is necessary to for cells to adapt the

composition of the CRL pool to the specific substrates and to ensure their sustained and efficient degradation. Furthermore, the CSN prevents the CRL to be constitutively active in the absence of substrate, as this results in auto-ubiquitination and degradation of the substrate receptor (Wolf et al., 2003).

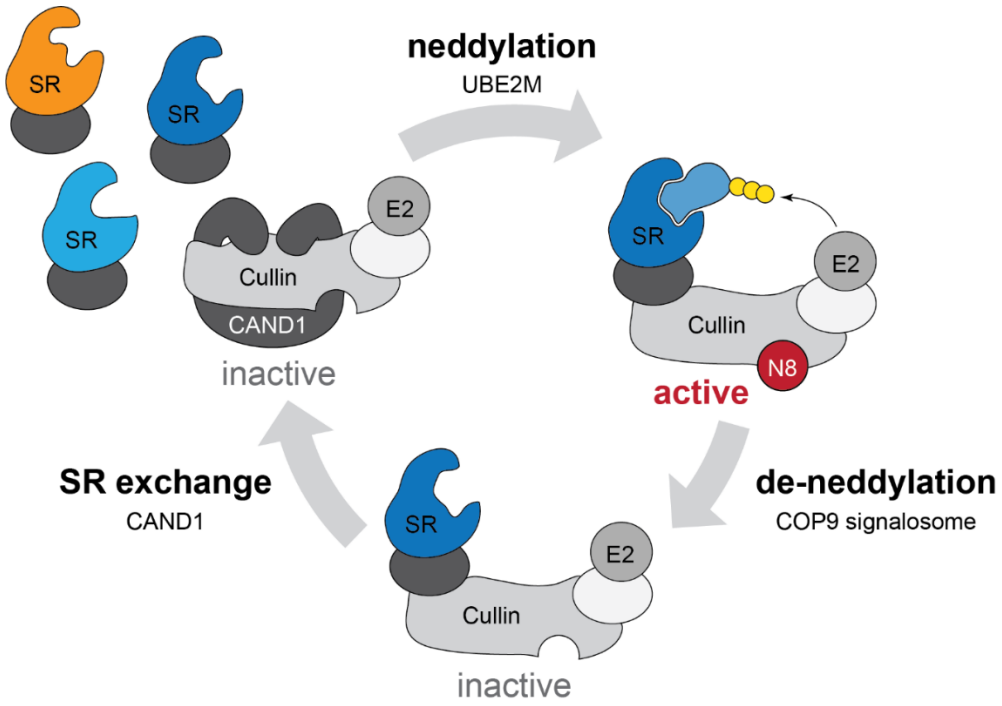

Figure 5 Schematic depiction of the CRL activation cycle. A free Cullin backbone engages a substrate receptor (SR) from the cellular pool. The CRL complex is then activated via deposition of a NEDD8-modification by UBE2M. Upon substrate depletion, the neddylation is removed by the COP9 signalosome, rendering the CRL accessible for binding by CAND1 and dissociation of the SR.

1.6 Drugging the UPS

With the precise characterization of the regulation of protein abundance by the UPS came novel opportunities for pharmacological modulation of cellular states. Instead of merely blocking protein activity, as a traditional enzymatic inhibitor does, targeting the UPS allows to modulate protein abundance.

1.6.1 Proteasome inhibitors

Proteasomal degradation is crucial for the regulation of fundamental cellular processes such as general protein homeostasis, cellular proliferation and signaling pathways. However, it also became apparent that malignant cells are more dependent on its correct functioning than non-cancerous cells, as they have an increased need to remove misfolded or damaged proteins due to their rapid proliferation and elevated mutational burden (Adams, 2004), thereby providing a rationale for the clinical investigation of proteasome inhibitors.

The first agent found to be able to inhibit proteasome activity was lactacystin, a natural metabolite isolated in the 1980s from Streptomyces. Lactacystin covalently binds the catalytic subunits of the proteasome and irreversibly inhibits all three peptidase activities (Fenteany et al., 1995). In contrast, the early inhibitor MG132 is a cell-permeable peptide aldehyde that reversibly inhibits the proteasome, but also targets other peptidases such as serine proteases (Hayashi et al., 1992). Although it never was clinically tested due to its rapid oxidation, it marked the lead molecule for the medicinal chemistry efforts that ultimately led to the development of bortezomib, a slowly reversible selective inhibitor of predominantly the chymotrypsin-like hydrolyzing activity. Bortezomib was the first proteasome inhibitor to enter the clinical use in 2003 after accelerated approval by the FDA and is currently used as first-line treatment in multiple myeloma (Richardson et al., 2003). Bortezomib's success prompted further exploration of the proteasome inhibitor space and resulted in the approval of two further drugs: carfilzomib, an irreversible inhibitor with higher selectivity for the chymotrypsin-like proteasome activity (Demo et al., 2007), and ixazomin, which stands out because of its oral bioavailability (Chauhan et al., 2011).

1.6.2 Ubiquitin ligase inhibitors

Inspired by the success of proteasome inhibitors, efforts have been made to pharmacologically modulate protein abundance by interfering with different steps of the ubiquitination cascade. However, since many of the players lack a canonical catalytic site and the ubiquitination cascade is for a considerable part regulated by hard-to-drug protein-protein interactions, progress so far has been slow.

A prime target is the RING E3 ligase MDM2, a crucial negative regulator of the tumor suppressor p53. In physiological conditions, p53 protein levels are kept low by rapid ubiquitination by MDM2 and consequent degradation. Therefore, MDM2 is overexpressed in many cancers by gene duplication or transcriptional upregulation, and high MDM2 levels correlate with a worse prognosis (Toledo and Wahl, 2006). The first MDM2 inhibitors are cis-imidazoline analogs called nutlins, a class of compounds identified by chemical screening. Nutlins occupy the p53-binding pocket of MDM2 and preventing its interaction with the target, resulting in accumulation of wild-type p53 (Vassilev et al., 2004). Several other MDM2 inhibitors with increased potency, such as idasanutlin, MI-77301 and MK-8242 are currently being tested in clinical trials (Tisato et al., 2017).

Inhibitors of Apoptosis Proteins (IAPs) are a family of 8 RING E3 ligases involved in caspase regulation that have been implicated in resistance to chemotherapy. IAP inhibitors were designed to mimic the endogenous IAP antagonist SMAC. Interestingly, these molecules

work as ‘suicidal degraders’, as they induce conformational rearrangements leading to IAP dimerization, autoubiquitination and ultimately degradation (Dueber et al., 2011).

Another emerging approach is the inhibition of the neddylation cascade, as it affects a multitude of CRLs that have a central role in cell proliferation. The most promising inhibitor is MLN4924 or pevonedistat, an inhibitor of the NEDD8 E1 activating enzyme NAE1 (Soucy et al., 2009). MLN4924 interacts with the nucleotide-binding pocket of NAE1 and covalently modifies NEDD8, preventing it from being utilized in further reactions. The adduct further blocks the NAE1 active site and inhibits its enzymatic activity (Brownell et al., 2010). MLN4924 is currently being evaluated in several clinical trials, showing promising preliminary results.

1.6.3 DUB inhibitors

Deubiquitinases (DUBs) are important regulators of protein fate, as they counter the outcome of ubiquitination. Since many of the targets stabilized by DUBs are oncoproteins, their expression and activity have been found to be dysregulated in several malignancies, making them interesting pharmacological targets. The field of DUB inhibitors is still in its infancy, in part because of the high degree of conservation of the catalytic domain which has hampered the development of selective inhibitors.

Among the most studied targets is USP7, which plays a role in the stabilization of the oncogenes N-MYC (Tavana et al., 2016) and has a paradoxical role in the regulation of p53. On one hand, USP7 can directly deubiquitinate p53 and protect it from proteasomal degradation. On the other hand, it regulates ubiquitination levels and consequently stability of MDM2, the E3 ligase responsible for p53 degradation. Since USP7-MDM2 binding has stronger affinity, the overall effect of USP7 overexpression is a reduction of p53 expression levels (Li et al., 2004). Promising molecules in pre-clinical development are HBX41108, an allosteric USP7 inhibitor (Colland et al., 2009), and P5091, a selective inhibitor with anti-multiple myeloma activity *in vitro* and *in vivo* (Chauhan et al., 2012).

1.7 Targeted protein degradation (TPD)

In recent years, the focus in pharmacological harnessing of the power of the UPS has shifted from inhibition of individual components to a far more sophisticated approach: chemically inducing novel protein-protein interactions to reprogram E3 ligases and redirect their activity to neo-substrates that wouldn’t otherwise be recognized.

The induction of protein dimerization by small molecules has first been described in the field of immunosuppression: extensive efforts to understand the mechanism of action of cyclosporine and FK506, two natural products with strong immunosuppressive effects clinically used to prevent transplant rejection, revealed that they inhibit the phosphatase

calcineurin by recruitment of the immunophilins cyclophilin and FKBP12, respectively (Liu et al., 1991). These and related compounds, such as the aforementioned mTOR inhibitor rapamycin, that mediate novel protein-protein interactions are collectively called ‘molecular glues’.

A first example of small molecule-induced targeted protein degradation came from plant biology. It was shown that the plant hormone auxin (also known as indole acetic acid, IAA) binds and reprograms the E3 ligase SCF^{TIR1}, promoting the interaction with Aux/IAA transcriptional repressors, resulting in their ubiquitination and removal by the proteasome (Dharmasiri et al., 2005). This mechanism is not an exception, as another plant hormone called jasmonate similarly reprograms the E3 ligase COI1 (Sheard et al., 2010).

Together, these insights lay the ground for the concept of TPD and created the notion that the target spectrum of the UPS can be artificially changed by small drug-like molecules, and that this could be therapeutically exploited to remove disease-causing proteins. Today, there are two main approaches to TPD, each with their distinct advantages and disadvantages: monovalent molecular glue degraders and hetero-bifunctional molecules.

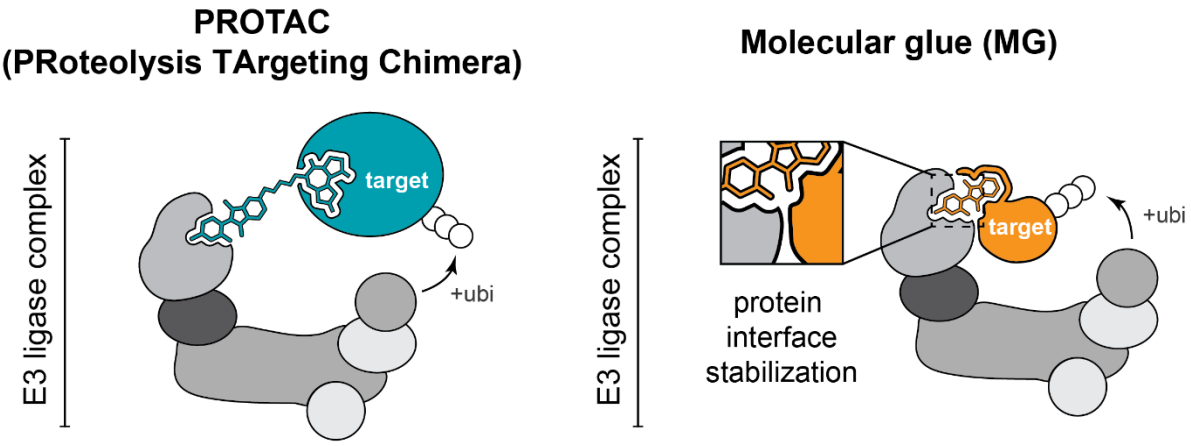

Figure 7 Overview of the two modalities of targeted protein degradation: heterobifunctional PROTACs and monovalent molecular glues.

1.7.1 Monovalent molecular glue degraders: immunomodulatory drugs and sulfonamides

Ironically, molecular glue degraders had been in clinical use long before the awareness for TPD arose, but it took more than 60 years of investigation to realize that.

The best example is thalidomide and its derivative molecules lenalidomide and pomalidomide, which are together named immunomodulatory drugs (IMiDs). Thalidomide is most known for its tragic history: originally developed as a sedative, it was marketed in the

late 1950s to treat anxiety and nausea, including morning sickness in pregnant women. It was however removed from the market a few years later because of its devastating teratogenic effects. IMiDs were later repurposed for treatment of multiple myeloma and showed excellent efficacy, but they're mechanism of action was not understood (Bartlett et al., 2004).

Only in 2010 it was discovered that the drug target of thalidomide and its analogs is CRBN, the substrate receptor of a $CRL4^{CRBN}$ E3 ligase complex (Ito et al., 2010). While it was first hypothesized that this binding would result in inhibition of CRBN and accumulation of its targets, seminal work from the Ebert and Kaelin labs later showed that upon lenalidomide binding, CRBN acquires the ability to recruit and ubiquitinate two transcription factors, IKZF1 and IKZF3, and target them for proteasomal degradation (Krönke et al., 2014; Lu et al., 2014). IKZF1 and IKZF3 are important transcription factors for the differentiation of the lymphoid lineage, explaining at least in part the therapeutic effect of IMiDs.

Since then, medicinal chemistry efforts have resulted in the identification of several other thalidomide analogs, such as CC-122 (Hagner et al., 2015) and CC-885 (Matyskiela et al., 2016). Interestingly, while all of the compounds induce degradation of IKZF1 and IKZF3, their target specificity slightly differs. For example, lenalidomide was found to recruit CK1α (Krönke et al., 2015), CC-885 induces degradation of the translation termination factor CC-885 (Matyskiela et al., 2016), and the developmental transcription factor SALL4 was identified as an additional target of thalidomide, contributing to its teratogenicity (Matyskiela et al., 2018). While these targets don't share any obvious conserved features in the primary sequence, structural analysis revealed a surface turn containing a conserved Gly residue which is shared among all known neo-substrates (Sievers et al.). Notably, IMiDs themselves don't display binding affinity for the target. Instead, they slightly modify the surface of the E3 ligase and thereby orchestrate novel protein-protein interactions with the neo-substrate to induce dimerization in a highly cooperative manner (Chamberlain and Hamann, 2019).

The molecular mechanism of IMiDs is not unique. Indisulam and related aryl sulfonamides have been recently described to hijack the $CRL4^{DCAF15}$ ubiquitin ligase resulting in degradation of the splicing factors RBM39 and RBM23 (Han et al., 2017; Uehara et al., 2017). Early structural characterization confirmed that sulfonamides act through a molecular glue mechanism. However, comparison with structures of IMiD ternary complexes suggest that more extensive surface interactions between DCAF15 and the substrate protein are necessary for complex stabilization, so the spectrum of potential neo-substrates is likely more limited than the IMiD target spectrum (Faust et al., 2020).

Overall, molecular glue degraders have proven that TPD has great potential and can deliver highly efficacious drugs. However, discovery of molecules that act via this novel pharmacology

has so far been completely luck-driven and the lack of rational discovery methods is a major obstacle to the field.

1.7.2 Hetero-bifunctional molecules: PROTACs

Targeted protein degradation is based on the ligand-based induction of molecular proximity between a ubiquitin ligase and a target protein. While, as noted above, we're still unable to rationally design monovalent molecules with such characteristics, this limitation is overcome by the strategy of hetero-bifunctional degraders, commonly called PROTACs (PRoteolysis-TArgeting Chimeras). Behaving like molecular bridges, these molecules are composed of an E3 binder and a ligand for the target to be degraded (often referred to as 'warhead'), connected by a short flexible linker. These molecules are of modular nature, as the individual components can be freely assembled and interchanged. Combined with existing methods to identify and develop ligands of a target protein, hetero-bifunctional degraders hold the promise to allow targeting of virtually the whole ligandable proteome.

Due to the lack of small molecule ligands for E3 ligases, the first PROTACs were of peptidic nature. The first successful attempt consisted of coupling ovalicin, a ligand of MetAP2, to a peptide that binds to the SCFβ-TrCP CRL complex (Sakamoto et al., 2001). A similar strategy was employed to develop AR and FKBP12 degraders using peptidic ligands of the $CRL2^{VHL}$ E3 ligase (Schneekloth, et al., 2004). These early experiments validated the concept of the technology. However, the peptidic nature of the E3 ligands strongly impacted cell permeability of the molecules, therefore microinjection of the drug into *Xenopus* eggs or very high PROTAC concentrations of 25-50 μM were necessary to ensure appreciable degradation of the target.

This changed with the discovery of nutlin as the first small molecule ligand of an E3 ligase (MDM2), opening the way to the first non-peptidic PROTACs. Indeed, a PROTAC which fused nutlin to a non-steroideal androgen receptor ligand via a PEG-based linker induced significant destabilization of AR at 10 μM in HeLa cells (Schneekloth et al., 2008). Soon thereafter, bestatin was used as ligand of the cIAP E3 ligase to generate small-molecule degraders of CRABP, further increasing potency to a low μM range and starting a new series of degraders called SNIPERs (Itoh et al., 2010).

The breakthrough in the PROTAC field came with the characterization of the mechanism of action of thalidomide and the identification of CRBN as a high-affinity interactor of IMiDs (Ito et al., 2010). These IMiDs could be utilized as small-molecule E3-recruiting group for potent PROTACs. For example, dBET1 was generated by coupling the competitive BET bromodomain inhibitor JQ1 with lenalidomide as a recruiting group for CRBN. dBET1 induced rapid and robust degradation of BRD4, displaying better efficacy in leukemia models than the parental inhibitor JQ1, indicating that complete removal of the target by degradation can be

preferable over mere inhibition of its function. Importantly, dBET1 also was the first PROTAC to show *in vivo* efficacy and delayed tumor growth in a leukemia xenograft mouse model (Winter et al., 2015).

Concurrently, the development and optimization of potent peptidomimetic small molecule VHL ligands paved the way for the synthesis of more potent VHL-based PROTACs (Buckley et al., 2012; Galdeano et al., 2014). Based on these ligands, all-small molecule hetero-bifunctional degraders recruiting ERRα and RIPK2 to VHL displayed >1000-fold increase in cellular potency compared to peptide-based PROTACs (Bondeson et al., 2015).

PROTACs have since then proven their wide applicability, as molecules targeting a plethora of target classes have been described. This includes among others (i) nuclear receptors, such as AR (Salami et al., 2018), (ii) protein kinases, such as EGFR (Burslem et al., 2018) and CDK9 (Olson et al., 2017), (iii) transcription factors, such as STAT3 (Bai et al., 2019), (iv) proteins involved in neurodegeneration, such as mutant Tau (Silva et al., 2019), and many more.

1.7.3 Features of targeted protein degradation

The pharmacology of small molecule degraders (both PROTACs and molecular glues) has several particularities that sets it apart from conventional inhibitors of protein activity. Some of these differences are so fundamental that targeted protein degradation is now viewed as a new paradigm in pharmacology and attracted great interest from the pharmaceutical industry.

Small-molecule enzymatic inhibitors work by a so called ‘occupancy-driven’ pharmacology: they generally occupy a well-defined binding pocket in an active site of the target protein and sterically prevent the interaction with its substrates, thereby blocking protein function. The small molecule only maintains its effectiveness if the binding pocket remains occupied, and inhibition is lost as soon as the active site is freed up again. With the exception of covalent inhibitors, drug binding is reversible and thus transient. Therefore, elevated drug concentrations must be achieved and maintained to ensure a degree of target inhibition that is sufficient to exert the therapeutic effect. This still represents one of the major challenges in drug development, because high dosages are hard to achieve and directly linked to undesirable off-target effects.

In contrast, targeted protein degradation pharmacology is ‘event-driven’: a short interaction between the small molecule and the target protein is sufficient to prime the latter for complete removal by the proteasome (Cromm and Crews, 2017). Additionally, the molecule is unaffected by the target degradation and is free to engage in several cycles of target

recognition and ubiquitination, so its action is of sub-stoichiometric and catalytic nature. Together, this eliminates the need to maintain elevated concentrations of the drug.

Traditional enzymatic inhibitors are further limited by the fact that they only inhibit one specific function of the target protein, without affecting other functional domains or scaffolding activities of the protein. Degraders instead holistically perturb the target protein by inducing its complete removal, affecting all of its functions, both enzymatic and structural (Burslem et al., 2018).

Closely related to this, small molecule inhibitors have a strong limitation of the targetable space inherent in their design: the molecule is required not only to bind the target with high affinity in a ligandable pocket on the protein surface, but the pocket also needs to be functionally relevant to the activity that is to be inhibited. The importance of this limitation is evident when looking at approved drugs, which together (including biologicals) only target less than 4% of the proteome, and estimates that predict only 10-20% of the proteome to be 'druggable' by conventional inhibitors (Hopkins and Groom, 2002). Particularly thanks to the modular nature of PROTAC design, targeted protein degradation limits the requirements to the identification of a ligand of the target protein, irrespectively of the binding site within the protein and with less restrictions on potency, as target occupancy is not required to be maintained long-term (Bai et al., 2019). Molecular glue degraders do not even require an accessible binding pocket and indeed several of their targets are transcription factors that would be considered undruggable by conventional means. Because of this, TPD holds the promise to open up virtually the whole proteome to pharmacological intervention.

Targeted protein degradation conserves the high kinetic resolution of traditional antagonists, as degradation typically occurs within a few hours after cellular treatment. Similarly, the effect is reversible upon washout of the drug, although for degraders the perturbation lasts longer compared to SMIs, as recovery is dependent on re-synthesis of the target (Bondeson et al., 2015). Similar to chemical inhibition, TPD allows dose-dependent modulation of its effects. However, PROTACs display a characteristic 'hook effect', with loss of degradation efficiency at high compound concentrations, as these trigger preferential assembly of binary assemblies (drug-E3 and drug-target) over the productive ternary complex (E3-drug-target).

A favorable feature of PROTACs is their exquisite selectivity: the notion has emerged that conversion of an inhibitor to a PROTAC often restricts its target profile, as exemplified among others by studies on promiscuous kinase inhibitors (Bondeson et al., 2018). Importantly, induction of degradation of a given protein does not correlate with its binding affinity for the compound. It is now understood that the nature, length and attachment of the linker plays an

important role in determining the target spectrum of PROTACs, as it influences the relative orientation of the components in the ternary complex. In principle, this characteristic of PROTACs would allow the engineering of extremely selective molecules, but further studies are required to fully understand the underlying rules.

However, PROTACs have their caveats. Most importantly, due to their hetero-bifunctional nature, these molecules are relatively large (typically 700-1200 Da) and lack several characteristics that are usually considered necessary for good bioavailability of a drug, as they influence absorption, distribution, metabolism and excretion (ADME) of a drug. While this generated initial worries about the clinical potential of hetero-bifunctional degraders, these challenges are at least partially counterbalanced by the benefits of an event-based pharmacology, since low drug exposure for a limited amount of time are sufficient for eliciting a therapeutic effect. Indeed, clinical trials with orally administered AR (ARV-110) and ER (ARV-471) PROTACs are ongoing and preliminary data showed promising *in vivo* antitumor activity (clinicaltrials.gov, NCT03888612, NCT04072952).

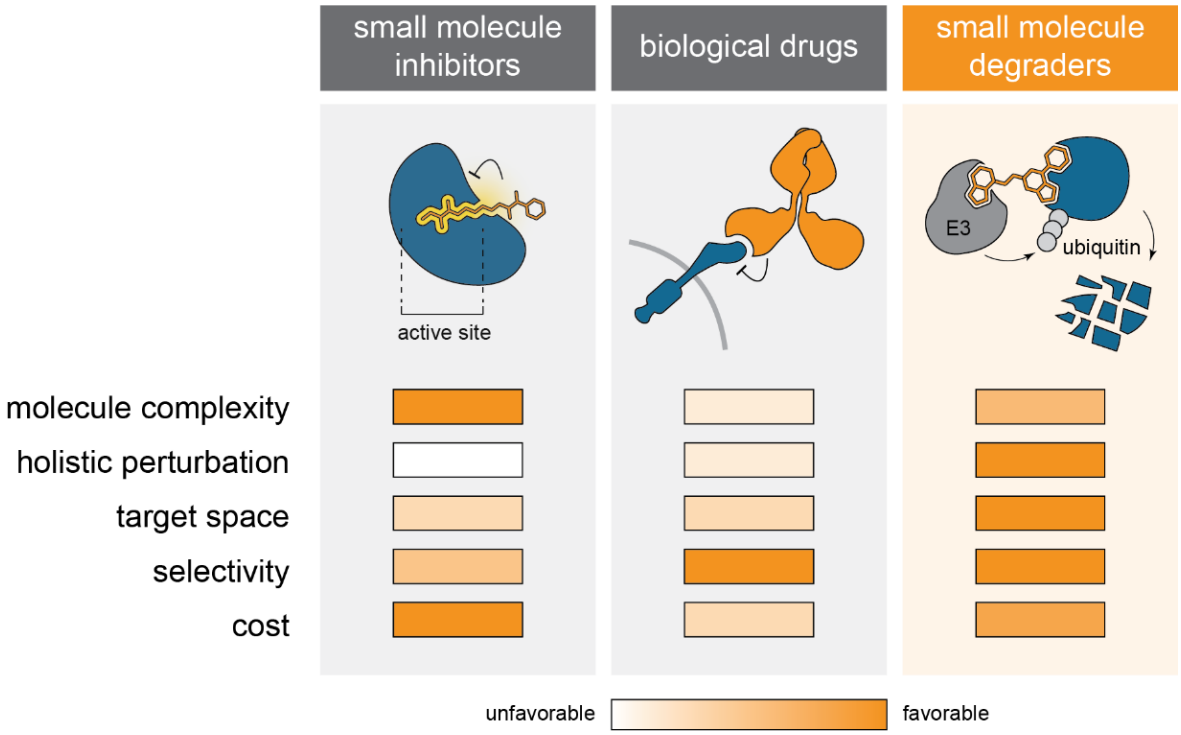

Figure 8 Comparison of targeted protein degradation through small molecule degraders to conventional targeted therapies.

1.8 Aims of this thesis

Small molecule-mediated targeted protein degradation has emerged in the last years as a new paradigm in drug discovery. Through its approach of directing disease-driving proteins to destruction by the ubiquitin-proteasome system, TPD holds the promise to access the 80% of the proteome that are considered ‘undruggable’ by conventional small molecule inhibitors. As such, it has generated lots of excitement and considerable investments in the pharma and biotech industry, resulting in the first PROTACs entering clinical testing in 2019.

In this thesis, we set out to further explore the therapeutic potential and advantages of the PROTAC technology; in particular, we aimed to:

(i) test the limits of PROTAC target selectivity by generating a homolog-selective degrader of CDK6;

(ii) identify the cellular components required for degrader sensitivity through genome-wide genetic resistance screens;

(iii) systematically characterize the emergence of genetic resistance to this novel pharmacology.

2. Results

2.1 Homolog-selective degradation as a strategy to probe the function of CDK6 in AML

2.1.1 Prologue

In this work, we designed and characterized BSJ-03-123, a CRBN-based PROTAC built off the CDK4/6 inhibitor palbociclib. BSJ-03-123 induces rapid degradation of CDK6 with exquisite selectivity without affecting cellular levels of its homolog CDK4, despite the two proteins sharing 94% sequence identity in the active pocket bound by the molecule. We found that BSJ-03-123 similarly engaged CDK4 and CDK6, but that ternary complex formation with the E3 ligase CRBN is only induced for CDK6, thereby explaining the selectivity of the probe.

BSJ-03-123 treatment recapitulates genetic dependency on CDK6 in cellular models. Selective and acute perturbation of CDK6 further allowed to characterize its role in the cellular signaling networks on a transcriptional and phosphoproteome level in acute myeloid leukemia.

The author of this thesis performed the majority of experiments and associated bioinformatic analyses, including western blots, proliferation assays and luminescence-based protein proximity assays, as well as RNA-seq and proteomic analyses. B Jiang synthesized BSJ-03-123 and BSJ-bump. S Bauer performed western blots, proliferation assays and CETSA experiments. G Winter and N Gray wrote the manuscript with input from all authors.

This manuscript has been featured in:

P Chamberlain, **Targeted Protein Degradation for Kinase Selectivity**, *Cell Chemical Biology* (2019)

2.1.2 PDF of the paper

Brief Communication

Cell Chemical Biology

Homolog-Selective Degradation as a Strategy to Probe the Function of CDK6 in AML

Graphical Abstract

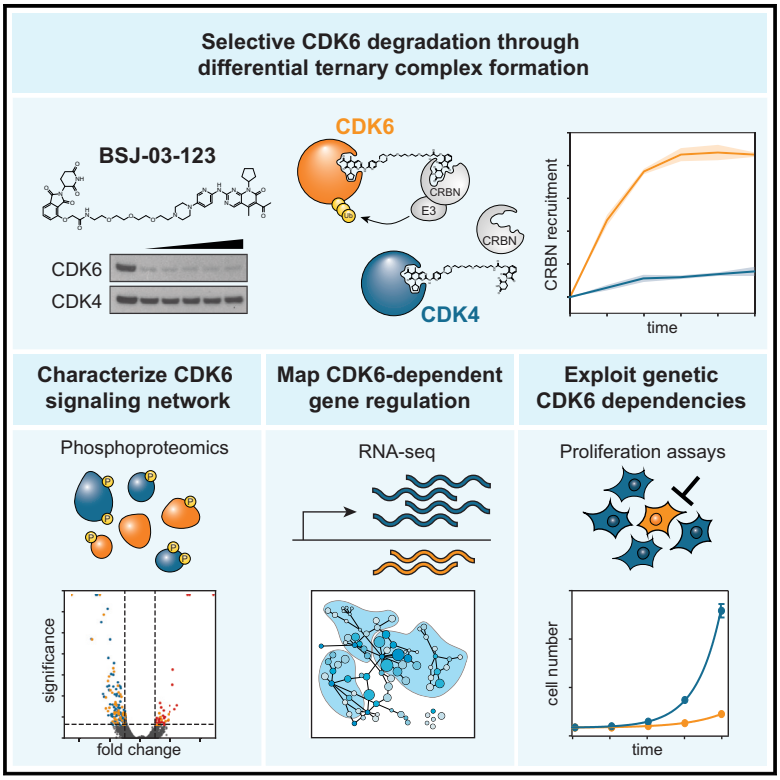

Highlights

- Development of a CDK6-selective small-molecule degrader
- Mechanistically understood selectivity via differential ternary complex formation
- Profiling of consequences of CDK6 degradation on signaling and gene regulation
- Precise exploitation of genetic dependencies through homolog-selective degradation

Authors

Matthias Brand, Baishan Jiang, Sophie Bauer, ..., Eric S. Fischer, Nathanael S. Gray, Georg E. Winter

Correspondence

nathanael_gray@dfci.harvard.edu (N.S.G.), gwinter@cemm.at (G.E.W.)

In Brief

Brand et al. describe BSJ-03-123, a degrader with proteome-wide selectivity for CDK6. Specificity emerges from differential ternary complex formation with the E3 ligase $CRL4^{CRBN}$. BSJ-03-123 exploits a dependency of AML cells on CDK6, and rapid degradation allowed assaying the role of CDK6 in coordinating signaling and gene control in AML.

Brand et al., 2019, Cell Chemical Biology *26*, 300–306
February 21, 2019
https://doi.org/10.1016/j.chembiol.2018.11.006

CellPress

CellPress

Cell Chemical Biology
Brief Communication

Homolog-Selective Degradation as a Strategy to Probe the Function of CDK6 in AML

Matthias Brand,[1,4] Baishan Jiang,[2,3,4] Sophie Bauer,[1] Katherine A. Donovan,[2,3] Yanke Liang,[2,3] Eric S. Wang,[2,3] Radosław P. Nowak,[2,3] Jingting C. Yuan,[2] Tinghu Zhang,[2,3] Nicholas Kwiatkowski,[2,3] André C. Müller,[1] Eric S. Fischer,[2,3] Nathanael S. Gray,[2,3,*] and Georg E. Winter[1,5,*]

[1]CeMM Research Center for Molecular Medicine of the Austrian Academy of Science, Vienna, Austria
[2]Department of Cancer Biology, Dana-Farber Cancer Institute, Boston, USA
[3]Department of Biological Chemistry and Molecular Pharmacology, Harvard Medical, Boston, USA
[4]These authors contributed equally
[5]Lead Contact
*Correspondence: nathanael_gray@dfci.harvard.edu (N.S.G.), gwinter@cemm.at (G.E.W.)
https://doi.org/10.1016/j.chembiol.2018.11.006

SUMMARY

The design of selective small molecules is often stymied by similar ligand binding pockets. Here, we report BSJ-03-123, a phthalimide-based degrader that exploits protein-interface determinants to achieve proteome-wide selectivity for the degradation of cyclin-dependent kinase 6 (CDK6). Pharmacologic CDK6 degradation targets a selective dependency of acute myeloid leukemia cells, and transcriptomics and phosphoproteomics profiling of acute degradation of CDK6 enabled dynamic mapping of its immediate role in coordinating signaling and transcription.

INTRODUCTION

Cyclin-dependent kinases (CDKs) orchestrate fundamental cellular processes such as cell cycle and transcription. CDKs are serine/threonine kinases and their activity is dependent on association with cyclins, enabling temporal control over enzymatic function. CDK4 and CDK6 control G1-S transition by associating with D-type cyclins to phosphorylate the tumor suppressor retinoblastoma (Rb). This relieves Rb-mediated repression of E2F transcription factors (TFs) to trigger gene expression required for S-phase entry. While CDK4 and CDK6 were long perceived as redundant, recent studies have identified homolog-specific functions. In particular, CDK6 emerged as a regulatory hub connecting cell cycle with metabolism (Wang et al., 2017) and transcription (Tigan et al., 2016). In several contexts, the transcriptional role of CDK6 is independent of its kinase function, but relies on molecular scaffolding (Kollmann et al., 2013; Tigan et al., 2016).

ATP-competitive CDK4/6 inhibitors have shown significant clinical activity, leading to approval of three drugs for breast cancer (O'Leary et al., 2016). However, none of these inhibitors can discriminate between CDK4 and CDK6, as they share 94% amino acid sequence identity in their ATP binding pockets. In addition, current inhibitors cannot disrupt scaffolding functions (Kollmann et al., 2013). To address this, we turned to a ligand-induced targeted protein degradation strategy based on heterobifunctional molecules that induce molecular proximity between a protein of interest (POI) and the $CRL4^{CRBN}$ E3 ligase complex (Lu et al., 2015; Winter et al., 2015; Zengerle et al., 2015). Interestingly, studies of degraders derived from multi-targeted warheads revealed that only a subset of targets were efficiently degraded, indicating the possibility of engineering selectivity into poly-pharmacologic scaffolds (Bondeson et al., 2018; Gadd et al., 2017; Huang et al., 2018; Olson et al., 2018; Winter et al., 2015). Along those lines, it was demonstrated that selective degradation can be achieved by exploiting amino acid differences in the POI-E3 interface and thus differential ternary complex formation (Gadd et al., 2017; Nowak et al., 2018).

Here, we explored the feasibility of homolog-selective degradation of CDK6 versus CDK4 using ligands that bind the ATP sites of both enzymes. We describe the discovery and characterization of BSJ-03-123 (BSJ), a selective degrader of CDK6 that uniquely enables rapid pharmacological interrogation of CDK6-dependent functions. Coupling acute CDK6 degradation with phosphoproteomic and transcriptomic profiling allowed us to establish a systems-level understanding of the sensitivity of acute myeloid leukemia (AML) cell lines to selective CDK6 ablation and to chart a network of CDK6-dependent signaling events.

RESULTS

Development of a Homolog-Selective CDK6 Degrader

Toward the development of CDK4/6 degraders, we chose palbociclib (palbo) as a starting point given its high selectivity and potency (Fry et al., 2004). Available crystal structures of palbo with CDK6 (PDB: 5L2I) highlighted the solvent-exposed piperazine moiety as an ideal site for linker conjugation (Chen et al., 2016). We installed a 3-polyethylene glycol linker conjugated to pomalidomide, resulting in the compound YKL-06-102 (YKL) (Figure 1A). Biochemical characterization indicated that phthalimide conjugation results in a comparable, albeit weakly reduced binding affinity to both CDK4 and CDK6 (Figure S1A; Table S1). Moreover, YKL bound to recombinant CRBN-DDB1 with comparable affinity as lenalidomide (Table S1). Unexpectedly, cellular treatment with YKL led to a selective destabilization of CDK6 (Figures S1B–S1D). To further survey degrader selectivity, we employed global proteomics following cellular treatment. While

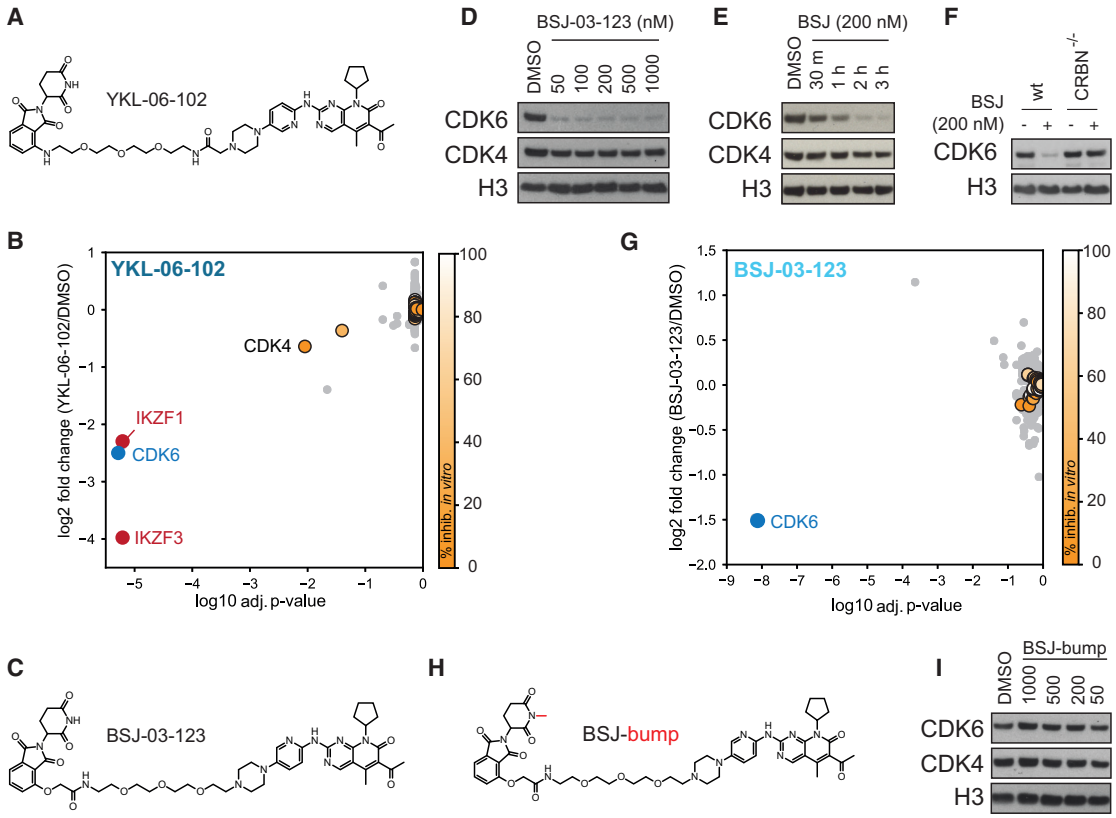

Figure 1. Development of a Homolog-Selective Degrader of CDK6

(A) Structure of YKL-06-102.

(B) Quantification of 5,945 proteins following treatment with YKL-06-102 (500 nM, 5 hr). False discovery rate (FDR)-adjusted p values. Kinases inhibited by palbociclib *in vitro* are color-coded by magnitude of inhibition.

(C) Structure of BSJ-03-123 (BSJ).

(D) Immunoblot for CDK4, CDK6, and histone 3 after 4 hr BSJ treatment.

(E) As in (D), but time-resolved at 200 nM BSJ.

(F) Immunoblot for CDK6 and histone 3. 200 nM BSJ, 4 hr, in CRBN-deficient and wild-type MV4-11.

(G) Quantification of 5,995 proteins following BSJ treatment (100 nM, 2 hr). FDR-adjusted p values. Kinase labeling as in (B).

(H) Structure of BSJ-bump.

(I) As in (D), but for BSJ-bump.

See also Figure S1 and Tables S1 and S2.

recapitulating the selective degradation of CDK6, we detected significant destabilization of IKZF1 and IKZF3 ($p = 6.19 \times 10^{-6}$) (Figure 1B), suggesting warhead-independent CRBN substrate modulation (An et al., 2017; Gandhi et al., 2014; Kronke et al., 2014; Lu et al., 2014). To remove IKZF1/3 activity of YKL, we designed BSJ by employing a phenoxyacetamide linker without altering the initial linker length (Figure 1C). Measurements of *in vitro* binding to recombinant kinase domains (KINOMEScan) confirmed that phthalimide conjugation preserves the narrow selectivity profile (Figure S1G; Table S2). BSJ induced CRBN-dependent, potent, fast, and homolog-selective degradation of CDK6 (Figures 1D–1F and S1E). In proteome-wide selectivity studies, CDK6 was the only destabilized protein (Figures 1G and S1F).

Based on BSJ, we furthermore synthesized an N-methylated glutarimide analog (BSJ-bump) incapable of CRBN binding *in vitro* (Figure 1H; Table S1). Accordingly, BSJ-bump was unable to degrade CDK4 or CDK6, thus serving as excellent negative control with matched physiochemical properties (Figure 1I).

BSJ Triggers Homolog-Selective Degradation via Differential Ternary Complex Formation

Next, we sought to understand the mechanism of CDK6 selectivity. *In vitro* kinase assays confirmed comparable affinity to both kinases (Figure S1A; Table S1). Similar cellular thermal stabilization of CDK4/6 further suggested that selectivity does not emerge from differential cellular target engagement (Figure 2A). We thus hypothesized that selectivity might stem from differential ternary complex formation. To monitor tripartite assembly in real time in intact cells, we designed a luciferase complementation assay based on NanoBiT technology (Figure 2B). We expressed C-terminal CDK4/6 LgBit fusions along with an N-terminal SmBit-CRBN fusion in $293T^{CRBN-/-}$ cells. BSJ induced rapid, dose-dependent ternary complex formation with CDK6

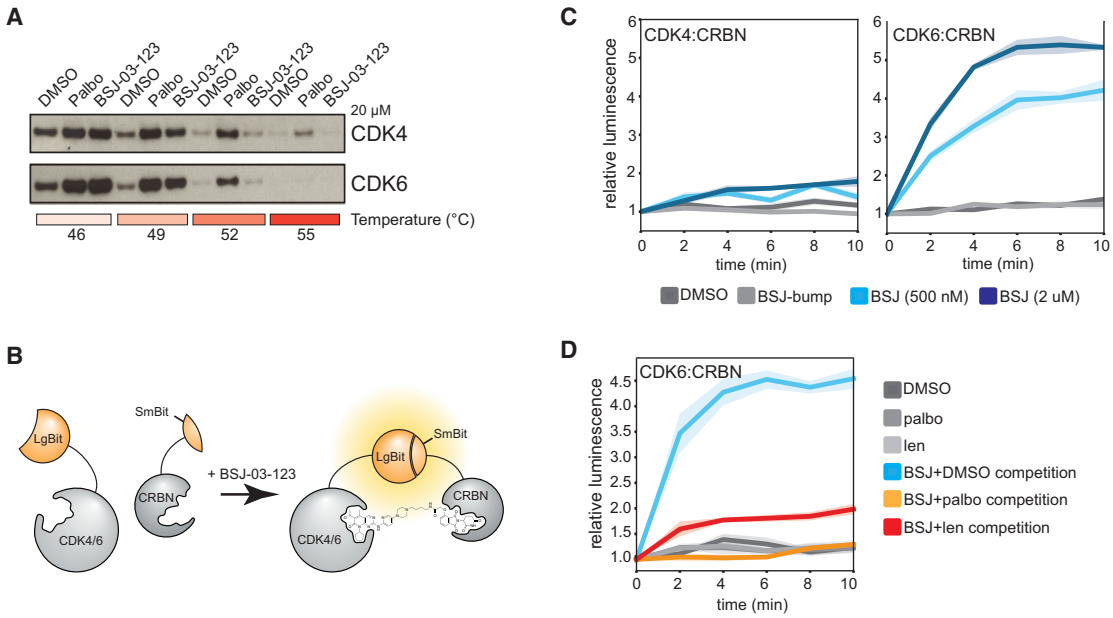

Figure 2. BSJ Selectivity Is Explained by Differential Ternary Complex Formation

(A) Immunoblot for CDK4 and CDK6 after thermal shift assay in MV4-11 CRBN$^{-/-}$ cells after cellular treatment with DMSO, palbociclib, or BSJ (both at 20 μM).

(B) Schematic representation of the luciferase complementation assay.

(C) Measurement of CDK4:CRBN and CDK6:CRBN binding via NanoBiT assay. Averages of five replicates are plotted, shaded areas represent 95% confidence intervals.

(D) Measurement of CDK6:CRBN complex formation after 1 hr pre-treatment with 20 μM palbociclib or lenalidomide. Statistics as in (C).

and CRBN, but not with CDK4 and CRBN (Figure 2C). Treatment with BSJ-bump failed to induce CDK6:CRBN interactions (Figure 2C). Ternary complex formation was prevented by blocking binding sites on CDK6 or CRBN via pretreatment with palbo or lenalidomide (Figure 2D). We thus concluded that BSJ exploits structural differences between CDK4 and CDK6 to achieve homolog-selective degradation of CDK6 via differential ternary complex formation.

BSJ Can Exploit Homolog-Selective Dependency on CDK6

To identify a cellular system that is disproportionally dependent on CDK6 over CDK4, we turned to genome-scale CRISPR/Cas9 screens in 342 cancer cell lines (Meyers et al., 2017). We identified a pronounced enrichment of AML cell lines among the most CDK6-addicted models (Figure 3A). None of these cell lines showed a comparable dependency on CDK4 (Figure S2A). Intersection with gene expression data did not unveil a correlation between essentiality and mRNA transcript levels (Figures 3A and S2A) (Klijn et al., 2015). Accordingly, CRISPR/Cas9-mediated genetic depletion of CDK4 in the AML cell line MV4-11 revealed largely preserved growth kinetics and cell-cycle distribution, supporting a dispensable role of CDK4 in the proliferation of AML cell lines (Figures S2B–S2D).

Given their lack of homolog-selectivity, CDK4/6 inhibitors are incapable of exploiting such fine-tuned genetic dependencies. Concomitant inhibition of both homologs is thus expected to limit the achievable therapeutic window. Therefore, we wanted to test if BSJ could target the genetic dependency of AML cells on CDK6, while sparing CDK4-dependent cancer cells lines. As expected, dual CDK4/6 inhibition severely impaired proliferation of CDK4-dependent cell lines, whereas selective degradation of CDK6 did not trigger a comparable effect (Figures 3B and S2E). In contrast, BSJ caused a pronounced anti-proliferative effect in CDK6-dependent AML cell lines by inducing a G1 cell-cycle arrest without a measurable increase in apoptosis (Figures 3C–3E). Of note, this effect exceeded the anti-proliferative consequences of cellular treatment with BSJ-bump (Figures 3C and S2F). The observed benefit of CDK6 degradation over CDK6 inhibition could be due to the disruption of additional, kinase activity-independent molecular mechanisms (Kollmann et al., 2013), or due to pharmacologic advantages of degraders, such as catalytic target turnover. To address this, we compared BSJ with the clinically approved palbo in CDK4-deficient MV4-11 cells to enable a CDK6-centric readout. In this experimental setup, selective degradation of CDK6 was not superior to enzymatic inhibition (Figure 3F). While interpretation of this comparison is non-trivial given the physicochemical differences between the molecules, it suggests that the dependency of AML cells on CDK6 is mostly dependent on its kinase function.

Impairment of Selective Regulatory Networks after CDK6 Degradation

We next investigated drug impact on the known CDK4/6 Rb phosphorylation site S780. Both BSJ and palbo treatment reduced levels of p-S780 (Figure 4A). Notably, BSJ-bump treatment failed to affect phosphorylation of Rb, indicating that, at the assayed concentration, enzymatic CDK4/6 inhibition is insignificant (Figure 4A). Measurable impact of BSJ-bump was only observed upon dose escalation (Figure S2G). In line with this,

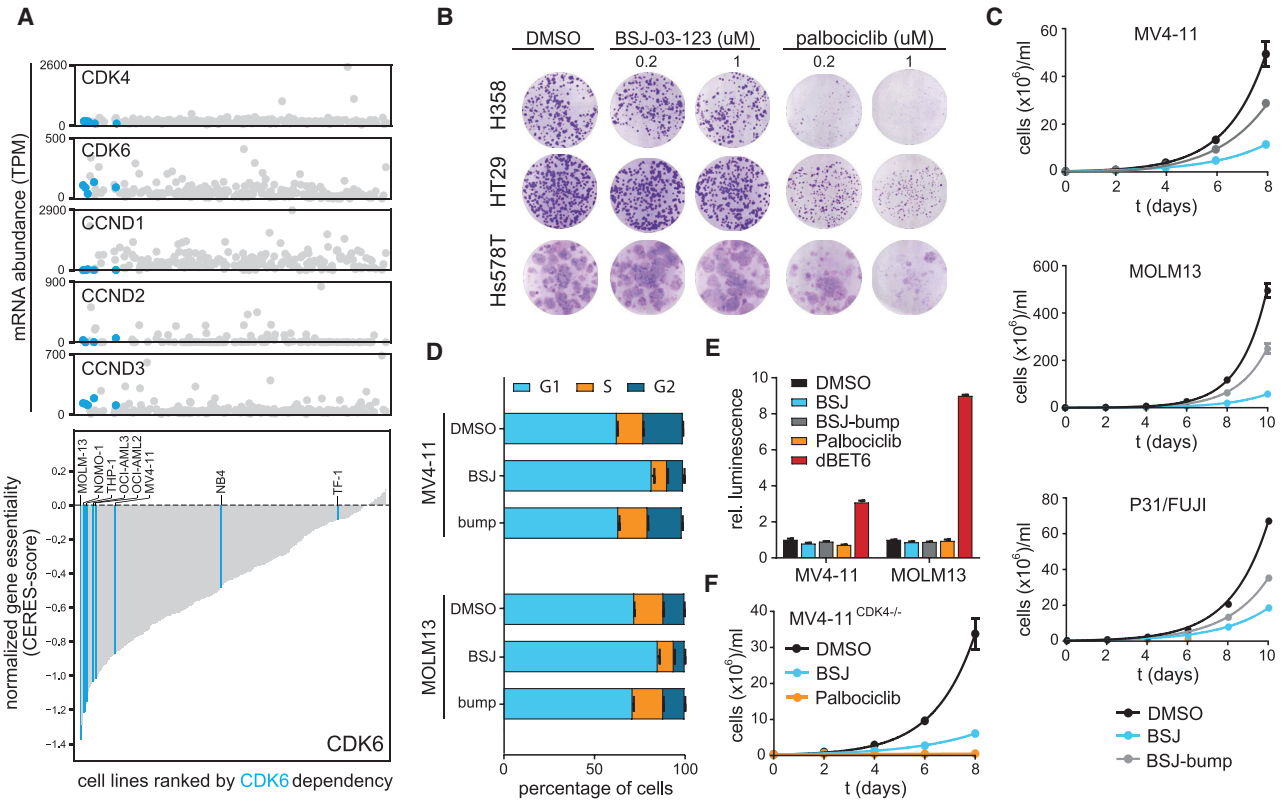

Figure 3. BSJ Exploits Homolog-Selective Dependencies

(A) Bottom: waterfall plot of 391 cell lines ranked by CDK6 dependency as determined in genome-wide CRISPR/Cas9 screens. CERES essentiality score is normalized for copy-number variation and scaled by setting the median of pan-essential genes to −1. Top: mRNA levels of CDK4, CDK6, and D-type cyclins.

(B) Colony-formation assays (12 days, refreshing the treatment every 2 days).

(C) Growth curves of AML cell lines treated with 200 nM BSJ, BSJ-bump, or DMSO. Cells were counted and treatment refreshed every 2 days.

(D) Cell cycle after treatment with 200 nM BSJ or BSJ-bump for 24 hr.

(E) Percentage of apoptotic cells after 24 hr treatment with 200 nM palbociclib, BSJ, BSJ-bump, or DMSO (Caspase-Glo 3/7 assay). BET protein degrader dBET6 served as positive control.

(F) Growth curves of CDK4-deficient MV4-11 treated with 200 nM BSJ, palbociclib, or DMSO.

See also Figure S2. Data presented in (C–F): mean ±SD, triplicate analysis.

the effect of BSJ treatment on Rb phosphorylation is rescued upon CRBN knockout (Figure S2H).

Given the plethora of functions assigned to CDK6, we globally extended our analysis to assay how acute and selective CDK6 disruption affects cellular signaling and gene activity in AML. Given the limited activity of BSJ-bump, we compared selective degradation of CDK6 via BSJ with catalytic CDK4/6 inhibition by palbo. We coupled acute drug treatment (2 hr, 200 nM each) to quantitative (Ser/Thr) phosphoproteomics to focus on direct drug effects. We quantified a total of 22,804 phosphopeptides in at least one technical replicate. In general, drug impact was modest, with 197 deregulated phosphopeptides after treatment with BSJ (44 up, 153 down), and 191 deregulated (57 up, 134 down) phosphopeptides following palbo treatment (Figures 4B and S3A). Changed sites were enriched for CDK motifs based on kinase-substrate enrichment analysis (Figures 4B and S3B), validating that short treatments biased for upstream events (Casado et al., 2013). Proteins with altered phosphosites were enriched for known regulators of cell-cycle progression (Figure S3C). Moreover, our data indicate a significant ($p = 4.49 \times 10^{-5}$) overlap with previously reported CDK4/6 substrates based on *in vitro* assays (Anders et al., 2011), but also uncovered undescribed substrates such as the splicing factor SRRM2 and the RSF chromatin-remodeling component RSF1 (Figures S3D and S3E).

In parallel, we compared the transcriptional response elicited by palbo and BSJ. This allowed us to determine if CDK6 orchestrates transcription independent of its kinase domain. As expected, transcriptional impact of YKL significantly differed from BSJ/palbo owing to off-target effects on IKZF1 and IKZF3. In contrast, enzymatic CDK4/6 inhibition and CDK6 degradation yielded a very similar and highly correlated ($R^2 = 0.9375$) transcriptional response, arguing that the transcriptional role of CDK6 in AML is mostly limited to its kinase function (Figures S4A–S4D). To further explore the functional implications of immediate CDK6 degradation, we performed gene ontology-term analysis of transcriptional changes elicited by CDK6 degradation and CDK4/6 inhibition (Figures 4D and S4E). Again, transcriptional consequences were similar, indicating that both converge on known pathways such as cell-cycle regulation, but also

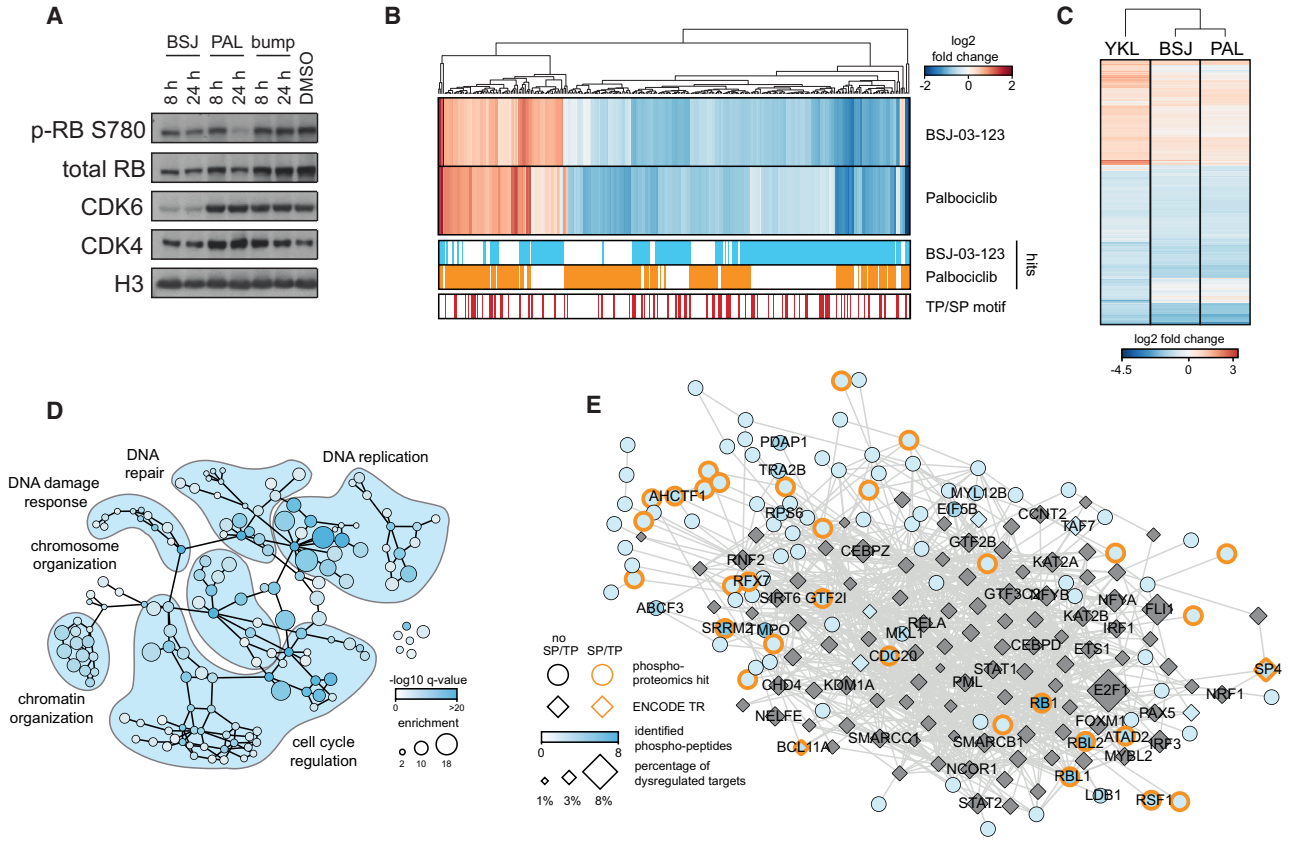

Figure 4. An Integrated View of the Effects of Acute CDK6 Degradation on Cellular Signaling and Transcription

(A) Immunoblot for p-RB S780, RB, CDK4, CDK6, and histone 3 after treatment with 200 nM BSJ, palbociclib, or BSJ-bump.

(B) Global phosphoproteomics. Heatmap depicting fold changes in peptide phosphorylation after BSJ or palbociclib treatment (200 nM, 2 hr) compared with DMSO for 305 differentially phosphorylated peptides. Hits (log2 fold change [FC] > 0.5 or < −0.5, adjusted p value < 0.05) and peptides phosphorylated at canonical SP/TP CDK phosphorylation motifs are annotated.

(C) Heatmap of DMSO-normalized fold changes in gene expression after BSJ, YKL, or palbociclib treatment (200 nM, 6 hr) for 993 significantly deregulated genes (log2 FC > 1.5 or < −1.5, adjusted p value < 0.05).

(D) Functional network of BSJ treatment. Nodes represent gene ontology (GO) terms enriched among genes that are differentially expressed upon treatment, scaled by magnitude, and color coded by significance of enrichment. Edges represent parent-child relationships of GO terms.

(E) Molecular network of BSJ treatment. Hits identified via global phosphoproteomics were mapped on a protein-protein interaction network and expanded to include first-order neighbors limited to ENCODE transcriptional regulators. Node shape distinguishes transcriptional regulators (TR) (diamonds) from phosphoproteomics hits (round). Node color represents the number of quantified phosphopeptides. Diamonds are scaled proportional to percentage of dysregulated TR target genes upon treatment. Proteins phosphorylated at CDK consensus motif (SP/TP) are annotated by edge color. Edges represent physical interaction between proteins.

See also Figures S3 and S4.

influence processes such as DNA replication, the DNA damage response, or chromatin organization.

To derive a systems-level understanding of the function of CDK6, we condensed data from transcriptional and phosphoproteomic profiling into a network centered around proteins with altered phosphopeptides after immediate CDK6 degradation (Figure 4E). Proteins were differentiated based on presence of a consensus CDK phosphorylation motif (SP/TP) in the detected phosphopeptides. Next, we expanded this network by adding ENCODE transcriptional regulators with established protein-protein interactions to members from the experimentally derived network. Network expansion was limited to factors with available genome-wide binding data. Dynamic transcriptional changes after CDK6 depletion were calculated and altered target genes were assigned to the network-resident TFs, which were visually scaled based on the percentage of dynamically regulated target genes (Figure 4E). This integrated network allowed identification of known, consensus downstream signaling axes such as Rb-E2F1, but also nodes such as BCL11A and NCOR2, previously not linked to CDK6. Network topologies are largely overlapping between BSJ or palbo treatment (Figure S3F), again supporting the notion that, in AML, CDK6 coordinates signaling and gene control predominantly via its kinase function.

DISCUSSION

The development of highly selective small molecules is a long-standing challenge in ligand discovery given the structural similarities of substrate or cofactor binding sites. This is a particular concern with ATP-competitive kinase inhibitors where a lack of

selectivity can limit the achievable therapeutic window. This hinders pharmacologic exploitation of genetically defined dependencies for therapeutic indications. Here, we present BSJ, a homolog-selective CDK6 degrader. BSJ features proteome-wide selectivity for CDK6 via differential ternary complex formation. Selectivity of BSJ enables exploitation of genetic dependencies beyond a resolution achievable with dual CDK4/6 inhibitors. In particular, we show that BSJ is capable of exploiting a homolog-selective dependency of AML cells on CDK6, thus outlining the potential for selective CDK6 degraders for further translational investigation, conceivably at reduced overall toxicity. Degradation of CDK6 is fast and potent, allowing us to map global consequences of acute CDK6 disruption on downstream signaling networks and transcriptional programs. While we cannot rule out that, at saturating concentrations, BSJ also catalytically inhibits CDK4, no inhibition was measured at the assayed concentration. Comparative profiling of CDK6 degradation and CDK4/6 inhibition suggest that, in AML, CDK6 integrates signaling and gene activity predominantly via its kinase activity. Our analysis uncovered several signaling nodes and transcriptional hubs previously not linked to CDK6, such as BCL11A and NCOR2, and future research will be necessary to explore the functional relevance of these pathways in AML and beyond. CDK6 features a prominent role in other malignancies as well as hematopoietic and leukemic stem cells. Selective degradation of CDK6 will facilitate differentiating relevant molecular mechanisms and further untangle kinase-dependent and -independent functions. Future medicinal chemistry efforts will be necessary to expand on the presented concept and to develop a toolbox of selective degraders to investigate the role of protein kinases at unprecedented precision and kinetic resolution.

SIGNIFICANCE

Traditionally, drug discovery efforts focus on the development of small-molecule inhibitors that block accessible hydrophobic pockets such as substrate or cofactor binding sites. However, due to the often high sequence conservation of these pockets, the design of selective inhibitors remains a continuous challenge. Here, we report a degrader that exploits structural differences outside of the ligand binding pocket to induce differential E3 ligase recruitment and ensuing degradation of CDK6, but not CDK4. We employed this exquisitely selective probe to dissect CDK6-dependent signaling and gene expression in AML, and showed that it allows unprecedented exploitation of genetically defined dependencies. This work showcases a framework for engineering selectivity into small-molecule probes and paves the way for the development of tools to functionally understand proteins at high kinetic resolution.

STAR★METHODS

Detailed methods are provided in the online version of this paper and include the following:

- KEY RESOURCES TABLE
- CONTACT FOR REAGENT AND RESOURCE SHARING
- EXPERIMENTAL MODEL AND SUBJECT DETAILS
- METHOD DETAILS
  - Knockout Generation
  - Proliferation Assays
  - Cell Cycle and Apoptosis
  - *In Vitro* CRBN Binding Assay
  - Immunoblotting
  - Cellular Thermal Shift Assay
  - NanoBiT® Assay
  - Expression Proteomics BSJ-03-123
  - Expression Proteomics YKL-06-102
  - Phosphoproteomics
  - RNA Sequencing
  - Chemical Synthesis of BSJ-03-123, BSJ-03-190/BSJ-bump, YKL-06-102
- QUANTIFICATION AND STATISTICAL ANALYSIS
  - Expression Proteomics BSJ-03-123
  - Expression Proteomics YKL-06-102
  - Phosphoproteomics
  - RNA Sequencing
- DATA AND SOFTWARE AVAILABILITY

SUPPLEMENTAL INFORMATION

Supplemental Information includes four figures, two tables, and one data file and can be found with this article online at https://doi.org/10.1016/j.chembiol.2018.11.006.

ACKNOWLEDGMENTS

We thank all members of the Gray and Winter labs. CeMM and the Winter lab are supported by the Austrian Academy of Sciences. This work was supported by an FWF grant to G.E.W. (project number FWF30271), and a Damon Runyon Cancer Research Fellowship DRG-2270-16 (to E.S.W.). The Gray lab is supported by NIH grant CA154303-06, and the Fischer lab by NIH NCI R01 CA214608-02. E.S.F. is a Damon Runyon-Rachleff Innovator supported in part by the Damon Runyon Cancer Research Foundation (DRR-50-18).

AUTHOR CONTRIBUTIONS

M.B. performed immunoblots, nluc-complementation assays, and proliferation assays. He also prepared samples for RNA sequencing and phosphoproteomics and expression proteomics, and performed the associated bioinformatic analysis. B.J. synthesized BSJ-03-123 and BSJ-bump. S.B. performed immunoblots and proliferation assays. K.A.D. performed, analyzed, and compared expression proteomics. Y.L. synthesized YKL-06-102. E.S.W. performed immunoblots and gave experimental advice. R.P.N. and J.C.Y. conducted recombinant CRBN binding assays. T.Z. and N.K. gave experimental and analytic advice. A.C.M. performed proteomics experiments. E.S.F. analyzed data and supervised aspects of the project. N.S.G. and G.E.W. wrote the manuscript, analyzed data, and have the overall project responsibility.

DECLARATION OF INTERESTS

E.S.F. is a member of the scientific advisory board of C4 Therapeutics and is a consultant to Novartis Pharmaceuticals. E.S.F. receives research funding from Novartis Pharmaceuticals and Astellas Pharma not related to this work. N.S.G. is equity holder and scientific advisor for Syros, Gatekeeper, Soltego, C4, Petra, and Aduro companies. N.S.G., B.J., T.Z., N.K., B.N., and E.S.F. are inventors on a patent covering CDK6 degraders owned by Dana-Farber.

Received: July 23, 2018
Revised: October 11, 2018
Accepted: November 6, 2018
Published: December 27, 2018

REFERENCES

Alanis-Lobato, G., Andrade-Navarro, M.A., and Schaefer, M.H. (2017). HIPPIE v2.0: enhancing meaningfulness and reliability of protein-protein interaction networks. Nucleic Acids Res. *45*, D408–D414.

An, J., Ponthier, C.M., Sack, R., Seebacher, J., Stadler, M.B., Donovan, K.A., and Fischer, E.S. (2017). pSILAC mass spectrometry reveals ZFP91 as IMiD-dependent substrate of the CRL4(CRBN) ubiquitin ligase. Nat. Commun. *8*, 15398.

Anders, L., Ke, N., Hydbring, P., Choi, Y.J., Widlund, H.R., Chick, J.M., Zhai, H., Vidal, M., Gygi, S.P., Braun, P., et al. (2011). A systematic screen for CDK4/6 substrates links FOXM1 phosphorylation to senescence suppression in cancer cells. Cancer Cell *20*, 620–634.

Bondeson, D.P., Smith, B.E., Burslem, G.M., Buhimschi, A.D., Hines, J., Jaime-Figueroa, S., Wang, J., Hamman, B.D., Ishchenko, A., and Crews, C.M. (2018). Lessons in PROTAC design from selective degradation with a promiscuous warhead. Cell Chem. Biol. *25*, 78–87.e5.

Casado, P., Rodriguez-Prados, J.C., Cosulich, S.C., Guichard, S., Vanhaesebroeck, B., Joel, S., and Cutillas, P.R. (2013). Kinase-substrate enrichment analysis provides insights into the heterogeneity of signaling pathway activation in leukemia cells. Sci. Signal. *6*, rs6.

Chen, P., Lee, N.V., Hu, W., Xu, M., Ferre, R.A., Lam, H., Bergqvist, S., Solowiej, J., Diehl, W., He, Y.A., et al. (2016). Spectrum and degree of CDK drug interactions predicts clinical performance. Mol. Cancer Ther. *15*, 2273–2281.

Fry, D.W., Harvey, P.J., Keller, P.R., Elliott, W.L., Meade, M., Trachet, E., Albassam, M., Zheng, X., Leopold, W.R., Pryer, N.K., et al. (2004). Specific inhibition of cyclin-dependent kinase 4/6 by PD 0332991 and associated antitumor activity in human tumor xenografts. Mol. Cancer Ther. *3*, 1427–1438.

Gadd, M.S., Testa, A., Lucas, X., Chan, K.H., Chen, W., Lamont, D.J., Zengerle, M., and Ciulli, A. (2017). Structural basis of PROTAC cooperative recognition for selective protein degradation. Nat. Chem. Biol. *13*, 514–521.

Gandhi, A.K., Kang, J., Havens, C.G., Conklin, T., Ning, Y., Wu, L., Ito, T., Ando, H., Waldman, M.F., Thakurta, A., et al. (2014). Immunomodulatory agents lenalidomide and pomalidomide co-stimulate T cells by inducing degradation of T cell repressors Ikaros and Aiolos via modulation of the E3 ubiquitin ligase complex CRL4(CRBN.). Br. J. Haematol. *164*, 811–821.

Huang, H.T., Dobrovolsky, D., Paulk, J., Yang, G., Weisberg, E.L., Doctor, Z.M., Buckley, D.L., Cho, J.H., Ko, E., Jang, J., et al. (2018). A chemoproteomic approach to query the degradable kinome using a multi-kinase degrader. Cell Chem. Biol. *25*, 88–99.e6.

Klijn, C., Durinck, S., Stawiski, E.W., Haverty, P.M., Jiang, Z., Liu, H., Degenhardt, J., Mayba, O., Gnad, F., Liu, J., et al. (2015). A comprehensive transcriptional portrait of human cancer cell lines. Nat. Biotechnol. *33*, 306–312.

Kollmann, K., Heller, G., Schneckenleithner, C., Warsch, W., Scheicher, R., Ott, R.G., Schafer, M., Fajmann, S., Schlederer, M., Schiefer, A.I., et al. (2013). A kinase-independent function of CDK6 links the cell cycle to tumor angiogenesis. Cancer Cell *24*, 167–181.

Kronke, J., Udeshi, N.D., Narla, A., Grauman, P., Hurst, S.N., McConkey, M., Svinkina, T., Heckl, D., Comer, E., Li, X., et al. (2014). Lenalidomide causes selective degradation of IKZF1 and IKZF3 in multiple myeloma cells. Science *343*, 301–305.

Lu, G., Middleton, R.E., Sun, H., Naniong, M., Ott, C.J., Mitsiades, C.S., Wong, K.K., Bradner, J.E., and Kaelin, W.G., Jr. (2014). The myeloma drug lenalidomide promotes the cereblon-dependent destruction of Ikaros proteins. Science *343*, 305–309.

Lu, J., Qian, Y., Altieri, M., Dong, H., Wang, J., Raina, K., Hines, J., Winkler, J.D., Crew, A.P., Coleman, K., et al. (2015). Hijacking the E3 ubiquitin ligase cereblon to efficiently target BRD4. Chem. Biol. *22*, 755–763.

Meyers, R.M., Bryan, J.G., McFarland, J.M., Weir, B.A., Sizemore, A.E., Xu, H., Dharia, N.V., Montgomery, P.G., Cowley, G.S., Pantel, S., et al. (2017). Computational correction of copy number effect improves specificity of CRISPR-Cas9 essentiality screens in cancer cells. Nat. Genet. *49*, 1779–1784.

Nowak, R.P., DeAngelo, S.L., Buckley, D., He, Z., Donovan, K.A., An, J., Safaee, N., Jedrychowski, M.P., Ponthier, C.M., Ishoey, M., et al. (2018). Plasticity in binding confers selectivity in ligand-induced protein degradation. Nat. Chem. Biol. *14*, 706–714.

O'Leary, B., Finn, R.S., and Turner, N.C. (2016). Treating cancer with selective CDK4/6 inhibitors. Nat. Rev. Clin. Oncol. *13*, 417–430.

Olson, C.M., Jiang, B., Erb, M.A., Liang, Y., Doctor, Z.M., Zhang, Z., Zhang, T., Kwiatkowski, N., Boukhali, M., Green, J.L., et al. (2018). Pharmacological perturbation of CDK9 using selective CDK9 inhibition or degradation. Nat. Chem. Biol. *14*, 163–170.

Remillard, D., Buckley, D.L., Paulk, J., Brien, G.L., Sonnett, M., Seo, H.S., Dastjerdi, S., Wuhr, M., Dhe-Paganon, S., Armstrong, S.A., et al. (2017). Degradation of the BAF complex factor BRD9 by heterobifunctional ligands. Angew. Chem. Int. Ed. *56*, 5738–5743.

Tigan, A.S., Bellutti, F., Kollmann, K., Tebb, G., and Sexl, V. (2016). CDK6 - a review of the past and a glimpse into the future: from cell-cycle control to transcriptional regulation. Oncogene *35*, 3083–3091.

Wang, H., Nicolay, B.N., Chick, J.M., Gao, X., Geng, Y., Ren, H., Gao, H., Yang, G., Williams, J.A., Suski, J.M., et al. (2017). The metabolic function of cyclin D3-CDK6 kinase in cancer cell survival. Nature *546*, 426–430.

Winter, G.E., Buckley, D.L., Paulk, J., Roberts, J.M., Souza, A., Dhe-Paganon, S., and Bradner, J.E. (2015). Drug development. Phthalimide conjugation as a strategy for in vivo target protein degradation. Science *348*, 1376–1381.

Zengerle, M., Chan, K.H., and Ciulli, A. (2015). Selective small molecule induced degradation of the BET bromodomain protein BRD4. ACS Chem. Biol. *10*, 1770–1777.

STAR★METHODS

KEY RESOURCES TABLE

REAGENT or RESOURCE	SOURCE	IDENTIFIER
Antibodies		
CDK4	Cell Signaling	Cat#12790; RRID: AB_2631166
CDK6	Santa Cruz	Cat#sc-7961; RRID: AB_627242
Histone 3	Abcam	Cat#ab1791; RRID: AB_302613
β-actin	Sigma-Aldrich	Cat#A5441; RRID: AB_476744
p-Rb S780	Cell Signaling	Cat#8180; RRID: AB_10950972
Rb	Cell Signaling	Cat#9309; RRID: AB_823629
Peroxidase-conjugated AffiniPure Goat Anti-Mouse IgG	Jackson Immuno Research	Cat#115-035-003; RRID: AB_10015289
Peroxidase-conjugated AffiniPure Goat Anti-Rabbit IgG	Jackson Immuno Research	Cat#111-035-003; RRID: AB_2313567
Chemicals, Peptides, and Recombinant Proteins		
BSJ-03-123	This study	N/A
BSJ-bump	This study	N/A
YKL-06-102	This study	N/A
Palbociclib	Selleckchem	Cat#S1116
Critical Commercial Assays		
Caspase-Glo 3/7	Promega	Cat#G8090
NanoBiT	Promega	Cat#N2011
Deposited Data		
Project Achilles: CRISPR-Cas9 Avana	Meyers et al., 2017	https://portals.broadinstitute.org/achilles/datasets/18/download
Gene expression data of 675 cell lines	Klijn et al., 2015	https://www.nature.com/articles/nbt.3080#supplementary-information
ENCODE transcription factor targets	ENCODE Consortium	http://amp.pharm.mssm.edu/Harmonizome/dataset/ENCODE+Transcription+Factor+Targets
Human protein-protein interaction network	Alanis-Lobato et al., 2017	http://cbdm-01.zdv.uni-mainz.de/~mschaefer/hippie/
Human reference genome NCBI build 38, GRCh38		http://hgdownload.cse.ucsc.edu/goldenPath/hg38/bigZips/
RNA sequencing upon CDK6 degradation	This study	GEO: GSE116187
CDK4/6 targets	Anders et al., 2011	https://doi.org/10.1016/j.ccr.2011.10.001
Experimental Models: Cell Lines		
MV4-11	ATCC	RRID: CVCL_0064
THP-1	ATCC	RRID: CVCL_0006
MOLM13	DMSZ	RRID: CVCL_2119
P31/FUJ	CCLE/Broad Institute	RRID: CVCL_1632
MOLT4	ATCC	RRID: CVCL_0013
NCI-H358	ATCC	RRID: CVCL_1559
HT29	ATCC	RRID: CVCL_0320
HEK293T	ATCC	RRID: CVCL_0063
Hs578T	ATCC	RRID: CVCL_0332
Oligonucleotides		
sgCDK4 sense (5'- CACCGAGCCACTGGCTCATATCGAG-3')	Sigma-Aldrich	N/A
sgCDK4 antisense (5'- AAACCTCGATATGAGCCAGTGGCTC-3')	Sigma-Aldrich	N/A

(*Continued on next page*)

Continued		
REAGENT or RESOURCE	SOURCE	IDENTIFIER
sgCRBN sense (5'- CACCGTAAACAGAC ATGGCCGGCGA-3')	Sigma-Aldrich	N/A
sgCRBN antisense (5'- AAACTCGCCGGCCATG TCTGTTTAC-3')	Sigma-Aldrich	N/A
Recombinant DNA		
Lenti_sgRNA_EFS_GFP	Addgene	https://www.addgene.org/65656
pBit1.1-C [TK/LgBiT]	Promega	Cat#N2014
pBit2.1-N [TK/SmBiT]	Promega	Cat#N2014
Software and Algorithms		
Cytoscape	Institute for Systems Biology	http://cytoscape.org; RRID: SCR_003032
GraphPad Prism		https://www.graphpad.com/scientific-software/prism/
Proteome Discoverer	Thermo Fisher Scientific	https://www.thermofisher.com/order/catalog/product/OPTON-30795
KSEA App		https://casecpb.shinyapps.io/ksea
STAR Aligner		https://github.com/alexdobin/STAR
limma		https://bioconductor.org/packages/release/bioc/html/limma.html
GOrilla		http://cbl-gorilla.cs.technion.ac.il/
networkx		https://networkx.github.io/

CONTACT FOR REAGENT AND RESOURCE SHARING

Further information and requests for resources and reagents should be directed to and will be fulfilled by the lead contact, Georg Winter (gwinter@cemm.at).

EXPERIMENTAL MODEL AND SUBJECT DETAILS

MV4-11 (RRID:CVCL_0064), THP-1 (RRID:CVCL_0006), MOLM13 (RRID:CVCL_2119), P31/FUJ (RRID:CVCL_1632), MOLT4 (RRID:CVCL_0013), NCI-H358 (RRID:CVCL_1559) and HT29 (RRID:CVCL_0320) cells were cultured in RPMI-1640 growth medium (Gibco) supplemented with 10% fetal bovine serum (Gibco) and 1% Penicillin/Streptomycin solution (ThermoFisher Scientific). HEK293T (RRID:CVCL_0063) and Hs578T (RRID:CVCL_0332) cells were cultured in DMEM (Gibco) supplemented with 10% fetal bovine serum (Gibco) and 1% Penicillin/Streptomycin solution (ThermoFisher Scientific). All cell lines were cultured at 37°C with 5% CO_2 and tested for mycoplasma contamination and cell identity.

Sex of human cell lines: MV4-11 (Male, 10 years old), THP-1 (Male, 1 year old), MOLM13 (Male, 20 years old), P31/FUJ (Male, 7 years old), MOLT4 (Male, 19 years old), NCI-H358 (Male, age unknown), HT29 (Female, 44 years old), HEK293T (Female, fetus), Hs578T (Female, 74 years old).

METHOD DETAILS

Knockout Generation

sgRNAs (CDK4: 5′-AGCCACTGGCTCATATCGAG-3′, CRBN: 5′- TAAACAGACATGGCCGGCGA-3') were cloned into Lenti_sgRNA_EFS_GFP (addgene #65656). Cells were transduced with lentiviral particles, selected by sorting for GFP positive cells and successful knockout verified by immunoblot and Sanger sequencing.

Proliferation Assays

For growth over time experiments of suspension cell lines, 300.000 cells per well were seeded in 24-well plates in triplicates. Cells were counted and treatments renewed every 2 days. For growth over time experiments of adherent cell lines, 100.000 cells per well were seeded in 12-well plates in triplicates. Cells were trypsinized and counted and treatments renewed every 3 days. For colony formation assays, 1000 cells per well were seeded in 6-well plates in duplicates. Every 2 days, culture medium was exchanged and treatments were renewed. After 12 days, cells were fixed in 1% PFA in PBS for 15 min at room temperature, washed 3 times with PBS and stained in Crystal Violet solution (0.1% in 10% EtOH) for 15 min at room temperature. The cells were again washed 3 times with PBS and left to dry overnight.

Cell Cycle and Apoptosis

For cell cycle measurement, 10^6 cells per well were seeded in 24-well plates in triplicates. After 24 h of drug treatment, cells were harvested by centrifugation at 500g for 5 min and washed in 1 ml cold PBS. Cells were spun down again, resuspended in 200 μl PBS and fixed by addition of 800 μl 70% EtOH and incubation for 20 min at -20°C. Cells were washed with 1 ml PBS and stained with 500 μl propidium iodide solution (50 μg/ml propidium iodide (Sigma Aldrich), 200 μg/ml RNase A (ThermoFisher Scientific), in PBS). Cellular DNA content was measured by flow cytometry using FACSCalibur (BD Biosciences) and analyzed using the FlowJo v10 software.

Analysis of apoptotic cells was performed using Caspase-Glo 3/7 (Promega) according to manufacturer's instructions. 20 000 cells per well were seeded in triplicate in a white 96-well plate in a total volume of 50 μl. After 24 h incubation with the treatment, 45 μl Caspase-Glo substrate were added per well. The plate was incubated at room temperature in the dark for 1 h and luminescence measured on a Victor X3 (Perkin Elmer) microplate reader. Luminescent signal was normalized to vehicle-treated cells.

In Vitro CRBN Binding Assay

Compounds in Atto565-Lenalidomide displacement assay were dispensed in a 384-well microplate (Corning, 4514) using D300e Digital Dispenser (HP) and normalized to 1% DMSO into 10 nM Atto565-Lenalidomide, 100 nM DDB1ΔB-CRBN, 50 mM Tris pH 7.5, 200 mM NaCl, 0.1% Pluronic F-68 solution (Sigma). The change in fluorescence polarization was monitored using a PHERAstar FS microplate reader (BMG Labtech) for 30 cycles of 187s each. Data from three independent measurements (n = 3) was plotted and IC50 values estimated using variable slope equation in GraphPad Prism 7.

Immunoblotting

$2x10^6$ cells were lysed in RIPA buffer (150 nM NaCl, 0.1% Triton X-100, 0.5% sodium deoxycholate, 0.1% SDS, 50 mM Tris-HCl (pH 8.0), protease inhibitors (Thermo Scientific), benzonase (Novagen)). Cell lysates containing 40 μg of protein were loaded on Bolt™ 4-12% Bis-Tris Plus Gels (Thermo Scientific) and ran for SDS-PAGE before transfer onto 0.45 μM nitrocellulose membrane (GE Healthcare). Following antibodies were used for detection:

Name	Origin	Cat. No.
CDK4	Cell Signaling	#12790
CDK6	Santa Cruz	sc-7961
Histone 3	Abcam	ab1791
β-actin	Sigma-Aldrich	A5441
p-Rb S780	Cell Signaling	#8180
Rb	Cell Signaling	#9309
Peroxidase-conjugated AffiniPure Goat Anti-Mouse IgG	Jackson Immuno Research	115-035-003
Peroxidase-conjugated AffiniPure Goat Anti-Rabbit IgG	Jackson Immuno Research	111-035-003

Cellular Thermal Shift Assay

$4x10^6$ MV4-11 CRBN-/- cells were treated for 3 h with 20 μM palbociclib, BSJ-03-123 or vehicle. $1x10^6$ cells were spun down at 500 x *g* for 5 min, and the supernatant removed. Pellets were incubated at 46, 49, 52 or 55°C for 3 min followed by 3 min incubation at room temperature. 30 μl of lysis buffer (20 mM Tris-HCl pH 8.0, 120 mM NaCl, 0.5% NP-40, protease inhibitors) were added and cells lysed by 3 rounds of snap freezing and thawing. Denatured proteins were removed by 20 min centrifugation at 14.000 x *g* at 4°C and supernatants analyzed by Western Blotting.

NanoBiT® Assay

The NanoBiT® assay (Promega) was performed following manufacturer's instructions. Full-length CDK4 and CDK6 were cloned into pBit1.1-C [TK/LgBiT] vector, full-length CRBN was cloned into pBit2.1-N [TK/SmBiT]. 400.000 CRBN-deficient HEK293T cells were seeded in a 6-well plate and transfected the day after with 750 μg each of CDK4/6-LgBit and CRBN-SmBit using Lipofectamine (Thermo Fisher Scientific) according to manufacturer's instructions. After 24 h, cells were detached and 50.000 cells per well seeded in a 96-well plate and allowed to attach overnight. Before the assay, the medium was exchanged with 100 μl of ambient temperature fresh medium supplemented with 25 mM HEPES and the plate incubated for 10 min at room temperature to equilibrate. 25 μl Nano-Glo® Live Cell Reagent was added per well, incubated for 5 min and baseline luminescence measured on a Victor X3 (Perkin Elmer) with 2 s integration time. 10 μl of 13.5X drug stock were added per well and emission of luminescent signal monitored by continuous measurement every 2 min. Signals were normalized to baseline and vehicle treated cells.

Expression Proteomics BSJ-03-123

Sample Preparation

15x10^6 MOLT4 cells were treated with 100 nM BSJ-03-123 for 2 h, in triplicate. Cells were washed three times with PBS, the supernatant aspirated and pellets snap-frozen in liquid N_2. Each washed cell pellet was lysed separately in 40 μL of freshly prepared lysis buffer containing 50 mM HEPES (pH 8.0), 2% SDS, 0.1 M DTT, 1 mM PMSF, and protease inhibitor cocktail (Sigma-Aldrich). Samples rested at RT for 20 minutes before heating to 99°C for 5 min. After cooling down to RT, DNA was sheared by sonication using a Covaris S2 high performance ultrasonicator. Cell debris were removed by centrifugation at 20.000 × g for 15 min at 20°C. Supernatant was transferred to fresh eppendorf tubes and protein concentration determined using the BCA protein assay kit (Pierce Biotechnology, Rockford, IL). FASP was performed using a 30 kDa molecular weight cutoff filter (VIVACON 500). Fifty microliters of each cleared protein extract were mixed with 200 μL of freshly prepared 8 M urea in 100 mM Tris-HCl (pH 8.5) (UA-solution) in the filter unit and centrifuged at 14.000 × g for 15 min at 20°C to remove SDS. Any residual SDS was washed out by a second washing step with 200 μL of UA. The proteins were alkylated with 100 μL of 50 mM iodoacetamide in the dark for 30 min at RT. Afterward, three washing steps with 100 μL of UA solution were performed, followed by three washing steps with 100μL of 50 mM TEAB buffer (Sigma-Aldrich). Proteins were digested with trypsin overnight at 37°C. Peptides were recovered using 40 μL of 50 mM TEAB buffer followed by 50 μL of 0.5 M NaCl (Sigma-Aldrich). Peptides were desalted using C18 solid phase extraction spin columns (The Nest Group, Southborough, MA). After desalting, peptides were labeled with TMT 10plex™ reagents according to the manufacturer (Pierce, Rockford, IL). After quenching of the labeling reaction, labeled peptides were pooled, organic solvent removed in a vacuum concentrator at 45°C and reconstituted in 5% acetonitrile containing 20mM ammonia formate buffer, pH 10 for offline fractionation using high pH reversed phase liquid chromatography (2D-RP/RP-HPLC).

2D-RP/RP Liquid Chromatography Mass Spectrometry

Two-dimensional liquid chromatography was performed by reverse-phase chromatography at high and low pH. In the first dimension, peptides were separated on a Gemini-NX C18 (150 × 2 mm, 3 μm, 110 Å, Phenomenex, Torrance, USA) in 20 mM ammonia formate buffer, pH 10, and eluted over 45 min by a 5-70% acetonitrile gradient at 100 μL/min using an Agilent 1200 HPLC system (Agilent Biotechnologies, Palo Alto, CA, USA). Ninty-six time-based fractions were collected and consolidated into 40 fractions. After solvent removal in a vacuum concentrator, samples were reconstituted in 5% formic acid for LC-MS/MS analysis. Mass spectrometry was performed on an Orbitrap Fusion Lumos mass spectrometer (ThermoFisher Scientific, San Jose, CA) coupled to an Agilent 1200 HPLC nanoflow system (Agilent Biotechnologies, Palo Alto, CA) via nanoflex source interface. Tryptic peptides were loaded onto a trap column (Zorbax 300SB-C18 5 μm, 5 × 0.3 mm, Agilent Biotechnologies) at a flow rate of 45 μL/min using 0.1% TFA as loading buffer. After loading, the trap column was switched in-line with a 25 cm, 75 μm inner diameter analytical column (packed in-house with ReproSil-Pur 120 C18-AQ, 3 μm, Dr. Maisch, Ammerbuch-Entringen, Germany). Mobile-phase A consisted of 0.4% formic acid in water and mobile-phase B of 0.4% formic acid in a mix of 90% acetonitrile and 10% water. The flow rate was set to 230 nL/min and a 90 min gradient used (6 to 30% solvent B within 81 min, 30 to 65% solvent B within 8 min and, 65 to 100% solvent B within 1 min, 100% solvent B for 6 min before equilibrating at 6% solvent B for 18 min). Analysis was performed in a data-dependent acquisition mode using the multi-notch MS3-based TMT method (termed SPS-MS3 on the Lumos instrument). MS1 spectra were acquired within a mass range of 350 - 1550 m/z in the orbitrap at a resolution of 120,000 (at 200Th). Automatic gain control (AGC) was set to a target of 2 × 10^5 and a maximum injection time of 50 ms. Precursor ions for MS2/MS3 analysis were selected using a Top10 dependent scan approach. MS2 spectra were acquired in the linear quadrupole ion trap (IT) using a quadrupole isolation window of 0.8Da; collision induced dissociation (CID) for fragmentation; a normalized collision energy (NCE) of 35%; an AGC target of 4 × 10^3; and a maximum injection time of 150 ms. For TMT quantitation, each MS2 scan followed a SPS-MS3 scan of the same precursor ion using the multiple frequency notches approach 3. The quadrupole isolation window for MS3 scans was set to 2 Da and the top 5 most intense MS2 fragment ions were isolated by SPS for fragmentation by higher energy collision-induced dissociation (HCD) using a NCE of 65%. Resulting fragment ions were analyzed in the Orbitrap at a resolution of 50,000 (at 200 Th). AGC settings were 5 × 10^4 and a maximum injection time of 150 ms. Dynamic exclusion for selected ions was 60 s. A single lock mass at m/z 445.120024 was employed. Xcalibur version 4.0.0 and Tune 2.1 were used to operate the instrument.

Expression Proteomics YKL-06-102

MOLT4 cells were treated with DMSO or 500 nM of compound YKL-06-102 in biological triplicates for 5 hours and cells harvested by centrifugation. Lysis buffer (8 M Urea, 50 mM NaCl, 50 mM 4-(2hydroxyethyl)-1-piperazineethanesulfonic acid (EPPS) pH 8.5, Protease and Phosphatase inhibitors from Roche) was added to the cell pellets and homogenized by 20 passes through a 21 gauge (1.25 in. long) needle to achieve a cell lysate with a protein concentration between 1 – 4 mg mL-1. A micro-BCA assay (Pierce) was used to determine the final protein concentration in the cell lysate. 200 μg of protein for each sample were reduced and alkylated.

Proteins were precipitated using methanol/chloroform. In brief, four volumes of methanol were added to the cell lysate, followed by one volume of chloroform, and finally three volumes of water. The mixture was vortexed and centrifuged to separate the chloroform phase from the aqueous phase. The precipitated protein was washed with three volumes of methanol, centrifuged and the resulting washed precipitated protein was allowed to air dry. Precipitated protein was resuspended in 4 M Urea, 50 mM HEPES pH 7.4, followed by dilution to 1 M urea with the addition of 200 mM EPPS, pH 8. Proteins were first digested with LysC (1:50; enzyme:protein) for 12 hours at room temperature. The LysC digestion was diluted to 0.5 M Urea with 200 mM EPPS pH 8 followed by digestion with trypsin (1:50; enzyme:protein) for 6 hours at 37°C. Tandem mass tag (TMT) reagents (Thermo Fisher Scientific) were dissolved in anhydrous acetonitrile (ACN) according to manufacturer's instructions. Anhydrous ACN was added to each peptide sample to a final

concentration of 30% v/v, and labeling was induced with the addition of TMT reagent to each sample at a ratio of 1:4 peptide:TMT label. The 10-plex labeling reactions were performed for 1.5 hours at room temperature and the reaction quenched by the addition of hydroxylamine to a final concentration of 0.3% for 15 minutes at room temperature. The sample channels were combined at a 1:1:1:1:1:1:1:1:1:1 ratio, desalted using C18 solid phase extraction cartridges (Waters) and analyzed by LC-MS for channel ratio comparison. Samples were then combined using the adjusted volumes determined in the channel ratio analysis and dried down in a speed vacuum. The combined sample was then resuspended in 1% formic acid, and acidified (pH 2−3) before being subjected to desalting with C18 SPE (Sep-Pak, Waters). Samples were then offline fractionated into 96 fractions by high pH reverse-phase HPLC (Agilent LC1260) through an aeris peptide xb-c18 column (phenomenex) with mobile phase A containing 5% acetonitrile and 10 mM NH4HCO3 in LC-MS grade H2O, and mobile phase B containing 90% acetonitrile and 10 mM NH4HCO3 in LC-MS grade H2O (both pH 8.0). The 96 resulting fractions were then pooled in a non-continuous manner into 24 fractions and these fractions were used for subsequent mass spectrometry analysis.

Data were collected using an Orbitrap Fusion Lumos mass spectrometer (Thermo Fisher Scientific, San Jose, CA, USA) coupled with a Proxeon EASY-nLC 1200 LC pump (Thermo Fisher Scientific). Peptides were separated on a 75 μM inner diameter microcapillary column packed with ∼40 cm of Accucore C18 resin (1.6 μM, 100 Å, Thermo Fisher Scientific). Peptides were separated using a 150 min gradient of 6–27% acetonitrile in 1.0% formic acid with a flow rate of 400 nL/min.

Each analysis used an MS3-based TMT method. The data were acquired using a mass range of m/z 340 – 1350, resolution 120,000, AGC target 1 x 106, maximum injection time 100 ms, dynamic exclusion of 120 seconds for the peptide measurements in the Orbitrap. Data dependent MS2 spectra were acquired in the ion trap with a normalized collision energy (NCE) set at 35%, AGC target set to 1.8 x 104 and a maximum injection time of 120 ms. MS3 scans were acquired in the Orbitrap with a HCD collision energy set to 55%, AGC target set to 1.5 x 105, maximum injection time of 150 ms, resolution at 50,000 and with a maximum synchronous precursor selection (SPS) precursors set to 10.

Phosphoproteomics

$15x10^6$ MV4-11 cells were treated with 200 nM BSJ-03-123 or Palbociclib for 2 h, in triplicate. Cells were washed three times with PBS, the supernatant aspirated and pellets snap-frozen in liquid N_2.

Each washed cell pellet was lysed separately in 40 μL of freshly prepared lysis buffer containing 50 mM HEPES (pH 8.0), 2% SDS, 0.1 M DTT, 1 mM PMSF, phosSTOP and protease inhibitor cocktail (Sigma-Aldrich). Samples rested at RT for 20 minutes before heating to 99°C for 5 min. After cooling down to RT, DNA was sheared by sonication using a Covaris S2 high performance ultrasonicator. Cell debris was removed by centrifugation at 20.000 X g for 15 min at 20°C. Supernatant was transferred to fresh eppendorf tubes and protein concentration determined using the BCA protein assay kit (Pierce Biotechnology, Rockford, IL). FASP was performed using a 30 kDa molecular weight cutoff filter (VIVACON 500). In brief, 100 μg total protein per sample were reduced by adding DTT at a final concentration of 83.3 mM followed by incubation at 99°C for 5 min. After cooling to room temperature, samples were mixed with 200 μL of freshly prepared 8 M urea in 100 mM Tris-HCl (pH 8.5) (UA-solution) in the filter unit and centrifuged at 14.000 × g for 15 min at 20°C to remove SDS. Any residual SDS was washed out by a second washing step with 200 μL of UA. The proteins were alkylated with 100 μL of 50 mM iodoacetamide in the dark for 30 min at RT. Afterward, three washing steps with 100 μL of UA solution were performed, followed by three washing steps with 100μL of 50 mM TEAB buffer (Sigma-Aldrich). Proteins were digested with trypsin at a ratio of 1:35 overnight at 37°C. Peptides were recovered using 40 μL of 50 mM TEAB buffer followed by 50 μL of 0.5 M NaCl (Sigma-Aldrich). Peptides were desalted using C18 solid phase extraction spin columns (The Nest Group, Southborough, MA). After desalting, peptides were labeled with TMT 10plex™ reagents (label 128N was omitted) according to the manufacturer (Pierce, Rockford, IL). After quenching of the labeling reaction, labeled peptides were pooled, organic solvent removed in vacuum concentrator and labelled peptides loaded onto a SPE column. Peptides were eluted with 300μL 80% acetonitrile containing 0.1% trifluoroacetic to achieve a final peptide concentration of ∼1μg/μl. Eluate was then used for phosphopeptide enrichment via immobilized metal affinity chromatography (IMAC). Briefly, two times 100 μL of Ni-NTA superflow slurry (QIAGEN Inc., Valencia, USA) were washed with LCMS-grade water and Ni^{2+} stripped off the beads by incubation with 100 mM of EDTA, pH 8 solution for 1 hr at room temperature. Stripped NTA resin was recharged with Fe^{3+}-ions by incubation with a fresh solution of $Fe(III)Cl_3$ and 2 x 110 μL of charged resin slurry used for the enrichment of a total of ∼900 μg TMT-labelled peptide. The unbound fraction was transferred to a fresh glass vial and used for offline fractionation for the analysis of the whole chromatome proteome. After washing the slurry with 0.1% TFA, phosphopeptides were eluted with a freshly prepared ammonia solution containing 3mM EDTA, pH 8 and all used for offline fractionation for the analysis of the phophoproteome.

Offline Fractionation via RP-HPLC at High pH

Peptides were re-buffered in 20 mM ammonium formiate buffer shortly before separation by reversed phase liquid chromatography at pH 10. Phosphopeptides was separated into 20 fractions on a Dionex column (500 μm × 50 mm PepSwift RP, monolithic, Dionex Corporation, Sunnyvale, CA, USA) using an Agilent 1200 series nanopump delivering solvent at 4 μL/min. Peptides were separated by applying a gradient of 90% aceonitrile containing 20 mM ammonium formiate, pH 10. After solvent removal in a vacuum concentrator, samples were reconstituted in 0.1% trifluroacetic acid (TFA) for LC-MS/MS analysis. Prepared samples were kept at -80°C until the analysis.

2D-RP/RP Liquid Chromatography Mass Spectrometry

Mass spectrometry was performed on an Orbitrap Fusion Lumos mass spectrometer (ThermoFisher Scientific, San Jose, CA) coupled to an Dionex Ultimate 3000RSLC nano system (ThermoFisher Scientific, San Jose, CA) via nanoflex source interface. Tryptic

peptides were loaded onto a trap column (Pepmap 100 5μm, 5 × 0.3 mm, ThermoFisher Scientific, San Jose, CA) at a flow rate of 10 μL/min using 2% ACN and 0.1% TFA as loading buffer. After loading, the trap column was switched in-line with a 30 cm, 75 μm inner diameter analytical column (packed in-house with ReproSil-Pur 120 C18-AQ, 3 μm, Dr. Maisch, Ammerbuch-Entringen, Germany). Mobile-phase A consisted of 0.4% formic acid in water and mobile-phase B of 0.4% formic acid in a mix of 90% acetonitrile and 10% water. The flow rate was set to 230 nL/min and a 90 min gradient used (6 to 30% solvent B within 81 min, 30 to 65% solvent B within 8 min and, 65 to 100% solvent B within 1 min, 100% solvent B for 6 min before equilibrating at 6% solvent B for 18 min). Analysis was performed in a data-dependent acquisition mode. Full MS scans were acquired with a mass range of 375 - 1650 m/z in the orbitrap at a resolution of 120,000 (at 200Th). Automatic gain control (AGC) was set to a target of 2×10^5 and a maximum injection time of 50 ms. Precursor ions for MS^2 analysis were selected using a TopN dependant scan approach with a cycle time of 3 seconds. MS^2 spectra were acquired in the orbitrap (FT) using a quadrupole isolation window of 1 Da and higher energy collision induced dissociation (HCD) at a normalized collision energy (NCE) of 38%. AGC target was set to 5×10^4 with a maximum injection time of 150 ms and MS^2 scans acquired at a resolution of 15,000 (at 200 Th). Dynamic exclusion for selected ions was 60 s. A single lock mass at *m/z* 445.120024 was employed. Xcalibur version 4.0.0 and Tune 2.1 were used to operate the instrument.

RNA Sequencing

$3x10^6$ MV4-11 cells per well were seeded in triplicate in a 12-well plate and treated with 200 nM BSJ-03-123, YKL-06-102, Palbociclib or vehicle for 6 h. Cells were lysed using QIAshredder columns (QIAGEN) and RNA isolated using RNeasy kit (QIAGEN) according to manufacturer's instructions.

The amount of total RNA was quantified using the Qubit Fluorometric Quantitation system (Life Technologies) and the RNA integrity number (RIN) was determined using the Experion Auto-mated Electrophoresis System (Bio-Rad). RNA-seq libraries were prepared with the TruSeq Stranded mRNA LT sample preparation kit (Illumina) using both, Sciclone and Zephyr liquid handling robotics (PerkinElmer). Library concentrations were quantified with the Qubit Fluorometric Quantitation system (Life Technologies) and the size distribution was assessed using the Experion Automated Electrophoresis System (Bio-Rad). For sequencing, samples were diluted and pooled into NGS libraries in equimolar amounts. Expression profiling libraries were sequenced on Illumina HiSeq 3000/4000 instruments in 50-base-pair-single-end mode and base calls provided by the Illumina Real-Time Analysis (RTA) software were subsequently converted into BAM format (Illumina2bam) before de-multiplexing (BamIndexDecoder) into individual, sample-specific BAM files via Illumina2bam tools (1.17.3).

Chemical Synthesis of BSJ-03-123, BSJ-03-190/BSJ-bump, YKL-06-102

Synthesis of 6a and 6b

2-((2-(2,6-dioxopiperidin-3-yl)-1,3-dioxoisoindolin-4-yl)oxy)acetic acid (6a). **6a** was prepared according to the literature (Remillard et al., 2017). 3-Hydroxyphthalic anhydride (**1**) (1.64 g, 10 mmol) and 3-aminopiperidine-2,6-dione hydrochloride (**2a**) (1.65 g, 10 mmol) were dissolved in pyridine (40 mL, 0.25 M) and heated to 110°C. After 14h, the mixture was cooled to room temperature and concentrated under reduced pressure. The residue was purification by column chromatography on silica gel (0-10% MeOH/DCM) to give 2-(2,6-dioxopiperidin-3-yl)-4-hydroxyisoindoline-1,3-dione (3a) as a grey solid (2.41 g, 88%). LC-MS: *m/z* 275 [M+1]. To a solution of **3a** (2.19 g, 8 mmol) in 8 mL of DMF was added K_2CO_3 (1.66 g, 12 mmol) and *t*-butyl bromoacetate (**4**) (1.18 mL, 8 mmol) respectively. The mixture was stirred at room temperature for 2h, then diluted with EtOAc and washed once with water then twice with brine. The organic layer was dried over anhydrous sodium sulfate, filtered and concentrated under reduced pressure. The residue was purification by column chromatography on silica gel (5-100%EtOAc/hexanes) to give *tert*-butyl 2-((2-(2,6-dioxopiperidin-3-yl)-1,3-dioxoisoindolin-4-yl)oxy)acetate (5a) as a cream colored solid (2.70 g, 87%). LC-MS: *m/z* 389 [M+1]. **5a** (2.06g, 5.3 mmol) was then dissolved in TFA (53 mL, 0.1M) at room temperature. After 4 hours, the solution was diluted with DCM and concentrated under reduced pressure to give **6a** as a cream colored solid (1.5 g, 85%) was deemed sufficiently pure and carried onto the next step without further purification. LC-MS: *m/z* 333 [M+1]. ^{1}H NMR (500 MHz, DMSO-*d*6) δ 11.09 (s, 1H), 7.79 (dd, *J* = 8.4, 7.4 Hz, 1H), 7.48 (d, *J* =7.4 Hz, 1H), 7.39 (d, *J* = 8.6 Hz, 1H), 5.10 (dd, *J* = 12.8, 5.4 Hz, 1H), 4.99 (s, 2H), 2.93-2.89 (m, 1H), 2.63-2.51 (m, 2H), 2.11-2.03 (m, 1H).

2-((2-(1-methyl-2,6-dioxopiperidin-3-yl)-1,3-dioxoisoindolin-4-yl)oxy)acetic acid (6b). **6b** was synthesized with similar procedures as **6a** from 3-Hydroxyphthalic anhydride (**1**) (328 mg, 2 mmol), 3-amino-1-methylpiperidine-2,6-dione (**2b**) (357 mg, 2 mmol) and *t*-butyl bromoacetate (**4**) (0.295 mL, 2 mmol). **6b** was obtained as an off-white solid (451 mg, 65% yield in 3 steps). LC-MS: *m/z* 347 [M+1]. ^{1}H NMR (500 MHz, DMSO-d_6) δ 13.24 (s, 1H), 7.80 (dd, *J* = 8.5, 7.3 Hz, 1H), 7.48 (d, *J* = 7.3 Hz, 1H), 7.40 (d, *J* = 8.5 Hz, 1H), 5.17 (dd, *J* = 13.0, 5.4 Hz, 1H), 4.99 (s, 2H), 3.02 (s, 3H), 2.99-2.91 (m, 1H), 2.80-2.73 (m, 1H), 2.59-2.52 (m, 1H), 2.09-2.02 (m, 1H). ^{13}C NMR (125 MHz, DMSO) δ 172.24, 170.14, 169.95, 167.17, 165.62, 155.61, 137.26, 133.70, 120.36, 116.76, 116.24, 65.46, 49.82, 31.56, 27.07, 21.65.

Synthesis of BSJ-03-123 and BSJ-03-190/BSJ-Bump

tert-butyl (2-(2-(2-(2-(4-(6-((6-acetyl-8-cyclopentyl-5-methyl-7-oxo-7,8-dihydropyrido[2,3-d]pyrimidin-2-yl)amino)pyridin-3-yl)piperazin-1-yl)ethoxy)ethoxy)ethoxy)ethyl)carbamate (9). To a suspension of Palbociclib (**7**) (100 mg, 0.22 mmol) in DMSO (5 mL) was added *tert*-butyl (2-(2-(2-(2-bromoethoxy)ethoxy)ethoxy)ethyl)carbamate (**8**) (156 mg, 0.44 mmol) and DIPEA (0.115 mL, 0.66 mmol). The mixture was heated to 80°C and kept stirring for 48h. The mixture was then cooled down to room temperature, extracted, dried, filtered and concentrated. The residue was purified by reverse phase HPLC (5-95% MeOH in H_2O) to give **9** (TFA salt) as a yellow solid (103mg, 65%). LC-MS: *m/z* 723 [M+1]. ^{1}H NMR (500 MHz, DMSO-d_6) δ 10.34 (s, 1H), 8.97 (s, 1H), 8.12 (d, *J* = 3.0 Hz,

1H), 7.90 (d, *J* = 9.1 Hz, 1H), 7.64-7.58 (m, 1H), 6.81-6.74 (m, 1H), 5.89-5.78 (m, 1H), 3.93-3.75 (m, 4H), 3.67-3.60 (m, 4H), 3.59-3.55 (m, 2H), 3.55-3.46 (m, 4H), 3.44-3.35 (m, 4H), 3.27 (br, 2H), 3.15-3.01 (m, 4H), 2.42 (s, 3H), 2.32 (s, 3H), 2.28-2.19 (m, 2H), 1.95-1.84 (m, 2H), 1.83-1.71 (m, 2H), 1.64-1.52 (m, 2H), 1.36 (s, 9H). ^{13}C NMR (126 MHz, DMSO) δ 202.38, 160.69, 158.32, 158.08, 157.98, 155.59, 154.77, 145.07, 141.96, 141.83, 134.97, 129.58, 126.24, 115.21, 106.93, 77.61, 69.67, 69.60, 69.52, 69.47, 69.17, 64.24, 54.85, 52.96, 50.95, 45.48, 31.29, 28.21, 27.57, 25.14, 13.65.

N-(2-(2-(2-(2-(4-(6-((6-acetyl-8-cyclopentyl-5-methyl-7-oxo-7,8-dihydropyrido[2,3-d]pyrimidin-2-yl)amino)pyridin-3-yl)piperazin-1-yl)ethoxy)ethoxy)ethoxy)ethyl)-2-((2-(2,6-dioxopiperidin-3-yl)-1,3-dioxoisoindolin-4-yl)oxy)acetamide (10a). To a solution of the **9** (30.5 mg, 0.0422 mmol) in DCM (2 mL) was added TFA (1 mL) and the resulting solution was stirred at room temperature for 1h. The mixture was concentrated and the residue was then dissolved in DMF (1 mL) followed by adding **6a** (14mg, 0.0422 mmol), HATU (33 mg, 0.0844 mmol) and DIPEA (37 μL, 0.211 mmol). The resulting mixture was stirred for 1h at room temperature, then evaporated the solvent and purified by reverse phase HPLC (5-95% MeOH in H_2O) to give **10a** (TFA salt) as a yellow solid (34.4 mg, 87%). LC-MS: *m/z* 937 [M+1]. ^{1}H NMR (500 MHz, DMSO-d_6) δ 11.2 (s, 1H, NH), 9.03 (s, 1H, AR-H), 8.09 (dt, *J* = 10.6, 3.1 Hz, 2H, AR-H), 7.87 (t, *J* = 8.5 Hz, 1H, AR-H), 7.79 (dd, *J* = 8.5, 7.3 Hz, 1H, AR-H), 7.47 (d, *J* = 7.2 Hz, 1H, AR-H), 7.40 (d, *J* = 8.5 Hz, 1H, AR-H), 5.89-5.80 (m, 1H, N-CH), 5.11 (dd, *J* = 12.8, 5.5 Hz, 1H, N-CH), 4.80 (s, 2H, CO-CH_2-O), 3.95-3.82 (m, 4H, 2xO-CH_2), 3.75-3.55 (m, 8H, 4xO-CH_2), 3.54-3.52 (m, 2H, N-CH_2), 3.51-3.45 (m, 2H, N-CH_2), 3.42-3.19 (m, 8H, 4xN-CH_2), 3.02-2.98 (br, 1H, H'$_{N\text{-}C\text{-}CH2}$), 2.65-2.52 (m, 2H, CO-CH_2), 2.44 (s, 3H, CO-CH_3), 2.35 (s, 3H, AR-CH_3), 2.28-2.12 (m, 2H, C-CH_2), 2.05 (ddt, *J* = 15.2, 7.8, 2.8 Hz, 1H, H'$_{N\text{-}C\text{-}CH2}$), 1.98-1.85 (m, 2H, C-CH_2), 1.82-1.74 (m, 2H, C-CH_2), 1.64-1.53 (m, 2H, C-CH_2).^{13}C NMR (126 MHz, DMSO) δ 202.43, 172.82, 169.90, 166.97, 166.72, 165.51, 160.70, 158.33, 158.23, 157.98, 154.92, 154.82, 144.95, 141.95, 141.83, 136.98, 133.03, 129.77, 126.77, 120.40, 116.78, 116.14, 115.35, 107.13, 69.71, 69.65, 69.63, 69.52, 68.83, 67.57, 64.19, 54.90, 53.00, 50.96, 48.85, 45.48, 38.40, 31.32, 30.98, 27.61, 25.19, 22.02, 13.70.

N-(2-(2-(2-(2-(4-(6-((6-acetyl-8-cyclopentyl-5-methyl-7-oxo-7,8-dihydropyrido[2,3-d]pyrimidin-2-yl)amino)pyridin-3-yl)piperazin-1-yl)ethoxy)ethoxy)ethoxy)ethyl)-2-((2-(1-methyl-2,6-dioxopiperidin-3-yl)-1,3-dioxoisoindolin-4-yl)oxy)acetamide (10b). **10b** was synthesized with similar procedures as **10a** from **9** (30.5 mg, 0.0422 mmol) and **6b** (14.6mg, 0.0422 mmol). **10b** was obtained as a yellow solid (33.7 mg, 84%). LC-MS: *m/z* 951 [M+1]. ^{1}H NMR (500 MHz, DMSO-d_6) δ 9.75 (br, 1H, NH), 8.97 (s, 1H, AR-H), 8.10 (d, *J* = 3.1 Hz, 1H, AR-H), 8.03-7.93 (m, 1H, AR-H), 7.87 (d, *J* = 9.1 Hz, 1H, AR-H), 7.85-7.76 (m, 1H, AR-H), 7.64 (dd, *J* = 9.2, 3.2 Hz, 1H, AR-H), 7.50 (d, *J* = 7.3 Hz, 1H, AR-H), 7.40 (d, *J* = 8.5 Hz, 1H, H_{AR}), 5.87-5.76 (m, 1H, N-CH), 5.21-5.10 (m, 1H, N-CH), 4.79 (s, 2H, CO-CH_2-O), 3.91-3.82 (m, 2H, O-CH_2), 3.81-3.77 (m, 2H, O-CH_2), 3.65-3.59 (m, 2H, O-CH_2), 3.58-3.55 (m, 2H, O-CH_2), 3.54 (br, 4H, 2xO-CH_2), 3.47 (t, *J* = 5.8 Hz, 2H, N-CH_2), 3.43-3.36 (m, 2H, N-CH_2), 3.35-3.30 (m, 2H, N-CH_2), 3.30-3.18 (m, 2H, N-CH_2), 3.13-3.04 (m, 2H, N-CH_2), 3.02 (s, 3H, N-CH_3), 2.99-2.91 (m, 2H, N-CH_2), 2.80-2.74 (m, 2H, CO-CH_2), 2.74-2.70 (m, 1H, H'$_{N\text{-}C\text{-}CH2}$), 2.43 (s, 3H, CO-CH_3), 2.32 (s, 3H, Ar-CH_3), 2.29-2.16 (m, 2H, C-CH_2), 2.06 (dtd, J = 13.0, 5.5, 2.4 Hz, 1H, H'$_{N\text{-}C\text{-}CH2}$), 1.95-1.84 (m, 2H, C-CH_2), 1.83-1.72 (m, 2H, C-CH_2), 1.65-1.51 (m, 2H, C-CH_2).^{13}C NMR (126 MHz, DMSO) δ 202.37, 171.75, 169.62, 166.93, 166.67, 165.47, 160.67, 158.32, 158.20, 158.03, 157.95, 154.95, 154.79, 144.90, 141.92, 141.79, 136.98, 133.00, 129.75, 126.78, 120.40, 116.73, 116.12, 115.34, 107.12, 69.68, 69.61, 69.49, 68.81, 67.55, 64.17, 54.86, 52.97, 50.92, 49.38, 45.45, 38.37, 31.30, 31.09, 27.59, 26.61, 25.16, 21.21, 13.68.

Synthesis of YKL-06-102

tert-butyl 2-(4-(6-((6-acetyl-8-cyclopentyl-5-methyl-7-oxo-7,8-dihydropyrido[2,3-d]pyrimidin-2-yl)amino)pyridin-3-yl)piperazin-1-yl) acetate (11). To a suspension of Palbociclib (**7**) (100 mg, 0.22 mmol) in DMSO (5 mL) were added *t*-butyl bromoacetate (**4**) (65 μL, 0.44 mmol) and DIPEA (0.115 mL, 0.66 mmol). The mixture was heated to 80°C and kept stirring for 24h. The mixture was then cooled down to room temperature, extracted, dried, filtered and concentrated. The residue was purified by reverse phase HPLC (5-95% MeOH in H_2O) to give **11** (TFA salt) as a yellow solid (90 mg, 73%). LC-MS: *m/z* 562 [M+1]. ^{1}H NMR (500 MHz, DMSO-d6) δ 10.09 (s, 1H), 8.95 (s, 1H), 8.05 (d, J = 3.0 Hz, 1H), 7.85 (d, J = 9.0 Hz, 1H), 7.49-7.43 (m, 1H), 5.88-5.75 (m, 1H), 3.20-3.13 (m, 6H), 2.67 (t, J = 4.9 Hz, 4H), 2.42 (s, 3H), 2.31 (s, 3H), 2.27-2.18 (m, 2H), 1.89 (br, 2H), 1.82-1.73 (m, 2H), 1.65-1.52 (m, 2H), 1.43 (s, 9H). ^{13}C NMR (126 MHz, DMSO) δ 202.91, 169.67, 161.22, 159.04, 158.74, 155.22, 144.77, 143.88, 142.55, 135.89, 125.21, 115.60, 107.02, 100.00, 80.72, 59.66, 53.36, 52.12, 48.78, 31.78, 28.29, 28.02, 25.58, 14.10.

2-(4-(6-((6-acetyl-8-cyclopentyl-5-methyl-7-oxo-7,8-dihydropyrido[2,3-d]pyrimidin-2-yl)amino)pyridin-3-yl)piperazin-1-yl)-N-(2-(2-(2-(2-((2-(2,6-dioxopiperidin-3-yl)-1,3-dioxoisoindolin-4-yl)amino)ethoxy)ethoxy)ethoxy)ethyl)acetamide (14). To a solution of the **11** (23.7 mg, 0.0422 mmol) in DCM (2 mL) was added TFA (1 mL) and the resulting solution was stirred for 1h at room temperature. The mixture was concentrated to give **12** which was used directly for the next step without further purification. **13** (23.1 mg, 0.0422 mmol), which was synthesized as previously described (Olson et al., 2018), was also dissolved in DCM (2 mL), TFA (1 mL) was added and the mixture was kept stirring for 1h at room temperature. Then the solvent was evaporated and the residue was re-dissolved in DMF (2mL). To the DMF solution were added **12**, HATU (33 mg, 0.0844 mmol) and DIPEA (37 μL, 0.211 mmol). The resulting mixture was stirred for 1h at room temperature, then evaporated the solvent and purified by reverse phase HPLC (5-95% MeOH in H_2O) to give **14** (TFA salt) as a yellow solid (34.4 mg, 77%). LC-MS: *m/z* 936 [M+1]. ^{1}H NMR (500 MHz, DMSO-d_6) δ 9.05 (s, 1H, AR-H), 8.90 (t, *J* = 5.6 Hz, 1H, NH), 8.19 (dd, *J* = 9.6, 2.8 Hz, 1H, AR-H), 8.12 (d, *J* = 2.9 Hz, 1H, AR-H), 7.93 (d, *J* = 9.4 Hz, 1H, AR-H), 7.57 (dd, *J* = 8.6, 7.1 Hz, 1H, AR-H), 7.13 (d, *J* = 8.6 Hz, 1H, AR-H), 7.02 (d, *J* = 7.0 Hz, 1H, AR-H), 5.90-5.75 (m, 1H, N-CH), 5.05 (dd, *J* = 12.8, 5.4 Hz, 1H, N-CH), 4.05 (s, 2H, CO-CH_2-N), 3.73-3.59 (m, 4H, 2xO-CH_2), 3.59-3.54 (m, 4H, 2xO-CH_2), 3.53-3.50 (m, 4H, 2xO-CH_2), 3.49-3.43 (m, 6H, 3xN-CH_2), 3.43-3.25 (m, 6H, 3xN-CH_2), 2.94-2.84 (m, 1H, H'$_{N\text{-}C\text{-}CH2}$), 2.63-2.51 (m, 2H, CO-CH_2), 2.44 (s, 3H, CO-CH_3), 2.35 (s, 3H, AR-CH_3), 2.28-2.15 (m, 2H, C-CH_2), 2.08–2.00 (m, 1H, H'$_{N\text{-}C\text{-}CH2}$), 1.99-1.91 (m, 2H, C-CH_2), 1.86-1.75 (m, 2H, C-CH_2), 1.65-1.53 (m, 2H, C-CH_2). ^{13}C NMR (126 MHz,

DMSO) δ 202.22, 172.82, 170.07, 168.94, 167.27, 163.93, 160.54, 157.29, 157.19, 154.95, 146.39, 143.30, 141.74, 141.59, 136.25, 132.07, 130.81, 117.46, 116.43, 110.71, 109.23, 108.31, 72.16, 70.52, 69.81, 69.77, 69.60, 68.89, 68.71, 60.18, 55.90, 53.12, 50.89, 48.57, 44.97, 43.62, 41.71, 31.27, 30.99, 27.68, 25.27, 22.16, 13.79.

QUANTIFICATION AND STATISTICAL ANALYSIS

Statistical parameters are reported in the figure legends of the paper.

Expression Proteomics BSJ-03-123

Acquired raw data files were processed using the Proteome Discoverer 2.2.0. platform, utilizing the Sequest HT database search engine and Percolator validation software node (V3.04) to remove false positives with a false discovery rate (FDR) of 1% on peptide and protein level under strict conditions. Searches were performed with full tryptic digestion against the human SwissProt database v2017.06 with up to two miscleavage sites. Oxidation (+15.9949 Da) of methionine was set as variable modification, whilst carbamidomethylation (+57.0214 Da) of cysteine residues and TMT 6-plex labelling of peptide N-termini and lysine residues were set as fixed modifications. Data was searched with mass tolerances of ±10 ppm and 0.6 Da on the precursor and fragment ions (CID), respectively. Results were filtered to include peptide spectrum matches (PSMs) with Sequest HT cross-correlation factor (Xcorr) scores of $\geq$1 and high peptide confidence. PSMs with precursor isolation interference values of $\geq$ 50% and average TMT-reporter ion signal-to-noise values (S/N) $\leq$ 10 were excluded from quantitation. Isotopic impurity correction and TMT channel-normalization based on total peptide amount were applied. For statistical analysis and p-value calculation, the integrated ANOVA hypothesis test was used. TMT ratios with p-values below 0.01 were considered as significant.

Expression Proteomics YKL-06-102

Proteome Discoverer 2.1 (Thermo Fisher Scientific) was used for .RAW file processing and controlling peptide and protein level false discovery rates, assembling proteins from peptides, and protein quantification from peptides. MS/MS spectra were searched against a Uniprot human database (September 2016) with both the forward and reverse sequences. Database search criteria are as follows: tryptic with two missed cleavages, a precursor mass tolerance of 20 ppm, fragment ion mass tolerance of 0.6 Da, static alkylation of cysteine (57.02146 Da), static TMT labelling of lysine residues and N-termini of peptides (229.16293 Da), and variable oxidation of methionine (15.99491 Da). TMT reporter ion intensities were measured using a 0.003 Da window around the theoretical m/z for each reporter ion in the MS3 scan. Peptide spectral matches with poor quality MS3 spectra were excluded from quantitation (summed signal-to-noise across 10 channels < 200 and precursor isolation specificity < 0.5), and resulting data was filtered to only include proteins that had a minimum of 3 unique peptides identified. Reporter ion intensities were normalised and scaled using in-house scripts in the R framework. Statistical analysis was carried out using the limma package within the R framework.

Phosphoproteomics

Acquired raw data files were processed using the Proteome Discoverer 2.2.0. platform, utilising the Sequest HT database search engine and Percolator validation software node (V3.04) to remove false positives with a false discovery rate (FDR) of 1% on peptide and protein level under strict conditions. Searches were performed with full tryptic digestion against the human SwissProt database v2017.12 with up to two miscleavage sites. Oxidation (+15.9949 Da) of methionine and phosphorylation (+79.9663 Da) of serine, threonine and tyrosine was set as variable modification, whilst carbamidomethylation (+57.0214 Da) of cysteine residues and TMT 10-plex labelling of peptide N-termini and lysine residues were set as fixed modifications. Data was searched with mass tolerances of ±10 ppm and 0.025 Da on the precursor and fragment ions (HCD), respectively. Results were filtered to include peptide spectrum matches (PSMs) with Sequest HT cross-correlation factor (Xcorr) scores of $\geq$1 and high peptide confidence. The ptmRS algorithm was additionally used to validate phospopeptides with a set score cutoff of 90. PSMs with precursor isolation interference values of $\geq$ 50% and average TMT-reporter ion signal-to-noise values (S/N) $\leq$ 10 were excluded from quantitation. Isotopic impurity correction and TMT channel-normalization based on total peptide amount were applied. For statistical analysis and p-value calculation, the integrated ANOVA hypothesis test was used. TMT ratios with p-values below 0.01 were considered as significant.

Hits identified via global phosphoproteomics (log2 fold change > 0.5 or < -0.5, FDR adj. p-value < 0.05) were mapped on a protein-protein interaction network using the networkx python package. The protein-protein interaction network was queried from the Human Integrated Protein-Protein Interaction rEference (HIPPIE) (Alanis-Lobato et al., 2017). Interactions without PubMed IDs were removed. The resulting subgraph was expanded to include first order neighbors limited to transcriptional regulators for which ENCODE genome localization data was available and visualized using Cytoscape. Kinase substrate prediction was performed with KSEA App (https://casecpb.shinyapps.io/ksea).

RNA Sequencing

NGS reads were trimmed based on quality and adapter sequence content with Trimmomatic in single-end (ILLUMINACLIP:TruSeq3-SE.fa:2:30:10:1:true, SLIDINGWINDOW:4:15, MINLEN:20) mode. The resulting reads were aligned with the "Spliced Transcripts Alignment to a Reference" (STAR) aligner to the hg38 reference genome assembly provided by the UCSC Genome Browser resembling the Genome Reference Consortium GRCh38 assembly. Ensembl transcript annotation from version e87 (December 2016) served as reference transcriptome. Reads were counted using htseq-count. Differential expression analysis was performed on

quantile-normalized read counts using the voom-limma R package. Following thresholds were applied for hit calling: fold change > 1.5 or < -1.5, FDR adj. p-value < 0.05. GO-term enrichment analysis was performed using GOrilla. For the network visualization of enriched GO-terms, parent-child relationships of terms were extracted from the go-basic.obo ontology and the network assembled using the python networkx package.

DATA AND SOFTWARE AVAILABILITY

The accession number for the RNA sequencing data reported in this paper is GEO: GSE116187.

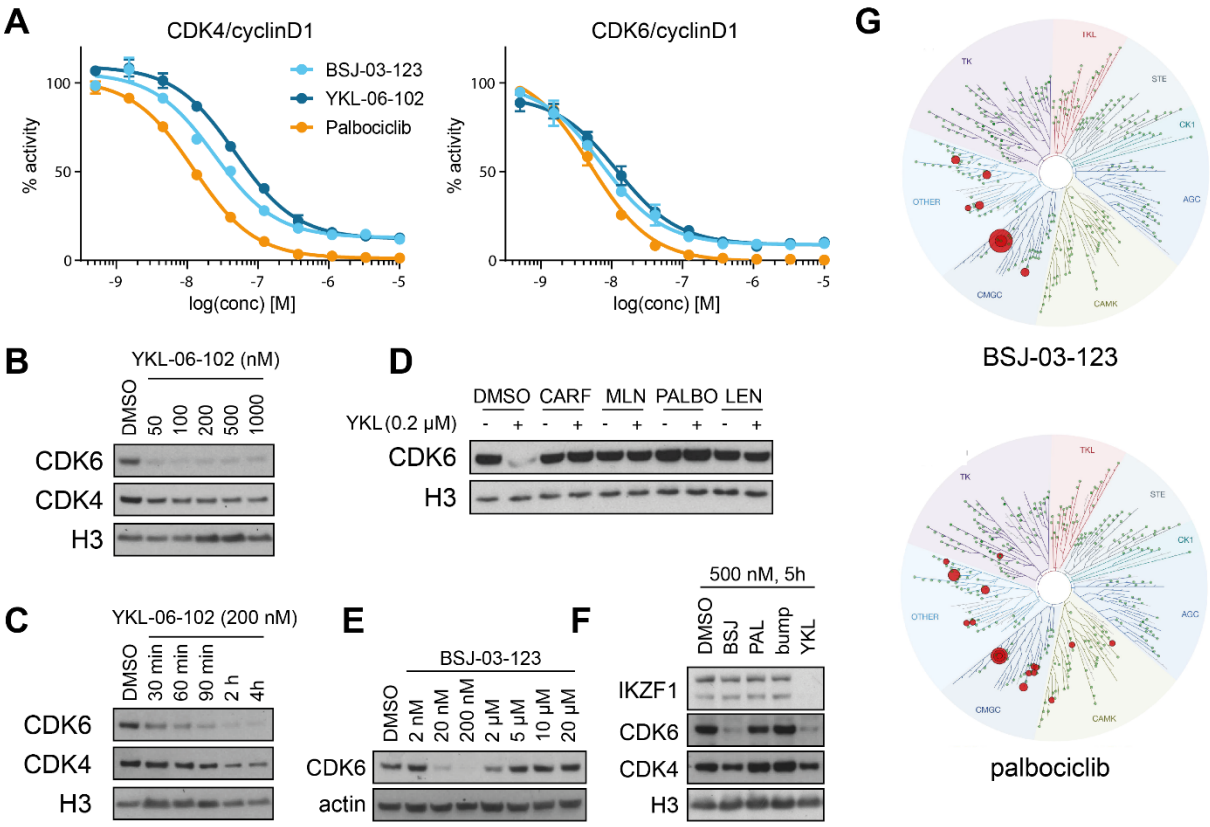

Supplementary Figure 1, related to Figure 1. (A) *In vitro* kinase inhibition assay for palbociclib, YKL-06-102 and BSJ-03-123 on recombinant CDK4/CyclinD1 and CDK6/CyclinD1. **(B)** Immunoblot for CDK4, CDK6 and histone 3 after dose-ranging treatment with YKL-06-102 for 4 hours. **(C)** Immunoblot for CDK4, CDK6 and histone 3 after time-resolved treatment with YKL-06-102 (200 nM). **(D)** Chemical competition experiment. Immunoblot for CDK6 and histone 3 after 1 h pre-treatment with DMSO, 500 nM carfilzomib (proteasome inhibitor, CARF), 1 µM MLN4924 (neddylation inhibitor, MLN), 10 µM palbociclib (PALBO) or 10 µM lenalidomide (LEN), followed by 2 h treatment with DMSO or 200 nM YKL-06-102. **(E)** Immunoblot for CDK6 and actin after extended dose-ranging treatment with BSJ-03-123 for 2 hours. **(F)** Immunoblot for IKZF1, CDK4, CDK6 and histone 3 after prolonged treatment (5h) with 500 nM BSJ-03-123, Palbociclib, YKL-06-102, BSJ-bump or DMSO. **(G)** Comparison of interaction of BSJ-03-123 and palbociclib with 468 human kinases (KINOMEscan). Compounds were tested at 1 µM concentration. Bound kinases are indicated by red circles of size proportional to the percentage of binding to each kinase.

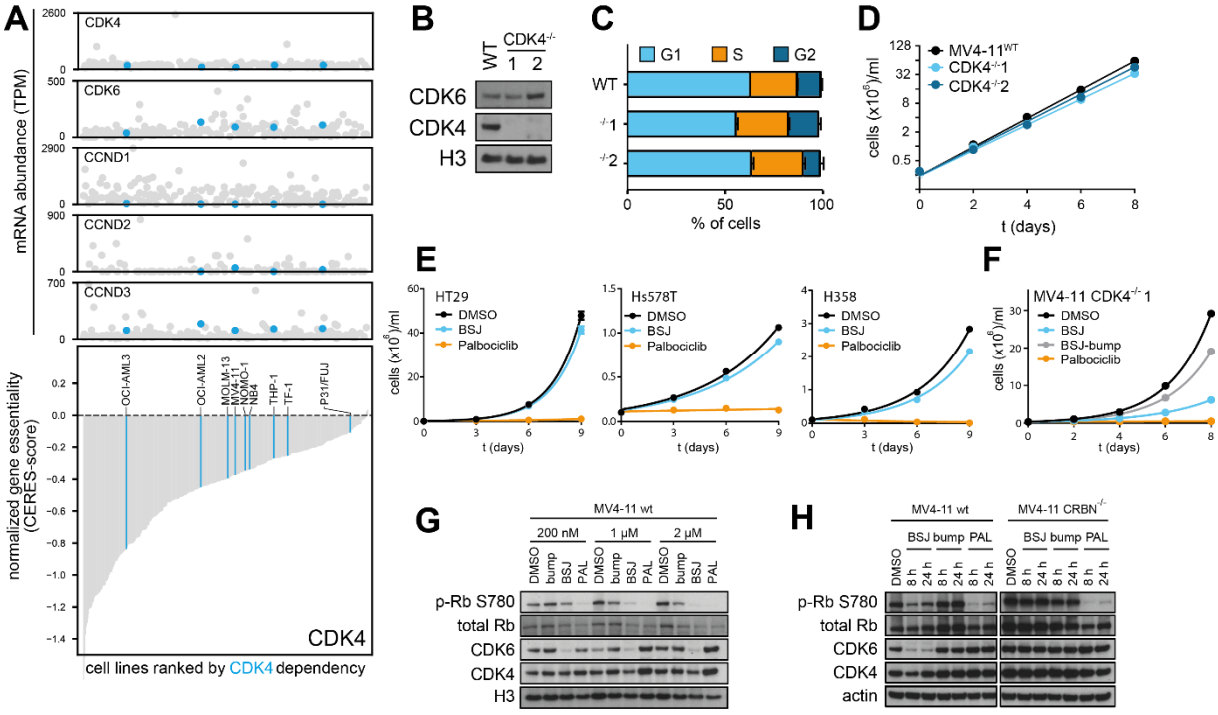

Supplementary Figure 2, related to Figure 3. (A) Bottom: Waterfall plot of 391 cell lines ranked by CKD4 dependency as determined in genome-wide CRISPR/Cas9 screens (Meyers et al., 2017). The CERES essentiality score is normalized for copy number variation of the gene of interest and scaled by setting the median of pan-essential genes to -1. Top: mRNA levels of CDK4, CDK6 and D-type cyclins extracted from RNA sequencing data in cancer cell lines (Klijn et al., 2015). AML cell lines are highlighted in blue. **(B)** Immunoblot for CDK4, CDK6 and histone 3 in MV4-11 wt and two CDK4-deficient clones. **(C)** Cell cycle distribution in *wild-type* and CDK4-deficient MV4-11 as determined by propidium iodide staining **(D)** Growth curves of *wild-type* and CDK4-deficient MV4-11. Cells were counted every 2 days. **(E)** Growth curves of CDK6-independent cell lines HT29, Hs578T and NCI-H358 treated with 200 nM BSJ-03-123, palbociclib or vehicle (DMSO). Cells were counted and re-seeded with drug every 3 days. **(F)** Growth curves of CDK4-deficient MV4-11 treated with 200 nM BSJ-03-123, BSJ-bump, palbociclib or vehicle (DMSO). Cells were counted and treatment refreshed every 2 days. **(G)** Immunoblot for p-Rb S780, total Rb, CDK4, CDK6 and histone 3 after 24 h treatment with BSJ-03-123, palbociclib or BSJ-bump at the indicated concentrations. **(H)** Immunoblot for p-Rb S780, total Rb, CDK4, CDK6 and actin after treatment with 200 nM BSJ-03-123, palbociclib, BSJ-bump or DMSO for the indicated time in *wild-type* or CRBN-deficient MV4-11.

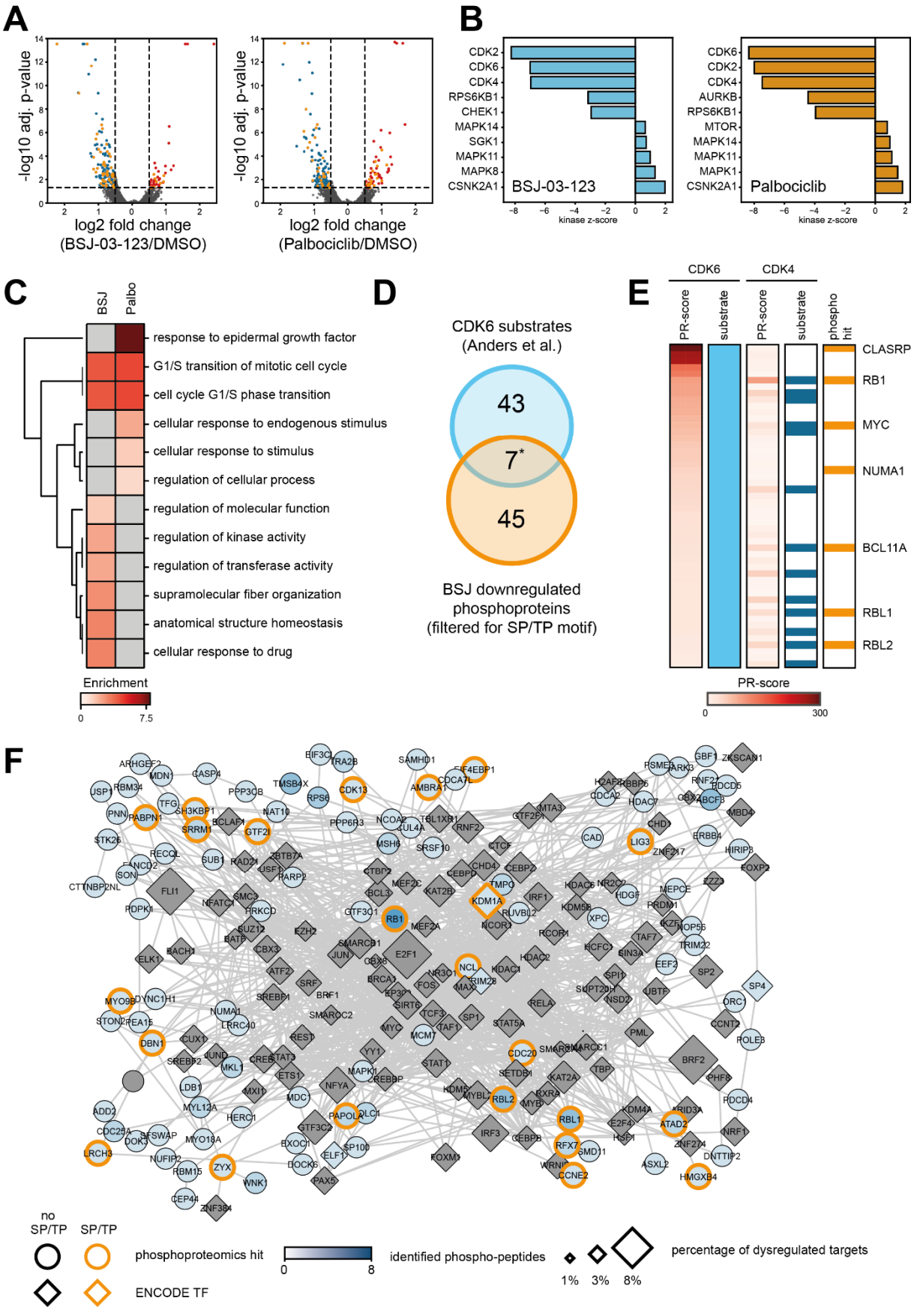

Supplementary Figure 3, related to Figure 4. (A) Global phosphoproteomics. Scatter plots of fold change of peptide phosphorylation relative to DMSO after BSJ-03-123 or palbociclib treatment (200 nM,

2h) versus significance. Downregulated phosphopeptides (log2 FC < -0.5, p-value < 0.05) are highlighted in blue, upregulated phosphopeptides (log2 FC > 0.5, p-value < 0.05) in red. Peptides phosphorylated at a CDK consensus motif SP/TP are highlighted in yellow. **(B)** z-score normalized kinase prediction scores as determined by kinase-substrate enrichment analysis on hits of the global phosphoproteomics experiment. Top 5 significantly enriched and depleted kinases are plotted. **(C)** Clustered heatmap of GO term enrichment analysis of differentially phosphorylated peptides. The color intensities indicate the level of enrichment score of each GO term. **(D)** Intersection of phosphoproteomics data with putative CDK6 targets (Anders et al., 2011). *p = 4.49×10^{-5} (hypergeometric test) **(E)** Relative phosphorylation (PR-) scores for CDK6 and CDK4 of the 50 CDK6 targets from Anders et al. detected in the phosphoproteomics experiment. Downregulated hits from the BSJ-03-123 phosphoproteomics are highlighted in orange. **(F)** Molecular network of palbociclib treatment. Hits identified via global phosphoproteomics were mapped on a protein-protein interaction network and expanded to include first order neighbors limited to ENCODE transcriptional regulators. Node shape distinguishes transcriptional regulators (TR, diamonds) from phosphoproteomics hits (round). Node color represents the number of quantified phosphopeptides. Diamonds are scaled proportional to percentage of dysregulated TR target genes upon treatment. Proteins phosphorylated at CDK consensus motif (SP/TP) are annotated by edge color. Edges represent physical interaction between proteins.

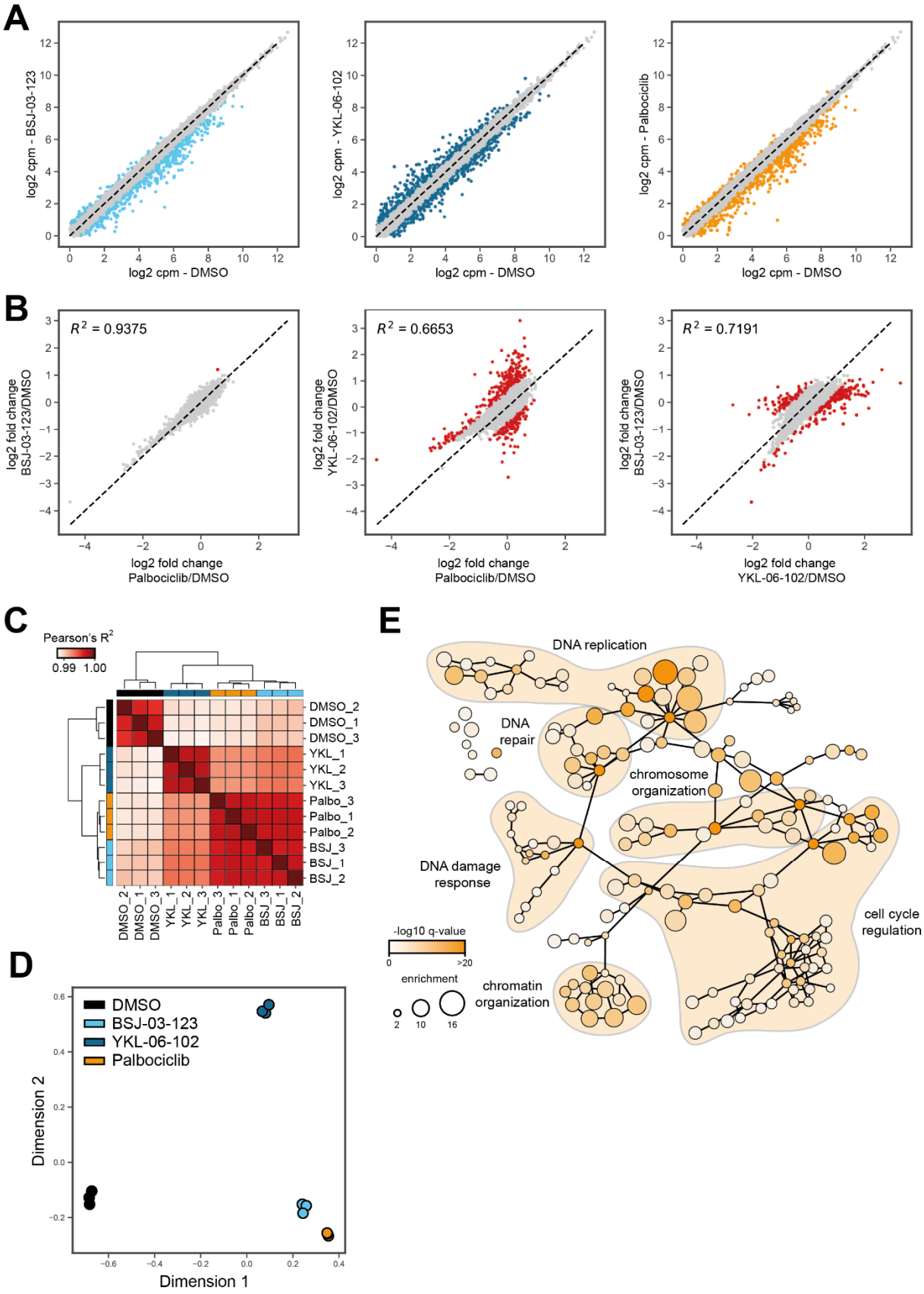

Supplementary Figure 4, related to Figure 4. (A) Scatter plots of expression levels for each gene in MV4-11 treated with BSJ-03-123, YKL-06-102 or palbociclib (200 nM, 6h) compared to DMSO. Significantly differentially expressed genes are highlighted. **(B)** Scatter plots of pairwise comparisons of

gene expression changes upon BSJ-03-123, YKL-06-102 or palbociclib treatment (200 nM, 6h). log2 transformed fold changes relative to DMSO control are plotted for each treatment. Significantly differentially expressed genes are highlighted in red. **(C)** Clustered heat map depicting the Pearson correlation coefficient of pairwise comparisons between technical replicates of the RNA sequencing experiment in MV4-11. **(D)** MDS plot of individual technical replicates of the RNA sequencing experiment in MV4-11. **(E)** Functional network of palbociclib treatment. Nodes represent GO-terms enriched among genes that are differentially expressed upon Palbociclib treatment, scaled by magnitude and color coded by significance of enrichment. Edges represent parent-child relationships of GO-terms.

Supplementary Table 1, related to Figure 1. Biochemical characterization of probes used in this study.

compound	IC50 CDK4-cyclin D1 (nM)	IC50 CDK4-cyclin D3 (nM)	IC50 CDK6-cyclin D1 (nM)	IC50 CDK6-cyclin D3 (nM)	IC50 CRBN (µM)*
Palbociclib	13.7	19.5	6.2	30.7	n.d.
YKL-06-102	74.6	47.8	13.5	305.7	2.2
BSJ-03-123	41.6	31.2	8.7	228.7	2.2
BSJ-bump	19.9	41.1	4.2	95.4	inactive

*lenalidomide 4.62 µM
n.d.=not determinded

2.2 Identification of genetic determinants of sensitivity to targeted protein degradation

2.2.1 Prologue

In this project, we started exploring potential resistance mechanisms to targeted protein degradation by mapping the cellular effectors required for small molecule degraders via genome-wide CRISPR/Cas9 screens. Comparing five different degraders that hijack three E3 ligase substrate receptors, we identified both shared as well as compound-specific determinants of drug efficacy. As expected, KO of the substrate receptor conferred strong resistance to the treatment. Furthermore, small molecule degrader efficacy depends on integrity of the regulatory machinery governing ubiquitination, including the neddylation cascade, the COPS signalosome and substrate receptor exchange factors.

The CRISPR/Cas9 screens presented herein were executed by M Jaeger. The author of this thesis performed the computational analysis and generated the figures. C Sin performed network analysis. C Mayor-Ruiz and GE Winter led the project.

These results have been published as part of a bigger project in:

C Mayor-Ruiz, MG Jaeger, S Bauer, M Brand, C Sin, A Hanzl, AC Mueller, J Menche, GE Winter, **Plasticity of the Cullin-RING Ligase Repertoire Shapes Sensitivity to Ligand-Induced Protein Degradation**, *Molecular Cell* (2019)

2.2.2 Results

To identify the genetic requirements for small molecule degrader sensitivity, we assembled a panel of well-characterized PROTACs and molecular glues covering a range of different target spectra and harnessed E3 ligases (**Fig 9A**). Three molecules hijack the $CRL4^{CRBN}$ ligase complex to induce degradation of CDK9 (THAL-SNS-032), GSPT1 (CC-885) or BRD4 and other BET proteins (dBET6). A second BET PROTAC shares the warhead of dBET6, but instead recruits a $CRL2^{VHL}$ E3 ligase (ARV-771). The last molecule is a molecular glue that induces degradation of RBM39 via a $CRL4^{DCAF15}$ complex (**Fig 9B**).

A

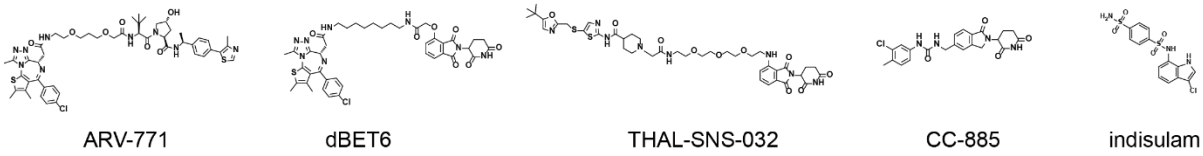

B

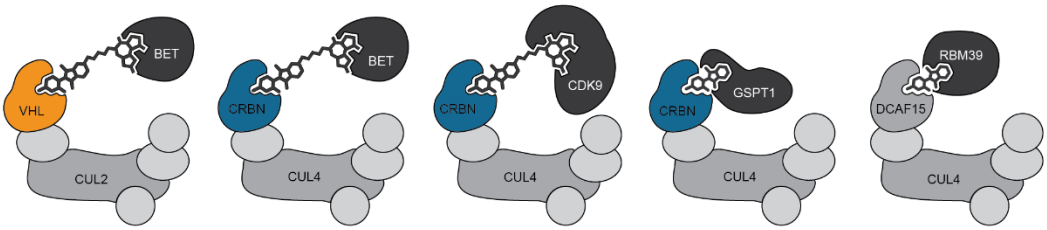

	ARV-771	dBET6	THAL-SNS-032	CC-885	indisulam
target	BET proteins	BET proteins	CDK9	GSPT1	RBM39
E3 ligase	$CRL2^{VHL}$	$CRL4^{CRBN}$	$CRL4^{CRBN}$	$CRL4^{CRBN}$	$CRL4^{DCAF15}$
modality	PROTAC	PROTAC	PROTAC	molecular glue	molecular glue

Figure 9 (**A**) Chemical structures of the degraders utilized in this study. (**B**) Overview of the target, the hijacked E3 ligase and the degradation modality of each molecule.

We performed genome-wide CRISPR/Cas9 drug resistance screens in the near-haploid leukemia cell line KBM7 using the Brunello sgRNA library (Doench et al., 2016). Cells were cultured under drug selective pressure for 20 days (**Fig 10A**) and subjected to next-generation sequencing to measure sgRNA abundance. As expected, sgRNAs targeting the co-opted substrate receptor were consistently found enriched upon selection with the respective degrader (**Fig 10B, 10C**). Unbiased Gene Ontology (GO) term analysis on the hits identified in our five screens revealed an enrichment of Cullin RING ligase complex subunits, as well as factors involved in the regulation of protein deneddylation, such as the COP9 signalosome (**Fig 10D**).

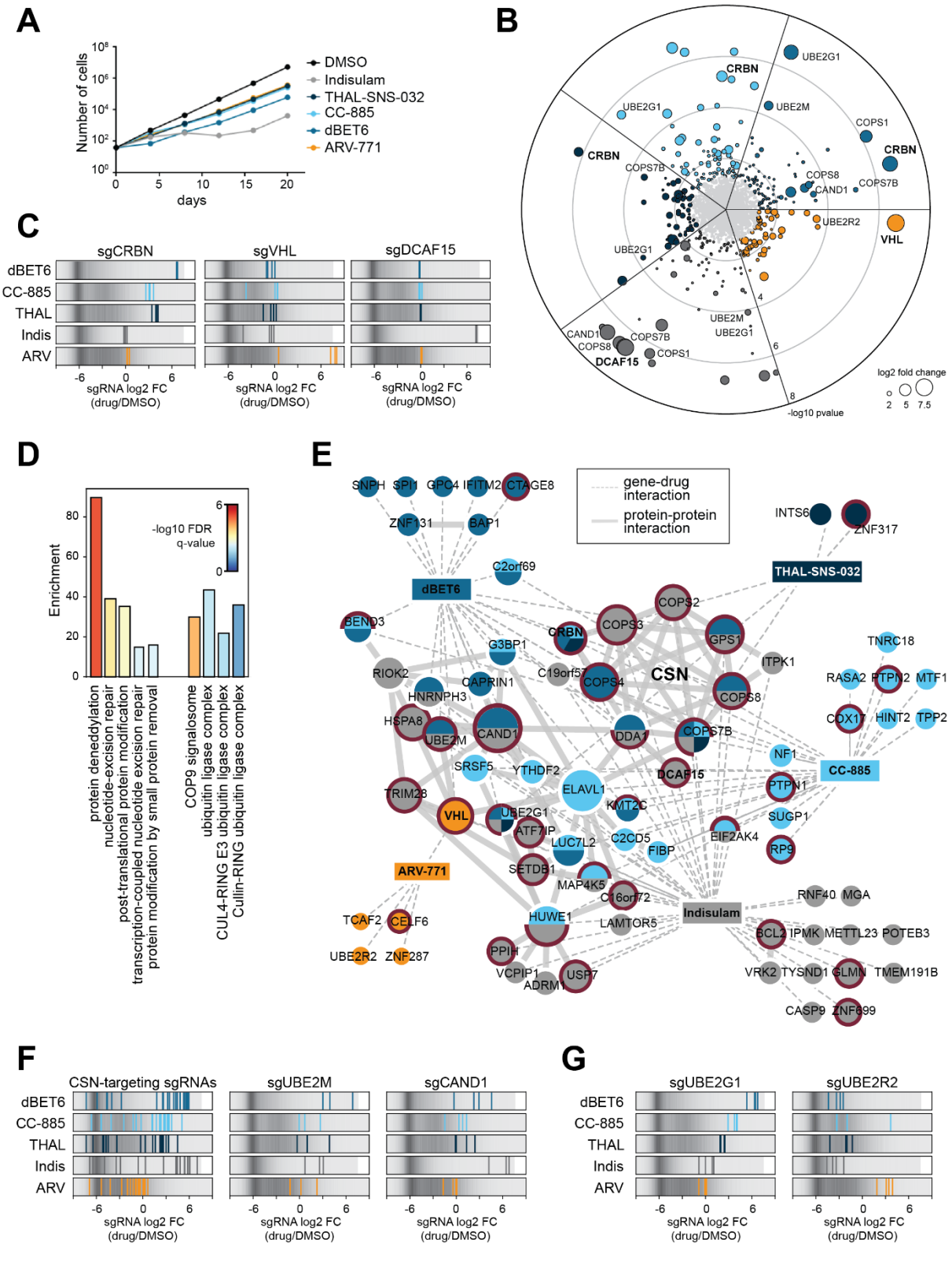

Figure 10 (**A**) Growth curves of the CRISPR/Cas9-mutagenized cell populations treated with degrader or vehicle. (**B**) Polar plot depicting enrichment of sgRNAs in the genome-wide CRISPR/Cas9 positive selection screens. Bubble size represents fold change over vehicle control, radial position indicates significance. (**C**) Enrichment of individual sgRNAs targeting the substrate receptors CRBN, VHL and DCAF15. Background represents the overall distribution of all sgRNAs in the respective screen. (**D**) Gene Ontology (GO) terms of Biological Processes (left) and Cellular Component (right) enriched among genes found enriched in at least one

screen (FDR q-value < 0.2). (**E**) Network analysis highlights shared and degrader-specific hits. Significant hits of each screen (FDR q-value < 0.05) were clustered based on protein-protein interactions (solid lines) and gene-drug interactions (dashed lines). Nodes are scaled based on connectivity and colored to indicate the screen. Strongest modulators (median sgRNA rank < 1000) are highlighted in red. (**F**-**G**) As C, for sgRNAs targeting regulators of CRL plasticity or E2 ubiquitin ligase genes.

Network analysis allowed us to further disentangle degrader-specific resistance genes from shared factors (**Fig 10E**). In line with the GO term enrichment analysis, several subunits of the COP9 signalosome are shared dependencies of CRL4-based degraders, irrespectively of implicated substrate receptor. Interestingly, none of these regulators of deneddylation appear to be determinants of sensitivity for the $CRL2^{VHL}$-based PROTAC (**Fig 10F**). Genetic ablation of other regulators of CRL activity, such as the ligase responsible for Cullin neddylation (UBE2M) or the substrate receptor exchange factor CAND1, can also confer resistance to multiple small-molecule degraders, indicating maintenance of CRL plasticity as a crucial determinant of sensitivity to this new pharmacology (**Fig 10F**).

Apart from general regulatory factors, the screens also highlighted drug-specific resistance genes. We identified UBE2G1 as a requirement for efficacy of all $CRL4^{CRBN}$-based degraders (**Fig 10G**), in line with previous studies that indicate it as the E2 enzyme associated with this complex (Lu et al., 2018). Our data further indicates that this interaction is also shared by the $CRL4^{DCAF15}$ ligase. Similarly, the significant enrichment of sgRNAs targeting UBE2R2 in the ARV-771 screen could suggest a comparable role as E2 ubiquitin-conjugating enzyme for $CRL2^{VHL}$ E3 ligases (**Fig 10G**). Drug-specific resistance genes can also be connected to biology of the target instead of impacting on the functionality of the ubiquitination machinery. For example, the resistance to the CDK9-degrader THAL-SNS-032 conferred by the INTS6 subunit of the integrator complex (**Fig 10B**) is likely related to its role in transcriptional regulation (Baillat et al., 2005).

Integration of five genetic drug resistance screens on small molecule degraders harnessing different E3 ligase complexes revealed shared and compound-specific resistance genes. Our data indicates that components of the co-opted CRL complexes and general regulators of the ubiquitination machinery are important determinants of efficacy of ligand-induced targeted protein degradation, while target-specific resistance genes were observed less frequently. Further studies are however needed to validate these findings in clinically more relevant experimental models.

2.3 Systematic characterization of genetic resistance mutations to PROTACs

2.3.1 Prologue

From our genetic screens, it emerged that the novel pharmacology of targeted protein degradation is subject to novel resistance mechanisms. In contrast to other targeted therapies, where most resistance mechanisms converge on the drug target or its signaling network, efficacy of small molecule degraders requires the correct functioning of complex protein machineries. Understanding the rules governing resistance to targeted protein degradation will be decisive to devise strategies to limit its emergence or overcome it with rational treatment protocols.

Here we set out to systematically chart genetic mutations that confer resistance to PROTAC degraders co-opting the CRL substrate receptors (SRs) most utilized in the field, CRBN and VHL. To identify potential gatekeeper-like mutations that would affect drug binding to the substrate receptor, we queried all SR residues at the PROTAC binding interface in a saturating mutagenesis experiment. Many of the resistance-conferring residues cluster around the ligand binding pocket. Others appear to affect protein-protein contacts between BRD4 and the E3 ligase or core secondary structures, possibly resulting in substrate receptor destabilization.

To further investigate the clinical relevance of the identified resistance mutations, we set up an experimental model of spontaneous drug resistance. Targeted sequencing of putative resistance genes in drug-resistant cellular pools recapitulated some of the mutations affecting the substrate receptor. Furthermore, we detected resistance-conferring variants in other components of the hijacked CRL complex, but not in general regulators of CRL activity. We detected quantitative and qualitative differences in emergence of PROTAC resistance depending on the recruited substrate receptor. Specifically, spontaneous resistance to a CRBN-based PROTAC was more frequent and characterized by more deleterious truncating mutations, compared to the equivalent VHL-based degrader.

This chapter collects data intended for publication in 2020. The author of this thesis designed the project together with GE Winter and planned and performed the majority of experiments and related bioinformatic analyses. H Imrichova analyzed the saturating mutagenesis experiment.

2.3.2 Results

Experimental system

The human genome encodes for about 600 different E3 ligases, but only four of them have so far been successfully co-opted by PROTACs. Significant efforts are therefore been made in the field to identify novel E3 ligands to expand the targetable E3 ligase space. We hypothesized the existence of differences in the frequency or modality of PROTAC resistance depending on the hijacked E3 ligase, a feature that would be crucial to thoroughly understand in order to optimize the discovery efforts of novel E3 ligase binders.

To test this hypothesis, we designed our experiments around two well-characterized PROTACs, dBET6 and ARV-771 (**Fig 11A**). Both molecules share JQ1 as the target-binding warhead, thus degrading BRD4 and related BET proteins. To our knowledge, no genetic resistance mutations to JQ1 have been reported so far, so the experimental system favors detection of resistance on the side of the ubiquitin machinery. The two molecules differ by the recruited E3 ligase: ARV-771 hijacks a CRL2 complex via the substrate receptor VHL, whereas dBET6 recruits a $CRL4^{CRBN}$ E3 ligase (**Fig 11B**). Of note, the two SRs have very different essentiality profiles based on CRISPR/Cas9-based systematic cataloguing of genetic vulnerabilities in 558 cancer cell lines (DepMap, 2019; Meyers et al., 2017). While VHL is essential (to a similar extent as core essential genes, such as ribosomal proteins) in almost all cell lines tested, genetic disruption of CRBN has barely any effect on cell viability and proliferation (**Fig 11C**). Importantly, this essentiality difference is maintained also in our cellular model of choice, the near-haploid human leukemia cell line KBM7 (**Fig 11D**). Both molecules have similar potency, with EC_{50} in KBM7 of about 10 nM (**Fig 11E**). Taken together, we believe that ARV-771 and dBET6 are excellent chemical probes to study the relevance of the E3 ligase machinery in the emergence of resistance to small molecule degraders.

Mapping of substrate receptor residues conferring PROTAC resistance via saturating mutagenesis

The substrate receptor is the subunit of the CRL complex that is directly engaged by the PROTAC. Moreover, its knockout conferred strong resistance in the genome-wide CRISPR screens (chapter 2.2) for all degraders. Thus, we first focused our investigations on VHL and CRBN. To systematically map resistance-conferring mutations, we designed a saturating mutagenesis library in which each residue within 10 Å of the PROTAC-binding interface (PDB: 5T35, 6BOY) was substituted by each other possible amino acid (**Fig 12A**). This resulted in a library of approximately 1450 and 1750 variants for VHL and CRBN, respectively.

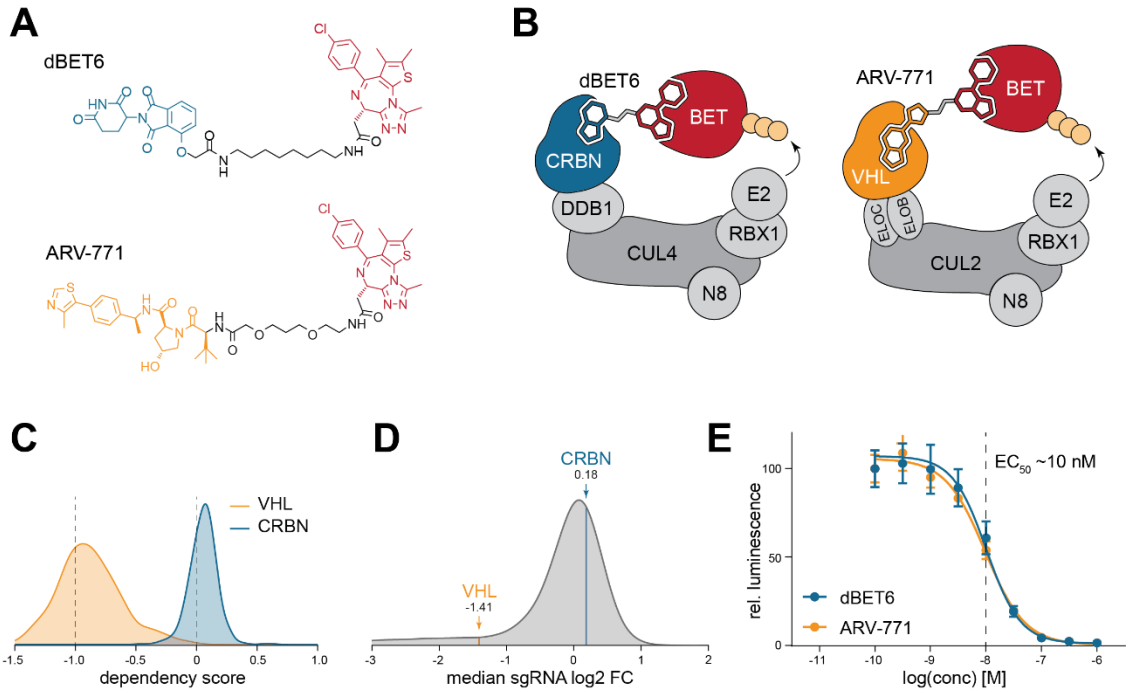

Figure 11 (**A**) Chemical structures of dBET6 and ARV-771. The shared warhead based on JQ1 is highlighted in red, the E3 recruiting moiety in blue and orange, respectively. (**B**) Schematic representation of the ternary complexes formed by the two PROTACs. (**C**) Distribution of normalized dependency scores across 558 cancer cell lines as determined by genome-wide CRISPR/Cas9 screens. A dependency score of -1 is equivalent to the median sgRNA depletion of a set of core essential genes. (**D**) Essentiality of VHL and CRBN in the utilized KBM7 cell line. The log2 fold change of sgRNA abundance (median of 4 sgRNAs per gene) upon a 20-day depletion screen is plotted. (**E**) Dose-response curves of dBET6 and ARV-771 treatment in KBM7 determined by 3-day Cell Titer Glo viability assay.

Colorectal carcinoma RKO cells, genetically engineered to be deficient for CRBN or VHL, were reconstituted with the respective variant library at a low titer and treated with dBET6 or ARV-771 for 7 days to enrich for resistance-conferring mutations. The abundance of individual variants was then quantified by next-generation sequencing (**Fig 12B**).

Several mutations were enriched upon drug exposure compared to vehicle-treated controls. Some residues appear to be of particular relevance, as PROTAC efficacy is abrogated upon change to most other amino acids. Importantly, these include positive controls such as VHL W88, Y98, S111, H115 and W117 (**Fig 12C, 12E**), which have been reported to mediate binding of the hydroxylated HIF1α peptide that structurally resembles the small-molecule VHL ligand (Min et al., 2002). Similarly, CRBN residues Y384 and W386, which are mutated in the CRBN$^{YW/AA}$ variant defective in IMiD binding (Lopez-Girona et al., 2012), were also enriched, validating our approach (**Fig 12D, 12H**).

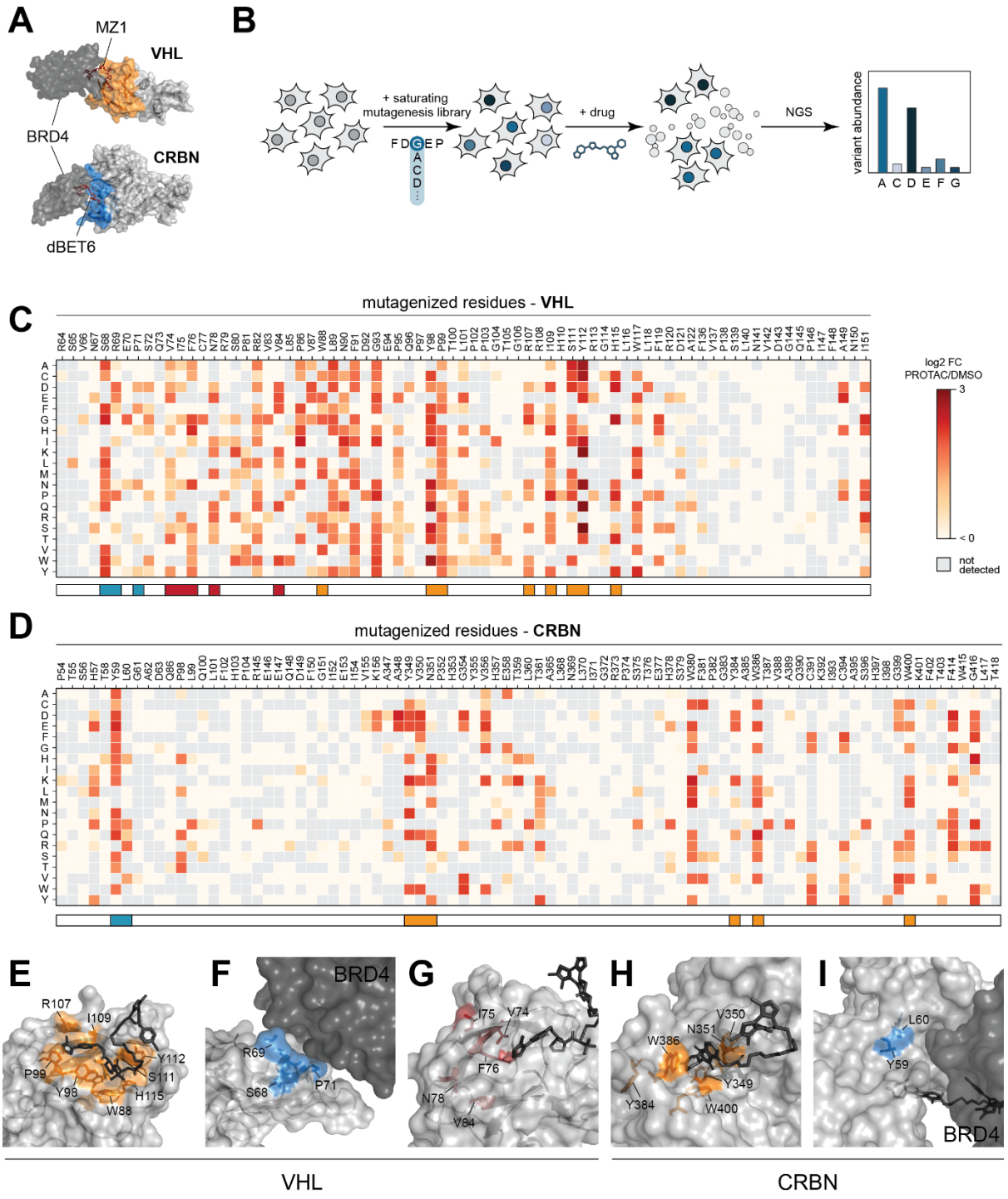

Figure 12 (**A**) Design of saturating mutagenesis libraries based on publicly available structures (PDB, CRBN: 6BOY, VHL: 5T35). Mutagenized residues in proximity of the PROTAC-binding interface are highlighted in color. (**B**) Overview of the experimental workflow. (**C**) Heatmap of resistance-conferring variants in VHL. Enrichment after 7-day treatment with 500 nM ARV-771 over vehicle is plotted. Residues displayed in (E-G) are highlighted in the respective color. (**D**) Heatmap of resistance-conferring variants in CRBN. Enrichment after 7-day treatment with 500 nM dBET6 over vehicle is plotted. Residues displayed in (H-I) are highlighted in the respective color. (**E-G**) Mapping of VHL residues determining ARV-771 efficacy on published structures (PDB: 5T35). Exemplary residues (E) at the liganded pocket, (F) at the interface with BRD4 (dark gray) and (G) in the structural core are shown. (**H-**

I) Mapping of CRBN residues determining dBET6 efficacy on published structures (PDB: 6BOY). Exemplary residues (H) at the liganded pocket and (I) at the interface with BRD4 (dark gray) are shown.

Variants conferring resistance to the CRBN-based degrader dBET6 were concentrated on few hotspots on the protein surface. Y349, V350, N351 and W400 are localized at the ligand interface (similarly to W386) and are likely gatekeeper-like residues that upon mutation hinder PROTAC binding (**Fig 12D, 12H**). A second cluster of variants is formed by H57, Y59 and L60. These residues are situated rather in proximity of the target BRD4 and might therefore be required for the cooperative formation of a ternary complex or conversely sterically hinder BRD4 recruitment when mutated to bulky or charged amino acids (**Fig 12D, 12I**).

VHL resistance mutations are instead more widespread. A large cluster of residues between V74 and G93 is localized in the core of the substrate receptor and contribute to the beta-sheets that form its structural scaffold. These mutants are likely to destabilize VHL altogether or induce conformational changes that interfere with formation of a ternary complex (**Fig 12C, 12G**). In a similar fashion to CRBN, other determinants of resistance are situated at the PROTAC-binding site (P99, R107, I109, Y112) (**Fig 12E**) or in proximity of the target protein (S68, R69, P71) (**Fig 12F**).

In summary, saturating mutagenesis proves to be a powerful method to systematically interrogate and identify resistance-conferring residues and a preliminary analysis allows to postulate theories about the potential mechanism of drug resistance. Of course, individual mutations will need to be functionally characterized to confirm our hypotheses. It will furthermore be important to verify whether these mutations can also arise in spontaneous drug resistance models and in patient samples.

Qualitative and quantitative analysis of spontaneous PROTAC resistance

We next set out to further investigate the emergence of PROTAC resistance in a spontaneous resistance model. In brief, near-haploid KBM7 cells were exposed to a one-time treatment with high doses (10X to 50X EC_{50}) of dBET6 or ARV-771 and resistant clones were monitored for outgrowth over 3 weeks.

First, we estimated resistance rates by fitting a binomial distribution to the number of wells in which outgrowth of resistant clones was observed. Resistance rates are inversely correlated with drug concentration and ranged between $1:10^5$ and $1:10^6$ at the highest tested concentrations. Importantly, resistance to dBET6 was about 10-fold more frequent than to ARV-771, probably due to differential essentiality of the co-opted substrate receptors (**Fig 13A**). No clonal outgrowth was observed upon treatment with the BET inhibitor JQ1,

suggesting that the mechanism of resistance is based on disruption of the degradation machinery and not on target biology.

To identify genetic mutations driving the resistance, we subjected pools of drug-resistant cells to targeted sequencing of putative resistance genes via hybridization-based capture coupled to next-generation sequencing (**Fig 13B**). We assembled a panel of 29 genes identified in the CRISPR screens described in chapter 2.2, comprising subunits of the CRL complexes, the related E2s, SR exchange factors and regulators of the neddylation and de-neddylation cascades (**Table 1**).

Gene	Class
CRBN	$CRL4^{CRBN}$ subunit
CUL4A	$CRL4^{CRBN}$ subunit
CUL4B	$CRL4^{CRBN}$ subunit
DDB1	$CRL4^{CRBN}$ subunit
RBX1	$CRL4^{CRBN}$/$CRL2^{VHL}$ subunit
VHL	$CRL2^{VHL}$ subunit
CUL2	$CRL2^{VHL}$ subunit
ELOB	$CRL2^{VHL}$ subunit
ELOC	$CRL2^{VHL}$ subunit
UBE2G1	E2 enzyme
UBE2R2	E2 enzyme
BRD2	target
BRD3	target
BRD4	target

Gene	Class
NAE1	neddylation
UBA3	neddylation
UBE2M	neddylation
UBE2F	neddylation
CAND1	SR exchange
CAND2	SR exchange
GPS1	de-neddylation
COPS2	de-neddylation
COPS3	de-neddylation
COPS4	de-neddylation
COPS5	de-neddylation
COPS6	de-neddylation
COPS7A	de-neddylation
COPS7B	de-neddylation
COPS8	de-neddylation
COPS9	de-neddylation

Table 1 List of genes in the targeted sequencing panel and rationale for inclusion.

Several of the identified mutations affect the substrate receptor directly (**Fig 13C**). For CRBN, we detected a predominance of deleterious frameshift mutations and premature stop codons, whereas more subtle point mutations were comparatively more frequent in VHL (**Fig 13D**). Many of the point mutations recapitulate our findings from the saturating mutagenesis screens, most notably CRBN^{Y59C} or VHL^{S111R} and VHL^{Y112C}. The VHL missense mutations conferring ARV-771 resistance have furthermore all been described in cancer patient samples, particularly renal cell carcinoma (Tate et al., 2018), thereby underscoring the clinical relevance of our approach.

While dBET6 resistance mutations affected almost exclusively CRBN itself, mutations on other subunits of the CRL complex were also enriched in ARV-771 resistant cells (**Fig 13C**). This could again be explained by the difference in essentiality: the lower fitness cost associated with CRBN loss of function favors the accumulation of deleterious frameshift mutations in the SR that overshadow the more moderate resistance mutations we found in CRL2^{VHL}. Importantly, mutations in general regulators of CRL activity, such as effectors of the neddylation cascade or the COP9 signalosome, appear to be much more infrequent, so cross-resistance to degraders that utilize different substrate receptors is unlikely to emerge.

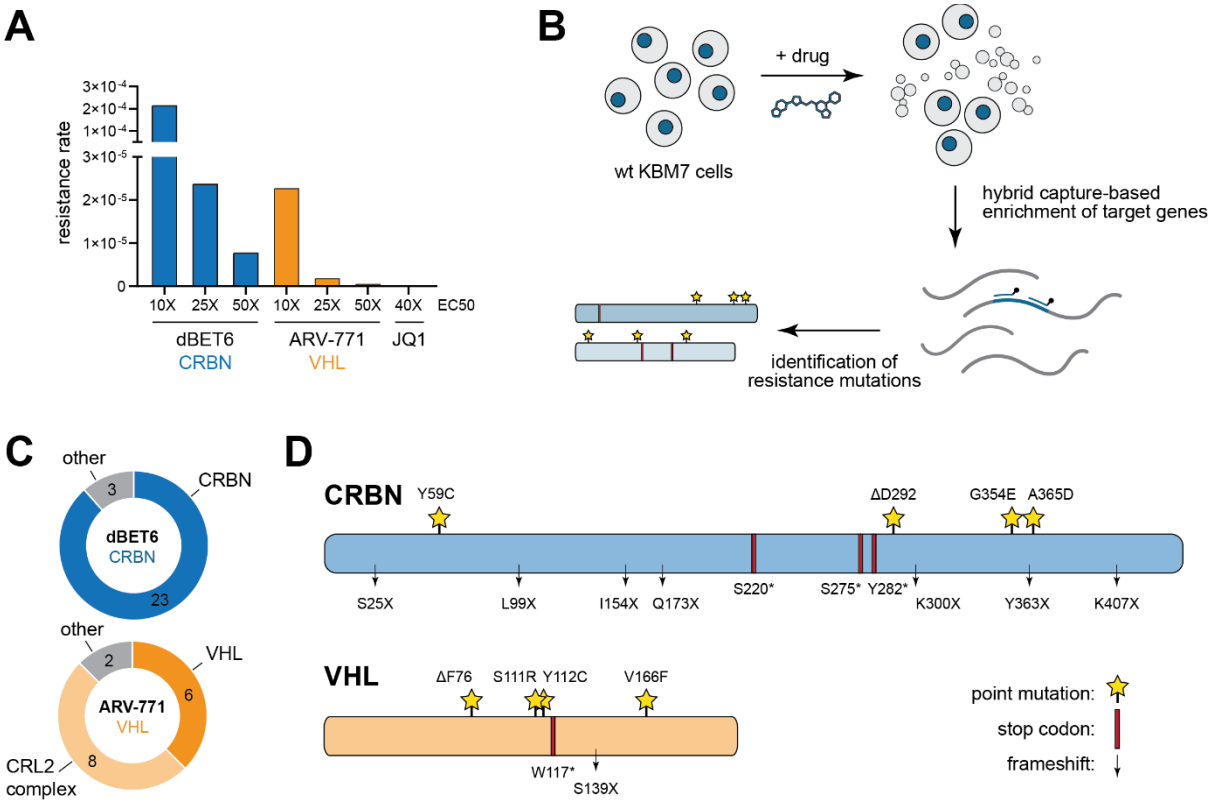

Figure 13 (**A**) Rate of spontaneous resistance in KBM7 cells treated with a single dose of dBET6 or ARV-771. (**B**) Experimental workflow for the identification of spontaneous resistance mutations via hybrid capture sequencing. (**C**) Distribution of identified mutations across components of the CRL machinery. (**D**) Schematic representation of the resistance mutations affecting CRBN and VHL.

Mapping of the ARV-771 resistance mutations on published structures of the CRL2^{VHL} E3 ligase complex revealed a clustering at important interaction surfaces (**Fig 14A**). VHL^{S111R} and VHL^{Y112C} likely act as classical gatekeeper mutations by modifying the drug-binding pocket: the hydroxyl group of S111 is a known hydrogen-bonding partner of the HIF1α peptide that guided the design of the small-molecule VHL ligand (Hon et al., 2002), whereas based on structural data, mutation of Y112 could affect interactions with the PROTAC linker (Gadd et al., 2017). F76 is buried within the protein, but computational studies suggested that its deletion enlarges and modifies the HIF1α binding cavity and could therefore interfere with PROTAC binding (Limaverde-Sousa et al., 2013) (**Fig 14B**, left panel).

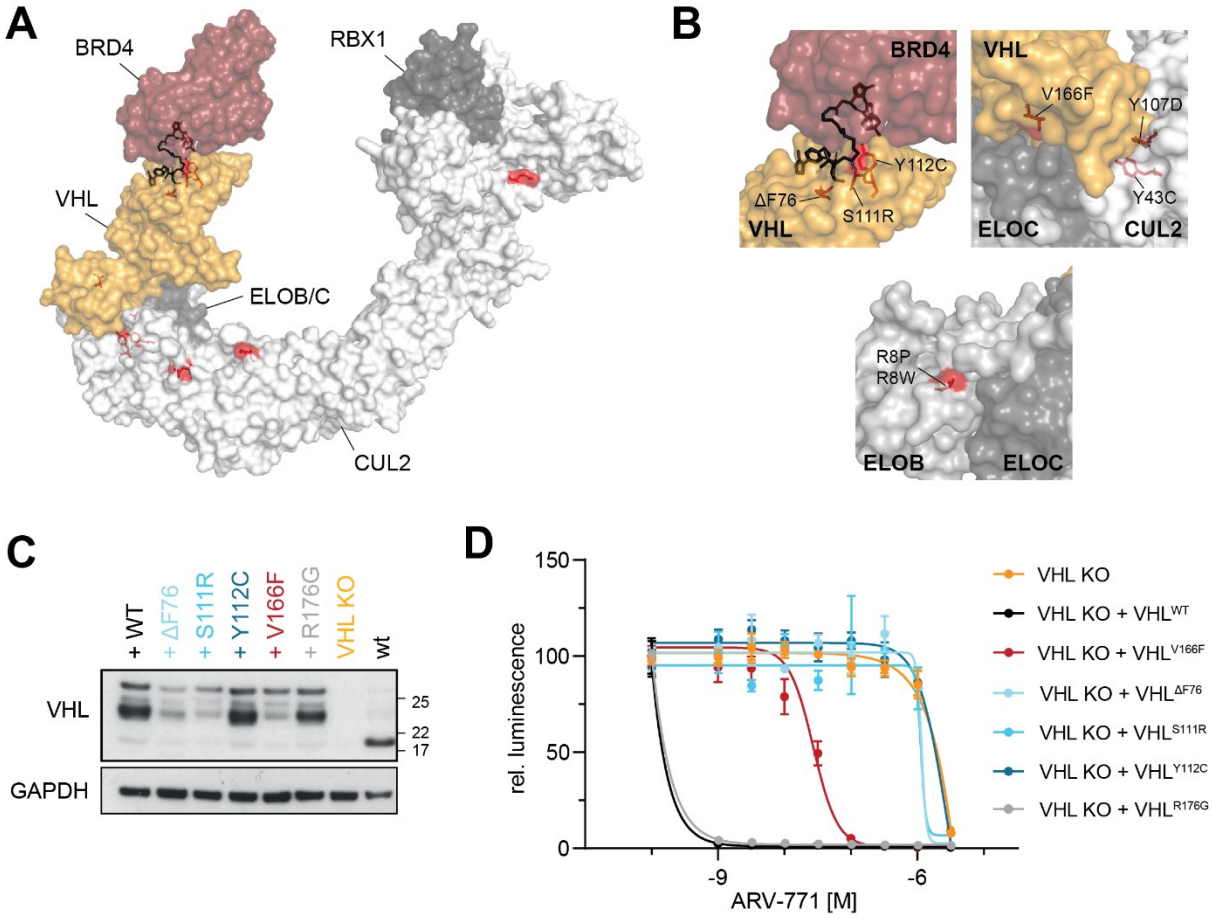

Figure 14 (**A**) Resistance-conferring residues (red) mapped on the structure of the CRL2^{VHL} complex (PDB: 5T35, 5N4W) (**B**) Zoom-in to mutations at critical interfaces: PROTAC-binding pocket on VHL (left), VHL:CUL2:ELOC (right) and ELOB:ELOC interaction surfaces (bottom). (**C**) Stable overexpression of VHL (p30 isoform) harboring identified mutations in RKO cells. (**D**) Dose-response curves ARV-771 treatment in VHL-mutant RKO cell lines determined by 3-day Cell Titer Glo viability assay.

Other mutated residues are located at protein-protein interaction surfaces and could therefore interfere with assembly and functionality of the CRL2^{VHL} complex. The residues Y43 and Y107 on CUL2 contribute to the binding surface to VHL and their mutation likely hinders incorporation of VHL into functional CRL2 complexes (**Fig 14B**, right panel). Similarly, the

VHL^{V166F} mutation could affect interaction with the adaptor protein ELOC (**Fig 14B**, second panel). Finally, the two substitutions of R8 on ELOB with bulky amino acids appear to interfere with dimerization with ELOC (**Fig 14B**, third panel).

To validate our findings, we reconstituted VHL KO cells with either VHL^{WT}, the point mutants that emerged from our spontaneous resistance experiments or a control mutant on R176, a surface-exposed VHL residue in proximity of the CUL2 binding site. Expression of all mutants was detectable by western blot, although some of the mutants appear to affect stability of the substrate receptor (**Fig 14C**). The mutations located at the drug-binding interface conferred >1000-fold resistance to ARV-771 treatment compared to the wild-type protein. This shift in sensitivity is comparable to the resistance observed in KO cells, further supporting the hypothesis that PROTAC binding is abrogated by the mutations (**Fig 14D**). The VHL^{V166F} mutant localized at the VHL-ELOC interaction surface confers more moderate resistance, likely by reducing the proportion of functional $CRL2^{VHL}$ E3 complexes in the cellular pool, whereas the control mutation doesn't impact drug sensitivity as expected (**Fig 14D**).

Overall, this study highlighted the contribution of mutations in the hijacked substrate receptor or the associated CRL machinery to the emergence of spontaneous drug resistance. We detected important differences in the type and frequency of resistance mutations depending on the targeted substrate receptor, possibly due to its essentiality. Most mutations specifically affect the co-opted CRL complex, rather than general factors involved in regulation of CRL activity, so cross-resistance to multiple degraders is likely to only emerge rarely. Further characterization and understanding of resistance to targeted protein degradation will be important to devise strategies to delay the its emergence and to design therapeutic regimens aimed to overcome it.

3. Discussion

Targeted protein degradation (TPD) has recently emerged as a novel paradigm in pharmacology. It is based on the ligand-mediated recruitment of a E3 ubiquitin ligase to a protein of interest and the consequent ubiquitination and proteasomal degradation of the latter. Two main modalities of TPD have been described: (i) molecular glue degraders are monovalent molecules that induce target recognition through orchestration of protein-protein interactions; (ii) PROTACs are modular bifunctional molecules composed of ligands for the target and the E3 ligase connected by a short linker.

TPD holds the promise to overcome some of the limitations of other therapeutic modalities. It therefore quickly generated research momentum, with a particular focus on PROTACs, that culminated in the first clinical trials on these molecules which started in 2019. In the context of this thesis, we sought to further explore the therapeutic potential of this innovative approach, with a particular focus on its benefits for drug selectivity and potential weaknesses in regards to drug resistance.

3.1 Engineering selectivity into molecular probes via PROTAC conversion

Conventional small molecule drugs inhibit the activity of a target protein by occupying accessible hydrophobic pockets on its surface, mostly corresponding to the catalytic site of an enzyme. However, due to their functional role, these pockets are generally highly conserved between proteins of the same family. In fact, off-target inhibition of proteins other than the target greatly contributes to the adverse effects of a drug. The design of molecules with high target selectivity is therefore an ongoing challenge in drug development.

PROTACs are bifunctional small molecule degraders that consist of a “warhead” ligand of a target protein and an E3 ligase recruitment moiety, connected by a short linker. PROTACs are of modular nature, therefore any small molecule ligand can in principle be utilized as a warhead and converted into a degrader. From early studies with PROTACs built off multi-targeted kinase inhibitors it emerged that their degradation spectrum is often more narrow than the binding spectrum of the parental inhibitor (Bondeson et al., 2018; Huang et al., 2018; Olson et al., 2017). The explanation for the selectivity was found in the pharmacology of PROTACs: the binary engagement of target:PROTAC is not sufficient to drive the pharmacological effect of the molecule, but the formation of a stable ternary target:PROTAC:E3 ligase complex is required. Protein-protein interactions between the target and the E3 ligase contribute to the stabilization of the ternary complex and explain the

discrepancy between the proteins that are engaged by the molecule and the smaller subset that is degraded (Bondeson et al., 2018).

Parallel studies on PROTACs targeting the BRD4 and related BET proteins highlighted the importance of the linker in determining the degradation specificity of a molecule. Structural characterization of the ternary complexes induced by PROTACs with different linker chemistries and lengths showed that the relative orientation of the target and E3 ligase are determined by the linker, and this in turn regulates the target selectivity of the molecule (Gadd et al., 2017; Nowak et al., 2018). Thus, conversion of an enzymatic inhibitor into a PROTAC and optimization of the linker chemistry open a promising avenue to engineer selectivity into multi-targeted chemical probes.

To showcase the approach and test its limits, we set out to design PROTACs that differentiate between two closely related homologs, CDK4 and CDK6. CDK4/6 are protein kinases with a well characterized role in the regulation of the transition from G1 to S phase during the cell cycle. Dual inhibitors targeting both kinases are in clinical use for the treatment of breast cancer, but since the two proteins share 94% sequence identity in the catalytic pocket bound by the molecules, it has so far not been possible to design inhibitors that selectively target a single homolog. However, some cancer lineages display selective dependency on one of the homologs. For example, through analysis of large-scale cancer dependency data, we identified acute myeloid leukemia (AML) as a cellular model with strong genetic dependency on CDK6, but not CDK4. Availability of homolog-specific drugs might therefore be very beneficial, as they would allow to target cancer vulnerabilities with conceivably lower overall toxicity.

We coupled palbociclib, a CDK4/6 inhibitor with comparable potency for both proteins, to a pomalidomide-derived CRBN-recruiting moiety via different linkers. YKL-06-102 emerged as a PROTAC that induced destabilization of CDK6, but not CDK4. However, in line with other studies reporting the possibility of off-targets that are independent of the warhead (Ishoey et al., 2018), we detected the pomalidomide targets IKZF1 and IKZF3 to be similarly degraded. Further engineering of the linker chemistry resulted in the degrader BSJ-03-123 (BSJ), with proteome-wide selectivity for CDK6.

Differential engagement of the target protein does not explain the selectivity, as we showed by cellular thermal shift assay that BSJ binds to both CDK4 and CDK6 in live cells. We further characterized the molecular basis for selectivity via a live-cell luciferase-based dimerization assay and were able to show that only CDK6, but not CDK4, is efficiently recruited to CRBN upon BSJ treatment. Further studies will be required to understand the cause of the difference in ternary complex formation, but based on published crystal structures of the two proteins

(PDB: 1JOW, 2W96), we speculate that a loop protruding prominently over the palbociclib binding pocket in CDK4 might provide steric hindrance and prevent recruitment of CRBN.

Since BSJ retains binding to both kinases, we cannot in principle rule out an inhibitory effect on CDK4. However, a control compound (BSJ-bump) that abrogates recruitment of the E3 ligase, but not engagement with the target, showed no detectable reduction of phosphorylation of the canonical target Rb at the assayed concentrations, indicating that the effect of BSJ as kinase inhibitor is negligible.

Overall, our study shows that targeted protein degradation allows selective perturbation of proteins with virtually identical ligand binding pockets, as showcased by CDK4 and CDK6. Importantly, modification of the linker chemistry allows tweaking of the target spectrum in both directions and PROTACs selective for CDK4 have been developed (Jiang et al., 2019). Since then, another study showed that similar selectivity can be achieved for other closely related targets, such as the MAPK isoforms p38α or p38δ (Smith et al., 2019). Taken together, these early reports support the promise of exquisite selectivity of PROTAC pharmacology. It will be interesting to study to what precision the selectivity of a PROTAC can be tuned, and whether it will allow to specifically degrade e.g. oncogenes harboring a specific mutation while sparing the wild-type counterpart in healthy cells.

3.2 Characterization of the role of CDK6 in acute myeloid leukemia

Historically, CDK4 and CDK6 were thought to have largely overlapping and redundant functions in the regulation of cell cycle, most notably the induction of progression into S-phase of the cell cycle via phosphorylation of the retinoblastoma (Rb) protein and consequent release of E2F transcription factors. This notion was supported by the ubiquitous expression of both kinases and mouse studies showing that individual KO mice are viable and fertile, whereas simultaneous deletion of both genes results in embryonic lethality due to severe anemia (Malumbres et al., 2004).

In recent years however, cell-cycle independent functions of CDK6 that are not shared with CDK4 started to emerge, particularly in the regulation of gene expression in the hematopoietic system and related malignancies (Tigan et al., 2016). Importantly, it has been shown that some of these functions are independent of the kinase activity of CDK6 and rather mediated by its binding to the chromatin and recruitment of transcription factors, such as STAT3, c-Jun and NF-κB (Handschick et al., 2014; Kollmann et al., 2013). However, further elucidation of the specific functions of the two homologs and the kinase-independent activity of CDK6 have respectively been hindered by the lack of selective chemical probes and experimental strategies to holistically abrogate protein function at high kinetic resolution.

We exploited the homolog-selectivity and fast kinetics of BSJ to characterize the role of CDK6 in cellular signaling via global phosphoproteomic profiling. Altered phospho-sites were enriched for CDK consensus motifs and known CDK4/6 substrates, arguing for detection of direct consequences of CDK6 depletion that would not be possible with alternative genetic strategies. In addition, we identified novel putative CDK6 targets, e.g. the splicing factor SRRM2 and the chromatin remodeling factor RSF1, which further support a role of CDK6 in the integration of cell proliferation and gene expression.

We further utilized BSJ to profile the acute transcriptional consequences of CDK6 degradation. As expected, the elicited transcriptional response mainly affected genes involved in the regulation of DNA replication and cell cycle progression, but also revealed an influence of CDK6 on DNA repair and the DNA damage response. It would be interesting to further explore this dual role, as it might inform on potential drug synergies that could be exploited by combination treatments.

The transcriptional effect of CDK6 degradation strongly correlated with the response to CDK4/6 inhibition by palbociclib. This indicates that in AML CDK6 appears to exert its gene regulatory role mostly through its catalytic activity, rather than through a scaffolding function. For the most part, the reported kinase-independent functions of CDK6 have been detected in cells of the lymphoid lineage, and it is not unlikely that the scaffolding function of CDK6 is specific to certain cell types. The further characterization of the kinase-independent role of CDK6 and other kinases and the identification of cellular determinants governing it will be challenges to be tackled in the next years. Selective small molecule degraders such as BSJ empower the accurate interrogation of protein biology at unprecedented kinetic resolution and have great potential to precisely target cancer vulnerabilities.

3.3 The CRL machinery is an important mediator of TPD resistance

The introduction of targeted therapies into clinical practice has contributed to improving patient survival and quality of life compared to conventional chemotherapy. However, it is well documented that cancer cells can evade the selective pressure of the drug via different mechanisms, resulting in the frequent emergence of resistance and tumor relapse. Molecular characterization of the resistance mechanisms has shown to provide valuable insights to delay or overcome the emergence of resistance. For example, novel chemistry has been developed to specifically target tumors harboring frequent genetic resistance mutations and rational combination therapies are an effective strategy to prevent the reactivation of oncogenic signaling pathways.

The general principles of drug resistance to small molecule inhibitors (SMIs) are by now relatively well understood. However, targeted protein degradation as a therapeutic modality

has introduced revolutionary novelties from a pharmacological perspective compared to traditional enzymatic inhibitors, so it is to be expected that drug resistance to these agents would underlie partially different rules. Considering that the field is still in its infancy, it will be beneficial to understand these rules early on and take them into consideration for drug discovery programs to direct ongoing efforts most efficiently.

An important resistance mechanism to SMIs is reactivation of oncogenic signaling by alteration of the drug target, e.g. through acquisition of gatekeeper mutations that reduce the inhibitor's binding affinity. Since the proteins targeted by these drugs are required for maintenance of the malignant phenotype, cancer cells must strike a tight balance between loss of fitness caused by mutation of the target and the consequent fitness gain due to escape of the drug action. Therefore, gatekeeper mutations tend to converge on few selected alterations, for example the T790M EGFR mutation.

Conversely, PROTAC efficacy is not only mediated by engagement of the target, but also requires the machinery of the UPS to be functional. Since its components are not directly involved in disease pathogenesis and the fitness deficit associated with their deactivation is likely minor, the ubiquitination machinery could be an important liability for the emergence of drug resistance. Anecdotic evidence supports this hypothesis, as depletion of CRBN or CUL2 have been reported to confer acquired resistance to a CRBN- or VHL-based BET PROTAC, respectively (Zhang et al., 2019a). A more methodical investigation of the role of the UPS machinery in PROTAC resistance, the type and scope of resistance mutations in its components and potential differences between hijacked CRL complexes is however required to draw meaningful conclusions.

Here, we set out to systematically map the cellular determinants of targeted protein degradation and identify potential resistance genes via genome-wide CRISPR/Cas9 screens. We compared five different small molecule degraders, PROTACs and molecular glues alike, with differences in the degraded target and co-opted CRL complex. Our screens uncovered both compound-specific requirements, mainly the recruited substrate receptors and other components of the CRL complex, as well as determinants shared amongst different degraders. Most importantly, we identified factors involved in the maintenance of CRL plasticity as major drivers of resistance of all CRL4-based degraders: this includes the SR exchange factor CAND1, the NEDD8-specific E2 enzyme UBE2M and components of the COPS9 signalosome required for deneddylation. This apparent paradox of opposing regulators being required for correct functioning of CRLs has already been studied in the context of SCF ligases (CRL1) (Schmidt et al., 2009), but based on our data extends to other complexes as well. Overall, our screens confirmed that impairment of the CRL machinery on multiple levels can drive resistance to different types of small molecule degraders.

Of the CRL components, the substrate receptor is likely of particular importance, as it is the direct interaction partner of the degrader. While a handful of SRs have potent ligands and are thereby amenable to PROTAC design, the field is largely focused on the CRL complexes around CRBN and VHL. The most striking difference between these two is their essentiality: loss of VHL causes strong fitness deficits across cell types, whereas CRBN deficiency is functionally neutral. The BET PROTACs dBET6 and ARV-771 share the same warhead, but recruit CRBN and VHL, respectively, and are therefore an ideal experimental model to investigate SR-dependent differences in PROTAC resistance.

First, we wanted to explore whether point mutations (which are by far less disruptive to protein function than the truncations caused by CRISPR/Cas9 mutagenesis) in these two SRs can confer resistance in a similar fashion to kinase gatekeeper mutations. By interrogating a saturating mutagenesis library, in which each residue in proximity to the PROTAC binding interface is substituted by each other possible amino acid, we identified several positions conferring resistance to the drug treatment when mutated. Mapping of the resistance residues on crystal structures of the complex revealed a strong clustering around the ligand-binding site, suggesting a gatekeeper-like resistance mechanism. We further identified functional residues that appear to be localized at the binding interface of the SR with the target, which support the possibility of target-specific resistance sites. However, the mutations could also impair SR activity via more general mechanisms, e.g. preventing proper folding of the protein or impacting its stability. In-depth characterization of individual mutants will be required to fully understand the underlying resistance mechanism.

We next sought to study the spontaneous emergence of resistance to PROTACs. For this, we selected the near-haploid cell line KBM7, originating from a chronic myelogenous leukemia patient, as cellular model. Favored by the genetic makeup of the cell line, a single high-dose PROTAC treatment is sufficient for outgrowth of resistant clones within a few weeks. Compared to the conventional method of generating resistant cell lines by prolonged passaging of the cells under increasing exposure to the drug, our method allows studies at scale with very limited hands-on work and on a much shorter timeframe. KBM7 cells are therefore in our eyes a great model for basic drug resistance studies in the absence of additional chemical mutagenesis.

We detected important differences when comparing the two PROTACs. On a quantitative side, the estimated resistance rates to the CRBN-based degrader were greater than 10-fold higher across tested drug doses compared to the VHL-based PROTAC. To assess qualitative differences, we performed targeted sequencing of 29 putative resistance genes in the selected cellular pools. dBET6-resistant cells showed a strong predominance of mutations in the substrate receptor CRBN, including a large proportion of deleterious frameshift mutations and premature stop codons. Similar observations have been made in a study on IMiD-refractory

multiple myeloma clinical samples, which identified mutations of CRBN (with a strong predominance of deleterious truncations and splicing mutations) as an important resistance mechanism (Kortüm et al., 2016). Conversely, variants detected in the population resistant to the VHL based PROTAC had a stronger predominance of more subtle point mutations that affected not only the SR, but also other components of the CRL complex.

While the data is still very preliminary and further studies will be needed to draw conclusions, a tempting explanation for the differences is the aforementioned differential essentiality of the SRs. Since no fitness deficit is associated with loss of CRBN, cells can easily tolerate deleterious mutations to overcome the selective pressure exerted by the drug. Other components of the complex are likely affected as well, but overshadowed by the much more preponderant mutations in the SR. In contrast, cells don't tolerate complete loss of function of the essential VHL, so rarer variants with mild phenotypes are selected upon drug treatment. If this observed effect of SR essentiality were indeed a generalizable principle, it would suggest to direct ongoing efforts to identify new E3-recruiting moieties towards essential SRs to limit emergence of drug resistance.

Of course, it will be important to assess the clinical relevance of the detected resistance mutations by genotyping patient samples upon relapse. For other targeted therapies, *in vitro* drug resistance studies like the one presented here have shown strong concordance with the mutations identified in clinical specimens, underscoring the value of functional genomics experiments in accelerating their characterization (Bhang et al., 2015; Hata et al., 2016; Joseph et al., 2013). In line with this, the majority of the mutations we identified in the spontaneous resistance experiments, particularly for VHL, have already been detected in human cancer samples (Tate et al., 2018). With the progression of ongoing clinical studies on PROTACs, it will be interesting to study the mechanisms of resistance in relapsed tumors to further assess the relevance of mutations in the CRL complex as a driver of resistance to targeted protein degradation.

3.4. TPD resistance and possible mechanisms to overcome it

Our results invite for preliminary speculation on possible mechanisms of resistance to targeted protein degradation and potential strategies that can be employed to overcome them. Several of the identified resistance mutations are substitutions of a single amino acid in proximity of the PROTAC-binding interface of the substrate receptor. Based on the successes with kinase inhibitors and gatekeeper mutations, one can imagine designing novel molecules that are able to recognize the mutated receptor. Thanks to the modular build of PROTACs, two strategies are possible:

(i) development of novel E3 ligands that bind to the SR despite the mutation.

(ii) alteration of the linker chemistry, while keeping the E3 and target ligands constant. The linker contributes significantly to the relative orientation of the components of an E3:PROTAC:target complex and can be exchanged with relative ease. Structural studies on BET degraders support this possibility. For example, the CRBN residue Y59 is according to our studies required for efficacy of dBET6, but has been reported dispensable for binding of the analog dBET57, which only differs in the linker (Nowak et al., 2018).

These approaches are likely only possible for mutations that abrogate PROTAC binding to the E3 ligase, but not if the functionality of the CRL complex is abrogated, e.g. through destabilizing point mutations, frameshifts and premature stop codons in the substrate receptor or other components of the CRL complex. In those cases, degradation of the target can be restored through switching the E3 ligand and thereby the ubiquitin ligase recruited by the PROTAC, a strategy that is again empowered by the modular nature of PROTACs. The lack of suitable ligands for E3 ligases is still the limiting factor for this approach, so it will be important to expand the arsenal of ubiquitin ligases that are amenable to PROTAC-based reprogramming.

Importantly, mutations that affect general regulators of CRL activity, such as the COPS9 signalosome or the neddylation cascade, appear to be rather infrequent. These mutations would likely confer cross-resistance to molecules harnessing the majority of CRLs. In this regard, it might be worthwhile to pursue discovery of ligands for E3 ligases of other families that are subject to different mechanisms of regulation.

The possibility of generating with relative ease several molecules that target the same protein via different E3 ligases calls for interesting considerations regarding treatment regimens. It might be beneficial to combine PROTACs that co-opt different E3 ligases to converge on degradation of a target in order to delay emergence of resistance. However, such a treatment plan would inevitably favor resistance mechanisms affecting general regulators of the ubiquitination cascade or the target itself, which will be harder to overcome than resistance mutations in individual CRL complexes. Administering the same molecules in sequential rounds of treatment could therefore be of advantage to prolong overall therapeutic efficacy of the drug class as a whole, even though resistance to the individual molecule would arise faster than in combination therapy.

The study presented herein was by design biased towards detection of resistance mechanisms on the E3 ligase machinery rather than the target. No genetic resistance mutations on BRD4 have been reported for the warhead ligand JQ1 shared by the two

PROTACs, likely because BET proteins have two bromodomains that can be bound by the inhibitor. This makes it highly unlikely for the cancer cell to simultaneously acquire independent gatekeeper mutations in both domains to escape the action of the drug. In line with this, no mutations in BRD2/3/4 were detected in the PROTAC-resistant cell pools. For other targets, abrogation of drug binding by acquisition of gatekeeper mutations will likely be an important resistance mechanism, but we see no reason to believe that it will be more prominent for PROTACs than for traditional inhibitors. On the contrary, since protein-protein contacts significantly contribute to the formation of the ternary complex and thanks to the catalytic mode of action of small molecule degraders, it is possible that mutations causing only a slight reduction in affinity will not be sufficient to drive drug resistance.

Overexpression of the target protein is another common drug resistance mechanism. Since the pharmacologic effect of small molecule inhibitors is dependent on target saturation, the occupancy of the target can be reduced to ineffective levels by increasing target abundance. It is tempting to speculate that the event-based pharmacology of targeted protein degradation could be beneficial in this regard, as the catalytic nature of drug action would be more robust to variations in target abundance, but this needs to be carefully investigated.

Due to the nature of the utilized assays, our study was exclusively focused on genetic resistance mutations and was therefore able to capture only a small fraction of the possible resistance mechanisms. While we clearly show that mutation of the CRL complex hijacked by PROTACs is a possible liability for the development of drug resistance, it will be important to quantify its importance relative to other genetic and epigenetic resistance mechanisms.

An important method for the precise quantification of drug resistance is molecular barcoding coupled to next-generation sequencing. Individual cells are tagged with unique DNA sequences that allow to quantitively determine enrichment of specific subclones upon application of selective pressure. Additionally, through barcoding approaches it is possible to distinguish between resistant clones that pre-exist in the cellular pool and *de novo* emergence of drug resistance (Bhang et al., 2015). However, the readout by sequencing is cell-destructive and therefore prevents functional profiling of the resistant clones. Novel barcoding methods overcome this limitation and allow isolation of clones of interest from the bulk population by their DNA barcodes (Akimov et al., 2019). This approach would allow to not only accurately quantify the resistance rates to PROTACs, but also to deconvolute the underlying mechanisms of resistance and estimate their relative frequency.

3.5 Future directions

Clinical translation of insights on important drivers of neoplastic growth have for many years been hindered by limitations in the available pharmacology. Only about 20% of the human proteome is estimated to harbor ligandable pockets on the protein surface, which are required for targeting by a small molecule inhibitor. Probes with sufficient selectivity and favorable physico-chemical properties have been developed for an even smaller subset and currently cover only ~600 proteins (Oprea et al., 2018). Therefore, several high-profile targets in oncology are not yet pharmacologically tractable.

The advent of targeted protein degradation via heterobifunctional molecules (PROTACs) has rapidly generated a lot of interest and considerable investments in related research thanks to the promise to open up all of the ligandable proteome to pharmacological modulation. While the majority of early proof-of-concept studies, including the first clinical trials, focused on PROTACs utilizing well-established inhibitors as warheads, first reports of degraders targeting proteins so far considered undruggable have recently been emerging (Bai et al., 2019; Silva et al., 2019).

It is now well accepted that an important determinant of PROTAC efficacy is the formation of a ternary complex composed of target:PROTAC:E3 ligase and the relative orientation of its constituents, largely mediated by the linker. Our study on CDK6 degradation outlined in this thesis further highlights the role of the linker in determining PROTAC selectivity. While the selection of the linker is for the moment mainly empirical, structural characterization of available molecules will hopefully empower rational design in the future. First promising work in this direction explored structure-guided design of macrocyclic PROTACs, which allows to constrain the molecule in specific conformations, thereby aiding degradation potency and discrimination between homologous targets (Testa et al., 2020). Other approaches to more precisely regulate PROTAC activity are being explored. For example, incorporation of photo-switchable chemical groups in the linker region allows precise and reversible spatio-temporal control of target degradation (Pfaff et al., 2019; Reynders et al., 2019).

As described in chapter 1.7.2, a big advantage of PROTACs is their modular assembly. Most efforts have so far been focused on recruitment of an E3 ligase to the target protein, directing the latter to proteasomal degradation. This approach however excludes degradation of extracellular and membrane-associated proteins. Therefore, other degradation pathways have been co-opted in a similar manner, such as lysosomal degradation by LYTACs (Banik et al.) and autophagy by AUTACs (Takahashi et al., 2019), further expanding the actionable space of TPD and even allowing induction of degradation of whole organelles. Importantly, the potential of heterobifunctional molecules is not limited to induction of degradation, as

exemplified by a recent proof-of-concept study describing PhoRCs. These molecules induce engagement of target proteins (AKT and EGFR) by the protein phosphatase PP1 and promote their de-phosphorylation (Yamazoe et al., 2020).

A major limitation of PROTACs and other bifunctional molecules is the requirement of potent and selective ligands for the target and the recruited effector. A very promising strategy to identify such ligands is chemical proteomic profiling of covalent fragments and molecules. For example, this recently led to the identification of novel ligands for the E3 ligases RNF114 and DCAF16 (Spradlin et al., 2019; Zhang et al., 2019b). These E3 recruiters were also successfully converted to bifunctional PROTACs. Potentially, PROTACs that irreversibly engage the E3 ligase could have important kinetic advantages, as they only require a binary interaction between the bound E3 ligase and the target instead of the assembly of three independent components. Precise characterization of their pharmacological properties and *in vivo* studies will be required to fully understand the translational potential of covalent PROTACs.

Monovalent molecular glue degraders (MGs) instead circumvent the requirement for ligandable pockets completely and therefore have biggest potential for “drugging the undruggable”. Many of the characterized targets of molecular glue degraders, including transcription factors IKZF1/3 and splicing factor RBM39, are devoid of binding pockets. Yet, they are engaged and efficiently degraded by MGs through formation of ternary complexes mediated by highly cooperative binding (Faust et al., 2020; Fischer et al., 2014). Expansion of the target space of MGs can be achieved by exploration of the chemical space around existing molecular glues. This has been very successful for glues hijacking the $CRL4^{CRBN}$ ligase, as several analogs with different target spectra have been developed starting from thalidomide. MGs have also the potential to reconstitute recognition of a target protein by its cognate E3 ligase that is abrogated by mutational events. For example, a MG has been developed that reinforces recognition of mutated β-catenin by the SCFβ-TrCP E3 ligase complex (Simonetta et al., 2019). Alternatively, novel E3 ligases could be unlocked for modulation via molecular glues. The recent characterization of sulfonamides as $CRL4^{DCAF15}$-recruiting MG indicates that this mechanism of action is not unique to IMiDs, but scalable strategies for the identification of such molecules will be required to truly unlock the potential of this promising pharmacological strategy.

While still in its infancy, the field of targeted protein degradation has incredible potential to unlock the vast areas of the proteome that were so far considered pharmacologically untractable and thereby revolutionize drug discovery. Further challenges await in the years to come, including opening up additional E3 ligases to modulation by molecular glues and

PROTACs, clinical exploration of the efficacy of bifunctional degraders and thorough characterization of possible resistance mechanisms to empower their rapid detection and circumvention.

References

Adams, J. (2004). The proteasome: A suitable antineoplastic target. Nat. Rev. Cancer *4*, 349–360.

Akimov, Y., Bulanova, D., Abyzova, M., Wennerberg, K., and Aittokallio, T. (2019). DNA barcode-guided lentiviral CRISPRa tool to trace and isolate individual clonal lineages in heterogeneous cancer cell populations. BioRxiv 622506.

Ampbell, P.J., Getz, G., Korbel, J.O., Stuart, J.M., Jennings, J.L., Stein, L.D., Perry, M.D., Nahal-Bose, H.K., Ouellette, B.F.F., Li, C.H., et al. (2020). Pan-cancer analysis of whole genomes. Nature *578*, 82–93.

Aravind, L., and Koonin, E. V. (2000). The U box is a modified RING finger - A common domain in ubiquitination. Curr. Biol. *10*.

Bai, L., Zhou, H., Xu, R., Zhao, Y., Chinnaswamy, K., McEachern, D., Chen, J., Yang, C.Y., Liu, Z., Wang, M., et al. (2019). A Potent and Selective Small-Molecule Degrader of STAT3 Achieves Complete Tumor Regression In Vivo. Cancer Cell *36*, 498-511.e17.

Baillat, D., Hakimi, M.A., Näär, A.M., Shilatifard, A., Cooch, N., and Shiekhattar, R. (2005). Integrator, a multiprotein mediator of small nuclear RNA processing, associates with the C-terminal repeat of RNA polymerase II. Cell *123*, 265–276.

Banik, S., Pedram, K., Wisnovsky, S., Riley, N., and Bertozzi, C. Lysosome Targeting Chimeras (LYTACs) for the Degradation of Secreted and Membrane Proteins.

Barker, A.J., Gibson, K.H., Grundy, W., Godfrey, A.A., Barlow, J.J., Healy, M.P., Woodburn, J.R., Ashton, S.E., Curry, B.J., Scarlett, L., et al. (2001). Studies leading to the identification of ZD1839 (Iressa^{TM}): An orally active, selective epidermal growth factor receptor tyrosine kinase inhibitor targeted to the treatment of cancer. Bioorganic Med. Chem. Lett. *11*, 1911–1914.

Barlow, P.N., Luisi, B., Milner, A., Elliott, M., and Everett, R. (1994). Structure of the C3HC4 domain by 1H-nuclear magnetic resonance spectroscopy. A new structural class of zinc-finger. J. Mol. Biol. *237*, 201–211.

Bartlett, J.B., Dredge, K., and Dalgleish, A.G. (2004). The evolution of thalidomide and its IMiD derivatives as anticancer agents. Nat. Rev. Cancer *4*, 314–322.

Baumeister, W., Walz, J., Zühl, F., and Seemüller, E. (1998). The proteasome: Paradigm of a self-compartmentalizing protease. Cell *92*, 367–380.

Bean, J., Brennan, C., Shih, J.Y., Riely, G., Viale, A., Wang, L., Chitale, D., Motoi, N., Szoke, J., Broderick, S., et al. (2007). MET amplification occurs with or without T790M mutations in EGFR mutant lung tumors with acquired resistance to gefitinib or erlotinib. Proc. Natl. Acad. Sci. U. S. A. *104*, 20932–20937.

Beaver, J.A., Amiri-Kordestani, L., Charlab, R., Chen, W., Palmby, T., Tilley, A., Zirkelbach, J.F., Yu, J., Liu, Q., Zhao, L., et al. (2015). FDA approval: Palbociclib for the treatment of postmenopausal patients with estrogen receptor-positive, HER2-negative metastatic breast cancer. Clin. Cancer Res. *21*, 4760–4766.

Bhang, H.E.C., Ruddy, D.A., Radhakrishna, V.K., Caushi, J.X., Zhao, R., Hims, M.M., Singh, A.P., Kao, I., Rakiec, D., Shaw, P., et al. (2015). Studying clonal dynamics in response to cancer therapy using high-complexity barcoding. Nat. Med. *21*, 440–448.

Bondeson, D.P., Mares, A., Smith, I.E.D., Ko, E., Campos, S., Miah, A.H., Mulholland, K.E., Routly, N., Buckley, D.L., Gustafson, J.L., et al. (2015). Catalytic in vivo protein knockdown by

small-molecule PROTACs. Nat. Chem. Biol. *11*, 611–617.

Bondeson, D.P., Smith, B.E., Burslem, G.M., Buhimschi, A.D., Hines, J., Jaime-Figueroa, S., Wang, J., Hamman, B.D., Ishchenko, A., and Crews, C.M. (2018). Lessons in PROTAC Design from Selective Degradation with a Promiscuous Warhead. Cell Chem. Biol. *25*, 78-87.e5.

Brookes, P., and Lawley, P. (1961). The reaction of mono- and di-functional alkylating agents with nucleic acids. Biochem. J. *80*, 496–503.

Brooks, P., Fuertes, G., Murray, R.Z., Bose, S., Knecht, E., Rechsteiner, M.C., Hendil, K.B., Tanaka, K., Dyson, J., and Rivett, A.J. (2000). Subcellular localization of proteasomes and their regulatory complexes in mammalian cells. Biochem. J. *346*, 155–161.

Brownell, J.E., Sintchak, M.D., Gavin, J.M., Liao, H., Bruzzese, F.J., Bump, N.J., Soucy, T.A., Milhollen, M.A., Yang, X., Burkhardt, A.L., et al. (2010). Substrate-Assisted Inhibition of Ubiquitin-like Protein-Activating Enzymes: The NEDD8 E1 Inhibitor MLN4924 Forms a NEDD8-AMP Mimetic In Situ. Mol. Cell *37*, 102–111.

Buckley, D.L., Gustafson, J.L., Van Molle, I., Roth, A.G., Tae, H.S., Gareiss, P.C., Jorgensen, W.L., Ciulli, A., and Crews, C.M. (2012). Small-Molecule Inhibitors of the Interaction between the E3 Ligase VHL and HIF1α. Angew. Chemie Int. Ed. *51*, 11463–11467.

Budhidarmo, R., Nakatani, Y., and Day, C.L. (2012). RINGs hold the key to ubiquitin transfer. Trends Biochem. Sci. *37*, 58–65.

Burslem, G.M., Smith, B.E., Lai, A.C., Jaime-Figueroa, S., McQuaid, D.C., Bondeson, D.P., Toure, M., Dong, H., Qian, Y., Wang, J., et al. (2018). The Advantages of Targeted Protein Degradation Over Inhibition: An RTK Case Study. Cell Chem. Biol. *25*, 67-77.e3.

Cappadocia, L., and Lima, C.D. (2018). Ubiquitin-like Protein Conjugation: Structures, Chemistry, and Mechanism. Chem. Rev. *118*, 889–918.

Carter, P., Presta, L., Gorman, C.M., Ridgway, J.B.B., Henner, D., Wong, W.L.T., Rowland, A.M., Kotts, C., Carver, M.E., and Shepard, H.M. (1992). Humanization of an anti-p185HER2 antibody for human cancer therapy. Proc. Natl. Acad. Sci. U. S. A. *89*, 4285–4289.

Castro, A., Bernis, C., Vigneron, S., Labbé, J.C., and Lorca, T. (2005). The anaphase-promoting complex: A key factor in the regulation of cell cycle. Oncogene *24*, 314–325.

Chamberlain, P.P., and Hamann, L.G. (2019). Development of targeted protein degradation therapeutics. Nat. Chem. Biol. *15*, 937–944.

Chang, B., Partha, S., Hofmann, K., Lei, M., Goebl, M., Harper, J.W., and Elledge, S.J. (1996). SKP1 connects cell cycle regulators to the ubiquitin proteolysis machinery through a novel motif, the F-box. Cell *86*, 263–274.

Chapman, P.B., Hauschild, A., Robert, C., Haanen, J.B., Ascierto, P., Larkin, J., Dummer, R., Garbe, C., Testori, A., Maio, M., et al. (2011). Improved survival with vemurafenib in melanoma with BRAF V600E mutation. N. Engl. J. Med. *364*, 2507–2516.

Chau, V., Tobias, J.W., Bachmair, A., Marriott, D., Ecker, D.J., Gonda, D.K., and Varshavsky, A. (1989). A multiubiquitin chain is confined to specific lysine in a targeted short-lived protein. Science *243*, 1576–1583.

Chauhan, D., Tian, Z., Zhou, B., Kuhn, D., Orlowski, R., Raje, N., Richardson, P., and Anderson, K.C. (2011). In vitro and in vivo selective antitumor activity of a novel orally bioavailable proteasome inhibitor MLN9708 against multiple myeloma cells. Clin. Cancer Res. *17*, 5311–5321.

Chauhan, D., Tian, Z., Nicholson, B., Kumar, K.G.S., Zhou, B., Carrasco, R., McDermott, J.L.,

Leach, C.A., Fulcinniti, M., Kodrasov, M.P., et al. (2012). A Small Molecule Inhibitor of Ubiquitin-Specific Protease-7 Induces Apoptosis in Multiple Myeloma Cells and Overcomes Bortezomib Resistance. Cancer Cell *22*, 345–358.

Chen, C.D., Welsbie, D.S., Tran, C., Baek, S.H., Chen, R., Vessella, R., Rosenfeld, M.G., and Sawyers, C.L. (2004). Molecular determinants of resistance to antiandrogen therapy. Nat. Med. *10*, 33–39.

Coiffier, B., Haioun, C., Ketterer, N., Engert, A., Tilly, H., Ma, D., Johnson, P., Lister, A., Feuring-Buske, M., Radford, J.A., et al. (1998). Rituximab (anti-CD20 monoclonal antibody) for the treatment of patients with relapsing or refractory aggressive lymphoma: A multicenter phase II study. Blood *92*, 1927–1932.

Colland, F., Formstecher, E., Jacq, X., Reverdy, C., Planquette, C., Conrath, S., Trouplin, V., Bianchi, J., Aushev, V.N., Camonis, J., et al. (2009). Small-molecule inhibitor of USP7/HAUSP ubiquitin protease stabilizes and activates p53 in cells. Mol. Cancer Ther. *8*, 2286–2295.

Cope, G.A., and Deshaies, R.J. (2003). COP9 signalosome: A multifunctional regulator of SCF and other cullin-based ubiquitin ligases. Cell *114*, 663–671.

Cromm, P.M., and Crews, C.M. (2017). Targeted Protein Degradation: from Chemical Biology to Drug Discovery. Cell Chem. Biol. *24*, 1181–1190.

Darvin, P., Toor, S.M., Sasidharan Nair, V., and Elkord, E. (2018). Immune checkpoint inhibitors: recent progress and potential biomarkers. Exp. Mol. Med. *50*.

Davies, H., Bignell, G.R., Cox, C., Stephens, P., Edkins, S., Clegg, S., Teague, J., Woffendin, H., Garnett, M.J., Bottomley, W., et al. (2002). Mutations of the BRAF gene in human cancer. Nature *417*, 949–954.

Dawson, M.A., and Kouzarides, T. (2012). Cancer epigenetics: From mechanism to therapy. Cell *150*, 12–27.

Delaney, G., Jacob, S., Featherstone, C., and Barton, M. (2005). The role of radiotherapy in cancer treatment: Estimating optimal utilization from a review of evidence-based clinical guidelines. Cancer *104*, 1129–1137.

Delgado, J.L., Hsieh, C.M., Chan, N.L., and Hiasa, H. (2018). Topoisomerases as anticancer targets. Biochem. J. *475*, 373–398.

Delmore, J.E., Issa, G.C., Lemieux, M.E., Rahl, P.B., Shi, J., Jacobs, H.M., Kastritis, E., Gilpatrick, T., Paranal, R.M., Qi, J., et al. (2011). BET bromodomain inhibition as a therapeutic strategy to target c-Myc. Cell *146*, 904–917.

Demo, S.D., Kirk, C.J., Aujay, M.A., Buchholz, T.J., Dajee, M., Ho, M.N., Jiang, J., Laidig, G.J., Lewis, E.R., Parlati, F., et al. (2007). Antitumor activity of PR-171, a novel irreversible inhibitor of the proteasome. Cancer Res. *67*, 6383–6391.

DepMap (2019). DepMap Achilles 19Q1.

Dharmasiri, N., Dharmasiri, S., and Estelle, M. (2005). The F-box protein TIR1 is an auxin receptor. Nature *435*, 441–445.

Dilruba, S., and Kalayda, G. V. (2016). Platinum-based drugs: past, present and future. Cancer Chemother. Pharmacol. *77*, 1103–1124.

Doench, J.G., Fusi, N., Sullender, M., Hegde, M., Vaimberg, E.W., Donovan, K.F., Smith, I., Tothova, Z., Wilen, C., Orchard, R., et al. (2016). Optimized sgRNA design to maximize activity and minimize off-target effects of CRISPR-Cas9. Nat. Biotechnol. *34*, 184–191.

Druker, B.J., Tamura, S., Buchdunger, E., Ohno, S., Segal, G.M., Fanning, S., Zimmermann,

J., and Lydon, N.B. (1996). Effects of a selective inhibitor of the Ab1 tyrosine kinase on the growth of Bcr-Ab1 positive cells. Nat. Med. *2*, 561–566.

Duda, D.M., Borg, L.A., Scott, D.C., Hunt, H.W., Hammel, M., and Schulman, B.A. (2008). Structural Insights into NEDD8 Activation of Cullin-RING Ligases: Conformational Control of Conjugation. Cell *134*, 995–1006.

Duda, D.M., Olszewski, J.L., Schuermann, J.P., Kurinov, I., Miller, D.J., Nourse, A., Alpi, A.F., and Schulman, B.A. (2013). Structure of HHARI, a RING-IBR-RING ubiquitin ligase: autoinhibition of an Ariadne-family E3 and insights into ligation mechanism. Structure *21*, 1030–1041.

Dueber, E.C., Schoeffler, A.J., Lingel, A., Elliott, J.M., Fedorova, A. V., Giannetti, A.M., Zobel, K., Maurer, B., Varfolomeev, E., Wu, P., et al. (2011). Antagonists induce a conformational change in cIAP1 that promotes autoubiquitination. Science *334*, 376–380.

Dummer, R., Ascierto, P.A., Gogas, H.J., Arance, A., Mandala, M., Liszkay, G., Garbe, C., Schadendorf, D., Krajsova, I., Gutzmer, R., et al. (2018). Overall survival in patients with BRAF-mutant melanoma receiving encorafenib plus binimetinib versus vemurafenib or encorafenib (COLUMBUS): a multicentre, open-label, randomised, phase 3 trial. Lancet Oncol. *19*, 1315–1327.

Edelman, A.M., Blumenthal, D.K., and Krebs, E.G. (1987). Protein Serine/Threonine Kinases. Annu. Rev. Biochem. *56*, 567–613.

Elsasser, S., Chandler-Mitilello, D., Müller, B., Hanna, J., and Finley, D. (2004). Rad23 and Rpn10 serve as alternate ubiquitin receptors for the proteasome. J. Biol. Chem. *279*, 26817–26822.

Emadi, A., Jones, R.J., and Brodsky, R.A. (2009). Cyclophosphamide and cancer: golden anniversary. Nat. Rev. Clin. Oncol. *6*, 638–647.

Engelman, J.A., Zejnullahu, K., Mitsudomi, T., Song, Y., Hyland, C., Joon, O.P., Lindeman, N., Gale, C.M., Zhao, X., Christensen, J., et al. (2007). MET amplification leads to gefitinib resistance in lung cancer by activating ERBB3 signaling. Science *316*, 1039–1043.

Estey, E.H. (2013). Epigenetics in clinical practice: The examples of azacitidine and decitabine in myelodysplasia and acute myeloid leukemia. Leukemia *27*, 1803–1812.

Fabbro, D. (2015). 25 Years of small molecular weight kinase inhibitors: Potentials and limitations. Mol. Pharmacol. *87*, 766–775.

Faust, T.B., Yoon, H., Nowak, R.P., Donovan, K.A., Li, Z., Cai, Q., Eleuteri, N.A., Zhang, T., Gray, N.S., and Fischer, E.S. (2020). Structural complementarity facilitates E7820-mediated degradation of RBM39 by DCAF15. Nat. Chem. Biol. *16*, 7–14.

Fenteany, G., Standaert, R.F., Lane, W.S., Choi, S., Corey, E.J., and Schreiber, S.L. (1995). Inhibition of proteasome activities and subunit-specific amino-terminal threonine modification by lactacystin. Science *268*, 726–731.

Ferrara, N., Hillan, K.J., Gerber, H.P., and Novotny, W. (2004). Discovery and development of bevacizumab, an anti-VEGF antibody for treating cancer. Nat. Rev. Drug Discov. *3*, 391–400.

Filippakopoulos, P., Qi, J., Picaud, S., Shen, Y., Smith, W.B., Fedorov, O., Morse, E.M., Keates, T., Hickman, T.T., Felletar, I., et al. (2010). Selective inhibition of BET bromodomains. Nature *468*, 1067–1073.

Fischer, E.S., Scrima, A., Böhm, K., Matsumoto, S., Lingaraju, G.M., Faty, M., Yasuda, T., Cavadini, S., Wakasugi, M., Hanaoka, F., et al. (2011). The molecular basis of CRL4

DDB2/CSA ubiquitin ligase architecture, targeting, and activation. Cell *147*, 1024–1039.

Fischer, E.S., Böhm, K., Lydeard, J.R., Yang, H., Stadler, M.B., Cavadini, S., Nagel, J., Serluca, F., Acker, V., Lingaraju, G.M., et al. (2014). Structure of the DDB1-CRBN E3 ubiquitin ligase in complex with thalidomide. Nature *512*, 49–53.

Flaherty, K.T., Robert, C., Hersey, P., Nathan, P., Garbe, C., Milhem, M., Demidov, L. V., Hassel, J.C., Rutkowski, P., Mohr, P., et al. (2012a). Improved Survival with MEK Inhibition in BRAF-Mutated Melanoma. N. Engl. J. Med. *367*, 107–114.

Flaherty, K.T., Infante, J.R., Daud, A., Gonzalez, R., Kefford, R.F., Sosman, J., Hamid, O., Schuchter, L., Cebon, J., Ibrahim, N., et al. (2012b). Combined BRAF and MEK Inhibition in Melanoma with BRAF V600 Mutations. N. Engl. J. Med. *367*, 1694–1703.

Fojo, A.T., Ueda, K., Slamon, D.J., Poplack, D.G., Gottesman, M.M., and Pastan, I. (1987). Expression of a multidrug-resistance gene in human tumors and tissues. Proc. Natl. Acad. Sci. U. S. A. *84*, 265–269.

Fornasier, G., Francescon, S., and Baldo, P. (2018). An Update of Efficacy and Safety of Cetuximab in Metastatic Colorectal Cancer: A Narrative Review. Adv. Ther. *35*, 1497–1509.

Gadd, M.S., Testa, A., Lucas, X., Chan, K.H., Chen, W., Lamont, D.J., Zengerle, M., and Ciulli, A. (2017). Structural basis of PROTAC cooperative recognition for selective protein degradation. Nat. Chem. Biol. *13*, 514–521.

Galdeano, C., Gadd, M.S., Soares, P., Scaffidi, S., Van Molle, I., Birced, I., Hewitt, S., Dias, D.M., and Ciulli, A. (2014). Structure-guided design and optimization of small molecules targeting the protein-protein interaction between the Von Hippel-Lindau (VHL) E3 ubiquitin ligase and the hypoxia inducible factor (HIF) alpha subunit with in vitro nanomolar affinities. J. Med. Chem. *57*, 8657–8663.

Geyer, C.E., Forster, J., Lindquist, D., Chan, S., Romieu, C.G., Pienkowski, T., Jagiello-Gruszfeld, A., Crown, J., Chan, A., Kaufman, B., et al. (2006). Lapatinib plus capecitabine for HER2-positive advanced breast cancer. N. Engl. J. Med. *355*, 2733–2743.

Goetz, M.P., Toi, M., Campone, M., Trédan, O., Bourayou, N., Sohn, J., Park, I.H., Paluch-Shimon, S., Huober, J., Chen, S.C., et al. (2017). MONARCH 3: Abemaciclib as initial therapy for advanced breast cancer. J. Clin. Oncol. *35*, 3638–3646.

Hagner, P.R., Man, H.W., Fontanillo, C., Wang, M., Couto, S., Breider, M., Bjorklund, C., Havens, C.G., Lu, G., Rychak, E., et al. (2015). CC-122, a pleiotropic pathway modifier, mimics an interferon response and has antitumor activity in DLBCL. Blood *126*, 779–789.

Hamed, A.R., Abdel-Azim, N.S., Shams, K.A., and Hammouda, F.M. (2019). Targeting multidrug resistance in cancer by natural chemosensitizers. Bull. Natl. Res. Cent. *43*.

Han, T., Goralski, M., Gaskill, N., Capota, E., Kim, J., Ting, T.C., Xie, Y., Williams, N.S., and Nijhawan, D. (2017). Anticancer sulfonamides target splicing by inducing RBM39 degradation via recruitment to DCAF15. Science *356*.

Hanahan, D., and Weinberg, R.A. (2000). The Hallmarks of Cancer. Cell *100*, 57–70.

Hanahan, D., and Weinberg, R.A. (2011). Hallmarks of cancer: The next generation. Cell *144*, 646–674.

Handschick, K., Beuerlein, K., Jurida, L., Bartkuhn, M., Müller, H., Soelch, J., Weber, A., Dittrich-Breiholz, O., Schneider, H., Scharfe, M., et al. (2014). Cyclin-Dependent Kinase 6 Is a Chromatin-Bound Cofactor for NF-κB-Dependent Gene Expression. Mol. Cell *53*, 193–208.

Hangauer, M.J., Viswanathan, V.S., Ryan, M.J., Bole, D., Eaton, J.K., Matov, A., Galeas, J., Dhruv, H.D., Berens, M.E., Schreiber, S.L., et al. (2017). Drug-tolerant persister cancer cells

are vulnerable to GPX4 inhibition. Nature *551*, 247–250.

Harbeck, N., Beckmann, M.W., Rody, A., Schneeweiss, A., Müller, V., Fehm, T., Marschner, N., Gluz, O., Schrader, I., Heinrich, G., et al. (2013). HER2 dimerization inhibitor pertuzumab - Mode of action and clinical data in breast cancer. Breast Care *8*, 49–55.

Hata, A.N., Niederst, M.J., Archibald, H.L., Gomez-Caraballo, M., Siddiqui, F.M., Mulvey, H.E., Maruvka, Y.E., Ji, F., Bhang, H.E.C., Radhakrishna, V.K., et al. (2016). Tumor cells can follow distinct evolutionary paths to become resistant to epidermal growth factor receptor inhibition. Nat. Med. *22*, 262–269.

Hauschild, A., Grob, J.J., Demidov, L. V., Jouary, T., Gutzmer, R., Millward, M., Rutkowski, P., Blank, C.U., Miller, W.H., Kaempgen, E., et al. (2012). Dabrafenib in BRAF-mutated metastatic melanoma: A multicentre, open-label, phase 3 randomised controlled trial. Lancet *380*, 358–365.

Hayashi, M., Saito, Y., and Kawashima, S. (1992). Calpain activation is essential for membrane fusion of erythrocytes in the presence of exogenous Ca2+. Biochem. Biophys. Res. Commun. *182*, 939–946.

Herman, J.G., and Baylin, S.B. (2003). Gene Silencing in Cancer in Association with Promoter Hypermethylation. N. Engl. J. Med. *349*, 2042–2054.

Hicke, L. (2001). Protein regulation by monoubiquitin. Nat. Rev. Mol. Cell Biol. *2*, 195–201.

Hodi, F.S., O'Day, S.J., McDermott, D.F., Weber, R.W., Sosman, J.A., Haanen, J.B., Gonzalez, R., Robert, C., Schadendorf, D., Hassel, J.C., et al. (2010). Improved survival with ipilimumab in patients with metastatic melanoma. N. Engl. J. Med. *363*, 711–723.

Hon, W.C., Wilson, M.I., Harlos, K., Claridge, T.D.W., Schofield, C.J., Pugh, C.W., Maxwell, P.H., Ratcliffe, P.J., Stuart, D.I., and Jones, E.Y. (2002). Structural basis for the recognition of hydroxyproline in HIF-1α by pVHL. Nature *417*, 975–978.

Hopkins, A.L., and Groom, C.R. (2002). The druggable genome. Nat. Rev. Drug Discov. *1*, 727–730.

Hortobagyi, G.N., Stemmer, S.M., Burris, H.A., Yap, Y.S., Sonke, G.S., Paluch-Shimon, S., Campone, M., Blackwell, K.L., Andre, F., Winer, E.P., et al. (2016). Ribociclib as first-line therapy for HR-positive, advanced breast cancer. N. Engl. J. Med. *375*, 1738–1748.

Howlader, N., Noone, A., Krapcho, M., Miller, D., Brest, A., Yu, M., Ruhl, J., Tatalovich, Z., Mariotto, A., Lewis, D., et al. (2019). Cancer Statistics Review, 1975-2016 - SEER Statistics.

Hu, R., Dunn, T.A., Wei, S., Isharwal, S., Veltri, R.W., Humphreys, E., Han, M., Partin, A.W., Vessella, R.L., Isaacs, W.B., et al. (2009). Ligand-independent androgen receptor variants derived from splicing of cryptic exons signify hormone-refractory prostate cancer. Cancer Res. *69*, 16–22.

Huang, H.T., Dobrovolsky, D., Paulk, J., Yang, G., Weisberg, E.L., Doctor, Z.M., Buckley, D.L., Cho, J.H., Ko, E., Jang, J., et al. (2018). A Chemoproteomic Approach to Query the Degradable Kinome Using a Multi-kinase Degrader. Cell Chem. Biol. *25*, 88-99.e6.

Huang, L., Kinnucan, E., Wang, G., Beaudenon, S., Howley, P.M., Huibregtse, J.M., and Pavletich, N.P. (1999). Structure of an E6AP-UbcH7 complex: Insights into ubiquitination by the E2-E3 enzyme cascade. Science *286*, 1321–1326.

Hudes, G., Carducci, M., Tomczak, P., Dutcher, J., Figlin, R., Kapoor, A., Staroslawska, E., Sosman, J., McDermott, D., Bodrogi, I., et al. (2007). Temsirolimus, Interferon Alfa, or Both for Advanced Renal-Cell Carcinoma. N. Engl. J. Med. *356*, 2271–2281.

Husnjak, K., Elsasser, S., Zhang, N., Chen, X., Randles, L., Shi, Y., Hofmann, K., Walters,

K.J., Finley, D., and Dikic, I. (2008). Proteasome subunit Rpn13 is a novel ubiquitin receptor. Nature *453*, 481–488.

Ingham, R.J., Gish, G., and Pawson, T. (2004). The Nedd4 family of E3 ubiquitin ligases: Functional diversity within a common modular architecture. Oncogene *23*, 1972–1984.

Ishoey, M., Chorn, S., Singh, N., Jaeger, M.G., Brand, M., Paulk, J., Bauer, S., Erb, M.A., Parapatics, K., Müller, A.C., et al. (2018). Translation Termination Factor GSPT1 Is a Phenotypically Relevant Off-Target of Heterobifunctional Phthalimide Degraders. ACS Chem. Biol. *13*, 553–560.

Ito, T., Ando, H., Suzuki, T., Ogura, T., Hotta, K., Imamura, Y., Yamaguchi, Y., and Handa, H. (2010). Identification of a primary target of thalidomide teratogenicity. Science *327*, 1345–1350.

Itoh, Y., Ishikawa, M., Naito, M., and Hashimoto, Y. (2010). Protein knockdown using methyl bestatin-ligand hybrid molecules: Design and synthesis of inducers of ubiquitination-mediated degradation of cellular retinoic acid-binding proteins. J. Am. Chem. Soc. *132*, 5820–5826.

Ivan, M., Kondo, K., Yang, H., Kim, W., Valiando, J., Ohh, M., Salic, A., Asara, J.M., Lane, W.S., and Kaelin, J. (2001). HIFα targeted for VHL-mediated destruction by proline hydroxylation: Implications for O2 sensing. Science *292*, 464–468.

Ivy, S.P., Wick, J.Y., and Kaufman, B.M. (2009). An overview of small-molecule inhibitors of VEGFR signaling. Nat. Rev. Clin. Oncol. *6*, 569–579.

Jiang, B., Wang, E.S., Donovan, K.A., Liang, Y., Fischer, E.S., Zhang, T., and Gray, N.S. (2019). Development of Dual and Selective Degraders of Cyclin-Dependent Kinases 4 and 6. Angew. Chemie - Int. Ed. *58*, 6321–6326.

Jin, L., Williamson, A., Banerjee, S., Philipp, I., and Rape, M. (2008). Mechanism of Ubiquitin-Chain Formation by the Human Anaphase-Promoting Complex. Cell *133*, 653–665.

Johnson, E.S., Ma, P.C.M., Ota, I.M., and Varshavsky, A. (1995). A proteolytic pathway that recognizes ubiquitin as a degradation signal. J. Biol. Chem. *270*, 17442–17456.

Jordan, M.A., and Wilson, L. (2004). Microtubules as a target for anticancer drugs. Nat. Rev. Cancer *4*, 253–265.

Joseph, J.D., Lu, N., Qian, J., Sensintaffar, J., Shao, G., Brigham, D., Moon, M., Maneval, E.C., Chen, I., Darimont, B., et al. (2013). A clinically relevant androgen receptor mutation confers resistance to second-generation antiandrogens enzalutamide and ARN-509. Cancer Discov. *3*, 1020–1029.

Kahan, B.D. (2015). Sirolimus-based immunosuppression: present state of the art. J. Nephrol. *17 Suppl 8*, S32-9.

Kalluri, R., and Weinberg, R.A. (2009). The basics of epithelial-mesenchymal transition. J. Clin. Invest. *119*, 1420–1428.

Kamura, T., Koepp, D.M., Conrad, M.N., Skowyra, D., Moreland, R.J., Iliopoulos, O., Lane, W.S., Kaelin, W.G., Elledge, S.J., Conaway, R.C., et al. (1999). Rbx1, a component of the VHL tumor suppressor complex and SCF ubiquitin ligase. Science *284*, 657–661.

Kawakami, T., Chiba, T., Suzuki, T., Iwai, K., Yamanaka, K., Minato, N., Suzuki, H., Shimbara, N., Hidaka, Y., Osaka, F., et al. (2001). NEDD8 recruits E2-ubiquitin to SCF E3 ligase. EMBO J. *20*, 4003–4012.

Kim, H.C., and Huibregtse, J.M. (2009). Polyubiquitination by HECT E3s and the determinants of chain type specificity. Mol. Cell. Biol. *29*, 3307–3318.

Kim, K.B., Kefford, R., Pavlick, A.C., Infante, J.R., Ribas, A., Sosman, J.A., Fecher, L.A., Millward, M., McArthur, G.A., Hwu, P., et al. (2013). Phase II study of the MEK1/MEK2 inhibitor trametinib in patients with metastatic BRAF-mutant cutaneous melanoma previously treated with or without a BRAF inhibitor. J. Clin. Oncol. *31*, 482–489.

Köhler, G., and Milstein, C. (1975). Continuous cultures of fused cells secreting antibody of predefined specificity. Nature *256*, 495–497.

Kollmann, K., Heller, G., Schneckenleithner, C., Warsch, W., Scheicher, R., Ott, R.G., Schäfer, M., Fajmann, S., Schlederer, M., Schiefer, A.I., et al. (2013). A kinase-independent function of CDK6 links the cell cycle to tumor angiogenesis. Cancer Cell *24*, 167–181.

Komander, D., and Rape, M. (2012). The Ubiquitin Code. Annu. Rev. Biochem. *81*, 203–29.

Komander, D., Clague, M.J., and Urbé, S. (2009). Breaking the chains: Structure and function of the deubiquitinases. Nat. Rev. Mol. Cell Biol. *10*, 550–563.

Kortüm, K.M., Mai, E.K., Hanafiah, N.H., Shi, C.X., Zhu, Y.X., Bruins, L., Barrio, S., Jedlowski, P., Merz, M., Xu, J., et al. (2016). Targeted sequencing of refractory myeloma reveals a high incidence of mutations in CRBN and Ras pathway genes. Blood *128*, 1226–1233.

Krönke, J., Udeshi, N.D., Narla, A., Grauman, P., Hurst, S.N., McConkey, M., Svinkina, T., Heckl, D., Comer, E., Li, X., et al. (2014). Lenalidomide causes selective degradation of IKZF1 and IKZF3 in multiple myeloma cells. Science *343*, 301–305.

Krönke, J., Fink, E.C., Hollenbach, P.W., MacBeth, K.J., Hurst, S.N., Udeshi, N.D., Chamberlain, P.P., Mani, D.R., Man, H.W., Gandhi, A.K., et al. (2015). Lenalidomide induces ubiquitination and degradation of CK1α in del(5q) MDS. Nature *523*, 183–188.

Kung, J.E., and Jura, N. (2016). Structural Basis for the Non-catalytic Functions of Protein Kinases. Structure *24*, 7–24.

Kurz, T., Özlü, N., Rudolf, F., O'Rourke, S.M., Luke, B., Hofmann, K., Hyman, A.A., Bowerman, B., and Peter, M. (2005). The conserved protein DCN-1/Dcn1p is required for cullin neddylation in C. elegans and S. cerevisiae. Nature *435*, 1257–1261.

Lampson, B.L., and Davids, M.S. (2017). The Development and Current Use of BCL-2 Inhibitors for the Treatment of Chronic Lymphocytic Leukemia. Curr. Hematol. Malig. Rep. *12*, 11–19.

Lander, G.C., Estrin, E., Matyskiela, M.E., Bashore, C., Nogales, E., and Martin, A. (2012). Complete subunit architecture of the proteasome regulatory particle. Nature *482*, 186–191.

Lanker, S., Valdivieso, M.H., and Wittenberg, C. (1996). Rapid degradation of the G1 cyclin Cln2 induced by CDK-dependent phosphorylation. Science *271*, 1597–1601.

Larkin, J., Ascierto, P.A., Dréno, B., Atkinson, V., Liszkay, G., Maio, M., Mandalà, M., Demidov, L., Stroyakovskiy, D., Thomas, L., et al. (2014). Combined Vemurafenib and Cobimetinib in BRAF-Mutated Melanoma James. N Engl J Med *20*, 1867–1876.

Lee, J.M., Lee, J.S., Kim, H., Kim, K., Park, H., Kim, J.Y., Lee, S.H., Kim, I.S., Kim, J., Lee, M., et al. (2012). EZH2 Generates a Methyl Degron that Is Recognized by the DCAF1/DDB1/CUL4 E3 Ubiquitin Ligase Complex. Mol. Cell *48*, 572–586.

Li, M., Brooks, C.L., Kon, N., and Gu, W. (2004). A dynamic role of HAUSP in the p53-Mdm2 pathway. Mol. Cell *13*, 879–886.

Li, W., Bengtson, M.H., Ulbrich, A., Matsuda, A., Reddy, V.A., Orth, A., Chanda, S.K., Batalov, S., and Joazeiro, C.A.P. (2008). Genome-wide and functional annotation of human E3 ubiquitin ligases identifies MULAN, a mitochondrial E3 that regulates the organelle's dynamics and signaling. PLoS One *3*.

Limaverde-Sousa, G., de Andrade Barreto, E., Ferreira, C.G., and Cláudio Casali-da-Rocha, J. (2013). Simulation of the mutation F76del on the von Hippel-Lindau tumor suppressor protein: Mechanism of the disease and implications for drug development. Proteins Struct. Funct. Bioinforma. *81*, 349–363.

Liu, S., and Kurzrock, R. (2014). Toxicity of targeted therapy: Implications for response and impact of genetic polymorphisms. Cancer Treat. Rev. *40*, 883–891.

Liu, J., Farmer, J.D., Lane, W.S., Friedman, J., Weissman, I., and Schreiber, S.L. (1991). Calcineurin is a common target of cyclophilin-cyclosporin A and FKBP-FK506 complexes. Cell *66*, 807–815.

Lopez-Girona, A., Mendy, D., Ito, T., Miller, K., Gandhi, A.K., Kang, J., Karasawa, S., Carmel, G., Jackson, P., Abbasian, M., et al. (2012). Cereblon is a direct protein target for immunomodulatory and antiproliferative activities of lenalidomide and pomalidomide. Leukemia *26*, 2326–2335.

Löwe, J., Stock, D., Jap, B., Zwickl, P., Baumeister, W., and Huber, R. (1995). Crystal structure of the 20S proteasome from the archaeon T. acidophilum at 3.4 Å resolution. Science *268*, 533–539.

Lu, G., Middleton, R.E., Sun, H., Naniong, M.V., Ott, C.J., Mitsiades, C.S., Wong, K.K., Bradner, J.E., and Kaelin, W.G. (2014). The myeloma drug lenalidomide promotes the cereblon-dependent destruction of ikaros proteins. Science *343*, 305–309.

Lu, G., Weng, S., Matyskiela, M., Zheng, X., Fang, W., Wood, S., Surka, C., Mizukoshi, R., Lu, C.C., Mendy, D., et al. (2018). UBE2G1 governs the destruction of cereblon neomorphic substrates. Elife *7*.

Lu, R.M., Hwang, Y.C., Liu, I.J., Lee, C.C., Tsai, H.Z., Li, H.J., and Wu, H.C. (2020). Development of therapeutic antibodies for the treatment of diseases. J. Biomed. Sci. *27*.

Lu, Y., Wang, W., and Kirschner, M.W. (2015). Specificity of the anaphase-promoting complex: A single-molecule study. Science *348*.

Lulla, P.D., Hill, L.C., Ramos, C.A., and Heslop, H.E. (2018). The use of chimeric antigen receptor T cells in patients with non-hodgkin lymphoma. Clin. Adv. Hematol. Oncol. *16*, 375–386.

Luo, J., Solimini, N.L., and Elledge, S.J. (2009). Principles of Cancer Therapy: Oncogene and Non-oncogene Addiction. Cell *136*, 823–837.

Lyapina, S., Cope, G., Shevchenko, A., Serino, G., Tsuge, T., Zhou, C., Wolf, D.A., Wei, N., Shevchenko, A., and Deshaies, R.J. (2001). Promotion of NEDD8-CUL1 conjugate cleavage by COP9 signalosome. Science *292*, 1382–1385.

Maemondo, M., Inoue, A., Kobayashi, K., Sugawara, S., Oizumi, S., Isobe, H., Gemma, A., Harada, M., Yoshizawa, H., Kinoshita, I., et al. (2010). Gefitinib or Chemotherapy for Non–Small-Cell Lung Cancer with Mutated EGFR. N. Engl. J. Med. *362*, 2380–2388.

Malumbres, M., Sotillo, R., Santamaría, D., Galán, J., Cerezo, A., Ortega, S., Dubus, P., and Barbacid, M. (2004). Mammalian cells cycle without the D-type cyclin-dependent kinases Cdk4 and Cdk6. Cell *118*, 493–504.

Marín, I., Lucas, J.I., Gradilla, A.C., and Ferrús, A. (2004). Parkin and relatives: The RBR family of ubiquitin ligases. Physiol. Genomics *17*, 253–263.

Martincorena, I., Raine, K.M., Gerstung, M., Dawson, K.J., Haase, K., Van Loo, P., Davies, H., Stratton, M.R., and Campbell, P.J. (2017). Universal Patterns of Selection in Cancer and Somatic Tissues. Cell *171*, 1029-1041.e21.

Matyskiela, M.E., Lu, G., Ito, T., Pagarigan, B., Lu, C.C., Miller, K., Fang, W., Wang, N.Y., Nguyen, D., Houston, J., et al. (2016). A novel cereblon modulator recruits GSPT1 to the CRL4 CRBN ubiquitin ligase. Nature *535*, 252–257.

Matyskiela, M.E., Couto, S., Zheng, X., Lu, G., Hui, J., Stamp, K., Drew, C., Ren, Y., Wang, M., Carpenter, A., et al. (2018). SALL4 mediates teratogenicity as a thalidomide-dependent cereblon substrate. Nat. Chem. Biol. *14*, 981–987.

McGowan, J. V., Chung, R., Maulik, A., Piotrowska, I., Walker, J.M., and Yellon, D.M. (2017). Anthracycline Chemotherapy and Cardiotoxicity. Cardiovasc. Drugs Ther. *31*, 63–75.

Meyer, H.-J., and Rape, M. (2014). Enhanced protein degradation by branched ubiquitin chains. Cell *157*, 910–921.

Meyers, R.M., Bryan, J.G., McFarland, J.M., Weir, B.A., Sizemore, A.E., Xu, H., Dharia, N. V., Montgomery, P.G., Cowley, G.S., Pantel, S., et al. (2017). Computational correction of copy number effect improves specificity of CRISPR-Cas9 essentiality screens in cancer cells. Nat. Genet. *49*, 1779–1784.

Min, J.H., Yang, H., Ivan, M., Gertler, F., Kaelin, W.G., and Pavietich, N.P. (2002). Structure of an HIF-1α-pVHL complex: Hydroxyproline recognition in signaling. Science *296*, 1886–1889.

Motzer, R.J., Escudier, B., Oudard, S., Hutson, T.E., Porta, C., Bracarda, S., Grünwald, V., Thompson, J.A., Figlin, R.A., Hollaender, N., et al. (2008). Efficacy of everolimus in advanced renal cell carcinoma: a double-blind, randomised, placebo-controlled phase III trial. Lancet *372*, 449–456.

Mukhopadhyay, D., and Riezman, H. (2007). Proteasome-independent functions of ubiquitin in endocytosis and signaling. Science *315*, 201–205.

Nazarian, R., Shi, H., Wang, Q., Kong, X., Koya, R.C., Lee, H., Chen, Z., Lee, M.K., Attar, N., Sazegar, H., et al. (2010). Melanomas acquire resistance to B-RAF(V600E) inhibition by RTK or N-RAS upregulation. Nature *468*, 973–977.

Niederst, M.J., Sequist, L. V., Poirier, J.T., Mermel, C.H., Lockerman, E.L., Garcia, A.R., Katayama, R., Costa, C., Ross, K.N., Moran, T., et al. (2015). RB loss in resistant EGFR mutant lung adenocarcinomas that transform to small-cell lung cancer. Nat. Commun. *6*.

Nissan, M.H., Pratilas, C.A., Jones, A.M., Ramirez, R., Won, H., Liu, C., Tiwari, S., Kong, L., Hanrahan, A.J., Yao, Z., et al. (2014). Loss of NF1 in cutaneous melanoma is associated with RAS activation and MEK dependence. Cancer Res. *74*, 2340–2350.

Nowak, R.P., Deangelo, S.L., Buckley, D., He, Z., Donovan, K.A., An, J., Safaee, N., Jedrychowski, M.P., Ponthier, C.M., Ishoey, M., et al. (2018). Plasticity in binding confers selectivity in ligand-induced protein degradation. Nat. Chem. Biol. *14*, 706–714.

Olson, C.M., Jiang, B., Erb, M.A., Liang, Y., Doctor, Z.M., Zhang, Z., Zhang, T., Kwiatkowski, N., Boukhali, M., Green, J.L., et al. (2017). Pharmacological perturbation of CDK9 using selective CDK9 inhibition or degradation. Nat. Chem. Biol. *14*, 163–170.

Oprea, T.I., Bologa, C.G., Brunak, S., Campbell, A., Gan, G.N., Gaulton, A., Gomez, S.M., Guha, R., Hersey, A., Holmes, J., et al. (2018). Unexplored therapeutic opportunities in the human genome. Nat. Rev. Drug Discov. *17*, 317–332.

Osaka, F. (2000). Covalent modifier NEDD8 is essential for SCF ubiquitin-ligase in fission yeast. EMBO J. *19*, 3475–3484.

Pfaff, P., Samarasinghe, K.T.G., Crews, C.M., and Carreira, E.M. (2019). Reversible Spatiotemporal Control of Induced Protein Degradation by Bistable PhotoPROTACs. ACS

Cent. Sci. *5*, 1682–1690.

Pickart, C.M. (2001). Mechanisms underlying ubiquitination. Annu. Rev. Biochem. *70*, 503–533.

Pickrell, A.M., and Youle, R.J. (2015). The roles of PINK1, parkin, and mitochondrial fidelity in Parkinson's disease. Neuron *85*, 257–273.

Pierce, N.W., Lee, J.E., Liu, X., Sweredoski, M.J., Graham, R.L.J., Larimore, E.A., Rome, M., Zheng, N., Clurman, B.E., Hess, S., et al. (2013). Cand1 promotes assembly of new SCF complexes through dynamic exchange of F box proteins. Cell *153*, 206–215.

Podust, V.N., Brownell, J.E., Gladysheva, T.B., Luo, R.S., Wang, C., Coggins, M.B., Pierce, J.W., Lightcap, E.S., and Chau, V. (2000). A Nedd8 conjugation pathway is essential for proteolytic targeting of p27Kip1 by ubiquitination. Proc. Natl. Acad. Sci. U. S. A. *97*, 4579–4584.

Pollyea, D.A., Tallman, M.S., de Botton, S., Kantarjian, H.M., Collins, R., Stein, A.S., Frattini, M.G., Xu, Q., Tosolini, A., See, W.L., et al. (2019). Enasidenib, an inhibitor of mutant IDH2 proteins, induces durable remissions in older patients with newly diagnosed acute myeloid leukemia. Leukemia *33*, 2575–2584.

Poulikakos, P.I., Persaud, Y., Janakiraman, M., Kong, X., Ng, C., Moriceau, G., Shi, H., Atefi, M., Titz, B., Gabay, M.T., et al. (2011). RAF inhibitor resistance is mediated by dimerization of aberrantly spliced BRAF(V600E). Nature *480*, 387–390.

Prince, H.M., Bishton, M.J., and Johnstone, R.W. (2009). Panobinostat (LBH589): A potent pan-deacetylase inhibitor with promising activity against hematologic and solid tumors. Futur. Oncol. *5*, 601–612.

Raut, C.P., Espat, N.J., Maki, R.G., Araujo, D.M., Trent, J., Williams, T.F., Purkayastha, D. Das, and Dematteo, R.P. (2018). Efficacy and Tolerability of 5-Year Adjuvant Imatinib Treatment for Patients With Resected Intermediate- or High-Risk Primary Gastrointestinal Stromal Tumor: The PERSIST-5 Clinical Trial. JAMA Oncol. *4*.

Read, M.A., Brownell, J.E., Gladysheva, T.B., Hottelet, M., Parent, L.A., Coggins, M.B., Pierce, J.W., Podust, V.N., Luo, R.-S., Chau, V., et al. (2000). Nedd8 Modification of Cul-1 Activates SCF-betaTrCP-Dependent Ubiquitination of IkBalpha. Mol. Cell. Biol. *20*, 2326–2333.

Reynders, M., Matsuura, B., Bérouti, M., Simoneschi, D., Marzio, A., Pagano, M., and Trauner, D. (2019). PHOTACs Enable Optical Control of Protein Degradation. Sci. Adv. *6*.

Richardson, P.G., Barlogie, B., Berenson, J., Singhal, S., Jagannath, S., Irwin, D., Rajkumar, S.V., Srkalovic, G., Alsina, M., Alexanian, R., et al. (2003). A phase 2 study of Bortezomib in relapsed, refractory myeloma. N. Engl. J. Med. *348*, 2609–2617.

Richon, V.M., Emiliani, S., Verdin, E., Webb, Y., Breslow, R., Rifkind, R.A., and Marks, P.A. (1998). A class of hybrid polar inducers of transformed cell differentiation inhibits histone deacetylases. Proc. Natl. Acad. Sci. U. S. A. *95*, 3003–3007.

Ronchi, V.P., Klein, J.M., Edwards, D.J., and Haas, A.L. (2014). The active form of E6-associated protein (E6AP)/UBE3A ubiquitin ligase is an oligomer. J. Biol. Chem. *289*, 1033–1048.

Rossari, F., Minutolo, F., and Orciuolo, E. (2018). Past, present, and future of Bcr-Abl inhibitors: from chemical development to clinical efficacy. J. Hematol. Oncol. *11*, 84.

Saha, A., and Deshaies, R.J. (2008). Multimodal Activation of the Ubiquitin Ligase SCF by Nedd8 Conjugation. Mol. Cell *32*, 21–31.

Sakamoto, K.M., Kim, K.B., Kumagai, A., Mercurio, F., Crews, C.M., and Deshaies, R.J. (2001). Protacs: Chimeric molecules that target proteins to the Skp1-Cullin-F box complex for ubiquitination and degradation. Proc. Natl. Acad. Sci. U. S. A. *98*, 8554–8559.

Salami, J., Alabi, S., Willard, R.R., Vitale, N.J., Wang, J., Dong, H., Jin, M., McDonnell, D.P., Crew, A.P., Neklesa, T.K., et al. (2018). Androgen receptor degradation by the proteolysis-targeting chimera ARCC-4 outperforms enzalutamide in cellular models of prostate cancer drug resistance. Commun. Biol. *1*.

Sánchez-Tena, S., Cubillos-Rojas, M., Schneider, T., and Rosa, J.L. (2016). Functional and pathological relevance of HERC family proteins: A decade later. Cell. Mol. Life Sci. *73*, 1955–1968.

Sander, B., Xu, W., Eilers, M., Popov, N., and Lorenz, S. (2017). A conformational switch regulates the ubiquitin ligase HUWE1. Elife *6*.

Saravanakumar, A., Sadighi, A., Ryu, R., and Akhlaghi, F. (2019). Physicochemical Properties, Biotransformation, and Transport Pathways of Established and Newly Approved Medications: A Systematic Review of the Top 200 Most Prescribed Drugs vs. the FDA-Approved Drugs Between 2005 and 2016. Clin. Pharmacokinet. *58*, 1281–1294.

El Sayed, R., El Jamal, L., El Iskandarani, S., Kort, J., Abdel Salam, M., and Assi, H. (2019). Endocrine and Targeted Therapy for Hormone-Receptor-Positive, HER2-Negative Advanced Breast Cancer: Insights to Sequencing Treatment and Overcoming Resistance Based on Clinical Trials. Front. Oncol. *9*.

Schmidt, M.W., McQuary, P.R., Wee, S., Hofmann, K., and Wolf, D.A. (2009). F-Box-Directed CRL Complex Assembly and Regulation by the CSN and CAND1. Mol. Cell *35*, 586–597.

Schneekloth, J.S., Fonseca, F.N., Koldobskiy, M., Mandal, A., Deshaies, R., Sakamoto, K., and Crews, C.M. (2004). Chemical Genetic Control of Protein Levels: Selective in Vivo Targeted Degradation. J. Am. Chem. Soc. *126*, 3748–3754.

Schneekloth, A.R., Pucheault, M., Tae, H.S., and Crews, C.M. (2008). Targeted intracellular protein degradation induced by a small molecule: En route to chemical proteomics. Bioorganic Med. Chem. Lett. *18*, 5904–5908.

Scott, D.C., Rhee, D.Y., Duda, D.M., Kelsall, I.R., Olszewski, J.L., Paulo, J.A., de Jong, A., Ovaa, H., Alpi, A.F., Harper, J.W., et al. (2016). Two Distinct Types of E3 Ligases Work in Unison to Regulate Substrate Ubiquitylation. Cell *166*, 1198-1214.e24.

Sharma, S. V., Lee, D.Y., Li, B., Quinlan, M.P., Takahashi, F., Maheswaran, S., McDermott, U., Azizian, N., Zou, L., Fischbach, M.A., et al. (2010). A Chromatin-Mediated Reversible Drug-Tolerant State in Cancer Cell Subpopulations. Cell *141*, 69–80.

Sharom, F.J. (2008). ABC multidrug transporters: Structure, function and role in chemoresistance. Pharmacogenomics *9*, 105–127.

Shaw, A.T., Kim, D.-W., Nakagawa, K., Seto, T., Crinó, L., Ahn, M.-J., De Pas, T., Besse, B., Solomon, B.J., Blackhall, F., et al. (2013). Crizotinib versus Chemotherapy in Advanced ALK-Positive Lung Cancer. N. Engl. J. Med. *368*, 2385–2394.

Sheard, L.B., Tan, X., Mao, H., Withers, J., Ben-Nissan, G., Hinds, T.R., Kobayashi, Y., Hsu, F.F., Sharon, M., Browse, J., et al. (2010). Jasmonate perception by inositol-phosphate-potentiated COI1-JAZ co-receptor. Nature *468*, 400–407.

Sievers, Q.L., Petzold, G., Bunker, R.D., Renneville, A., Słabicki, M., Liddicoat, B.J., Abdulrahman, W., Mikkelsen, T., Ebert, B.L., and Thomä, N.H. Defining the human C2H2 zinc finger degrome targeted by thalidomide analogs through CRBN.

Silva, M.C., Ferguson, F.M., Cai, Q., Donovan, K.A., Nandi, G., Patnaik, D., Zhang, T., Huang, H.T., Lucente, D.E., Dickerson, B.C., et al. (2019). Targeted degradation of aberrant tau in frontotemporal dementia patient-derived neuronal cell models. Elife *8*.

Simonetta, K.R., Taygerly, J., Boyle, K., Basham, S.E., Padovani, C., Lou, Y., Cummins, T.J., Yung, S.L., von Soly, S.K., Kayser, F., et al. (2019). Prospective discovery of small molecule enhancers of an E3 ligase-substrate interaction. Nat. Commun. *10*, 1–12.

Singh, S., Kumar, N.K., Dwiwedi, P., Charan, J., Kaur, R., Sidhu, P., and Chugh, V.K. (2018). Monoclonal Antibodies: A Review. Curr. Clin. Pharmacol. *13*, 85–99.

Smith, B.E., Wang, S.L., Jaime-Figueroa, S., Harbin, A., Wang, J., Hamman, B.D., and Crews, C.M. (2019). Differential PROTAC substrate specificity dictated by orientation of recruited E3 ligase. Nat. Commun. *10*, 1–13.

Song, L., and Rape, M. (2010). Regulated degradation of spindle assembly factors by the anaphase-promoting complex. Mol. Cell *38*, 369–382.

Soucy, T.A., Smith, P.G., Milhollen, M.A., Berger, A.J., Gavin, J.M., Adhikari, S., Brownell, J.E., Burke, K.E., Cardin, D.P., Critchley, S., et al. (2009). An inhibitor of NEDD8-activating enzyme as a new approach to treat cancer. Nature *458*, 732–736.

Soucy, T.A., Dick, L.R., Smith, P.G., Milhollen, M.A., and Brownell, J.E. (2010). The NEDD8 conjugation pathway and its relevance in cancer biology and therapy. Genes and Cancer *1*, 708–716.

Soverini, S., Colarossi, S., Gnani, A., Castagnetti, F., Rosti, G., Bosi, C., Paolini, S., Rondoni, M., Piccaluga, P.P., Palandri, F., et al. (2007). Resistance to dasatinib in Philadelphia-positive leukemia patients and the presence or the selection of mutations at residues 315 and 317 in the BCR-ABL kinase domain. Haematologica *92*, 401–404.

Spradlin, J.N., Hu, X., Ward, C.C., Brittain, S.M., Jones, M.D., Ou, L., To, M., Proudfoot, A., Ornelas, E., Woldegiorgis, M., et al. (2019). Harnessing the anti-cancer natural product nimbolide for targeted protein degradation. Nat. Chem. Biol. *15*, 747–755.

Steins, M., Thomas, M., and Geißler, M. (2018). Erlotinib. Recent Results Cancer Res. *211*, 1–17.

Stewart, M.D., Ritterhoff, T., Klevit, R.E., and Brzovic, P.S. (2016). E2 enzymes: more than just middle men. Cell Res. *26*, 423–440.

Stieglitz, B., Morris-Davies, A.C., Koliopoulos, M.G., Christodoulou, E., and Rittinger, K. (2012). LUBAC synthesizes linear ubiquitin chains via a thioester intermediate. EMBO Rep. *13*, 840–846.

Swaney, D.L., Rodríguez-Mias, R.A., and Villén, J. (2015). Phosphorylation of ubiquitin at Ser65 affects its polymerization, targets, and proteome-wide turnover. EMBO Rep. *16*, 1131–1144.

Takahashi, D., Moriyama, J., Nakamura, T., Miki, E., Takahashi, E., Sato, A., Akaike, T., Itto-Nakama, K., and Arimoto, H. (2019). AUTACs: Cargo-Specific Degraders Using Selective Autophagy. Mol. Cell *76*, 797-810.e10.

Takezawa, K., Pirazzoli, V., Arcila, M.E., Nebhan, C.A., Song, X., de Stanchina, E., Ohashi, K., Janjigian, Y.Y., Spitzler, P.J., Melnick, M.A., et al. (2012). HER2 amplification: A potential mechanism of acquired resistance to EGFR inhibition in EGFR-mutant lung cancers that lack the second-site EGFR T790M mutation. Cancer Discov. *2*, 922–933.

Tate, J.G., Bamford, S., Jubb, H.C., Sondka, Z., Beare, D.M., Bindal, N., Boutselakis, H., Cole, C.G., Creatore, C., Dawson, E., et al. (2018). COSMIC: the Catalogue Of Somatic Mutations

In Cancer. Nucleic Acids Res. *47*, 941–947.

Tavana, O., Li, D., Dai, C., Lopez, G., Banerjee, D., Kon, N., Chen, C., Califano, A., Yamashiro, D.J., Sun, H., et al. (2016). HAUSP deubiquitinates and stabilizes N-Myc in neuroblastoma. Nat. Med. *22*, 1180–1186.

Testa, A., Hughes, S.J., Lucas, X., Wright, J.E., and Ciulli, A. (2020). Structure-Based Design of a Macrocyclic PROTAC. Angew. Chemie - Int. Ed. *59*, 1727–1734.

Thrower, J.S. (2000). Recognition of the polyubiquitin proteolytic signal. EMBO J. *19*, 94–102.

Tigan, A.S., Bellutti, F., Kollmann, K., Tebb, G., and Sexl, V. (2016). CDK6-a review of the past and a glimpse into the future: From cell-cycle control to transcriptional regulation. Oncogene *35*, 3083–3091.

Tisato, V., Voltan, R., Gonelli, A., Secchiero, P., and Zauli, G. (2017). MDM2/X inhibitors under clinical evaluation: Perspectives for the management of hematological malignancies and pediatric cancer. J. Hematol. Oncol. *10*.

Tiwari, M. (2012). Antimetabolites: Established cancer therapy. J. Cancer Res. Ther. *8*, 510–519.

Toledo, F., and Wahl, G.M. (2006). Regulating the p53 pathway: In vitro hypotheses, in vivo veritas. Nat. Rev. Cancer *6*, 909–923.

Uehara, T., Minoshima, Y., Sagane, K., Sugi, N.H., Mitsuhashi, K.O., Yamamoto, N., Kamiyama, H., Takahashi, K., Kotake, Y., Uesugi, M., et al. (2017). Selective degradation of splicing factor CAPERα By anticancer sulfonamides. Nat. Chem. Biol. *13*, 675–680.

Uzunova, K., Göttsche, K., Miteva, M., Weisshaar, S.R., Glanemann, C., Schnellhardt, M., Niessen, M., Scheel, H., Hofmann, K., Johnson, E.S., et al. (2007). Ubiquitin-dependent proteolytic control of SUMO conjugates. J. Biol. Chem. *282*, 34167–34175.

Vassilev, L.T., Vu, B.T., Graves, B., Carvajal, D., Podlaski, F., Filipovic, Z., Kong, N., Kammlott, U., Lukacs, C., Klein, C., et al. (2004). In Vivo Activation of the p53 Pathway by Small-Molecule Antagonists of MDM2. Science *303*, 844–848.

Verma, R., Aravind, L., Oania, R., McDonald, W.H., Yates, J.R., Koonin, E. V., and Deshaies, R.J. (2002). Role of Rpn11 metalloprotease in deubiquitination and degradation by the 26S proteasome. Science *298*, 611–615.

Vijay-Kumar, S., Bugg, C.E., and Cook, W.J. (1987). Structure of ubiquitin refined at 1.8 Å resolution. J. Mol. Biol. *194*, 531–544.

Wang, S., Cang, S., and Liu, D. (2016a). Third-generation inhibitors targeting EGFR T790M mutation in advanced non-small cell lung cancer. J. Hematol. Oncol. *9*.

Wang, S., Tsui, S.T., Liu, C., Song, Y., and Liu, D. (2016b). EGFR C797S mutation mediates resistance to third-generation inhibitors in T790M-positive non-small cell lung cancer. J. Hematol. Oncol. *9*.

Weber, J., Polo, S., and Maspero, E. (2019). HECT E3 ligases: A tale with multiple facets. Front. Physiol. *10*, 370.

Weinstein, I.B. (2002). Cancer: Addiction to oncogenes - The Achilles heal of cancer. Science *297*, 63–64.

Wenzel, D.M., Lissounov, A., Brzovic, P.S., and Klevit, R.E. (2011). UBCH7 reactivity profile reveals parkin and HHARI to be RING/HECT hybrids. Nature *474*, 105–108.

Wertz, I.E., O'Rourke, K.M., Zhang, Z., Dornan, D., Arnott, D., Deshaies, R.J., and Dixit, V.M.

(2004). Human De-etiolated-1 regulates c-Jun by assembling a CUL4A ubiquitin ligase. Science *303*, 1371–1374.

Wiesner, S., Ogunjimi, A.A., Wang, H.R., Rotin, D., Sicheri, F., Wrana, J.L., and Forman-Kay, J.D. (2007). Autoinhibition of the HECT-Type Ubiquitin Ligase Smurf2 through Its C2 Domain. Cell *130*, 651–662.

Wilhelm, S.M., Adnane, L., Newell, P., Villanueva, A., Llovet, J.M., and Lynch, M. (2008). Preclinical overview of sorafenib, a multikinase inhibitor that targets both Raf and VEGF and PDGF receptor tyrosine kinase signaling. Mol. Cancer Ther. *7*, 3129–3140.

Winter, G.E., Buckley, D.L., Paulk, J., Roberts, J.M., Souza, A., Dhe-Paganon, S., and Bradner, J.E. (2015). Phthalimide conjugation as a strategy for in vivo target protein degradation. Science *348*, 1376–1381.

Wolf, D.A., Zhou, C., and Wee, S. (2003). The COP9 signalosome: An assembly and maintenance platform for cullin ubiquitin ligases? Nat. Cell Biol. *5*, 1029–1033.

Wood, A.J.J., Smith, I.E., and Dowsett, M. (2003). Aromatase Inhibitors in Breast Cancer.

Xu, L., Wei, Y., Reboul, J., Vaglio, P., Shin, T.-H., Vidal, M., Elledge, S.J., and Harper, J.W. (2003). BTB proteins are substrate-specific adaptors in an SCF-like modular ubiquitin ligase containing CUL-3. Nature *425*, 316–321.

Yamazoe, S., Tom, J., Fu, Y., Wu, W., Zeng, L., Sun, C., Liu, Q., Lin, J., Lin, K., Fairbrother, W.J., et al. (2020). Heterobifunctional Molecules Induce Dephosphorylation of Kinases-A Proof of Concept Study. J. Med. Chem.

Yang, H., Rudge, D.G., Koos, J.D., Vaidialingam, B., Yang, H.J., and Pavletich, N.P. (2013). mTOR kinase structure, mechanism and regulation. Nature *497*, 217–223.

Yau, R., and Rape, M. (2016). The increasing complexity of the ubiquitin code. Nat. Cell Biol. *18*, 579–586.

Yu, H.A., Arcila, M.E., Rekhtman, N., Sima, C.S., Zakowski, M.F., Pao, W., Kris, M.G., Miller, V.A., Ladanyi, M., and Riely, G.J. (2013). Analysis of tumor specimens at the time of acquired resistance to EGFR-TKI therapy in 155 patients with EGFR-mutant lung cancers. Clin. Cancer Res. *19*, 2240–2247.

Zhang, L., Riley-Gillis, B., Vijay, P., and Shen, Y. (2019a). Acquired resistance to BET-ProTACS (proteolysis-targeting chimeras) caused by genomic alterations in core components of E3 ligase complexes. Mol. Cancer Ther. *18*, 1302–1311.

Zhang, X., Crowley, V.M., Wucherpfennig, T.G., Dix, M.M., and Cravatt, B.F. (2019b). Electrophilic PROTACs that degrade nuclear proteins by engaging DCAF16. Nat. Chem. Biol. *15*, 737–746.

Zheng, N., and Shabek, N. (2017). Ubiquitin Ligases: Structure, Function, and Regulation. Annu. Rev. Biochem. *86*, 129–157.

Zheng, J., Yang, X., Harrell, J.M., Ryzhikov, S., Shim, E.H., Lykke-Andersen, K., Wei, N., Sun, H., Kobayashi, R., and Zhang, H. (2002a). CAND1 binds to unneddylated CUL1 and regulates the formation of SCF ubiquitin E3 ligase complex. Mol. Cell *10*, 1519–1526.

Zheng, N., Schulman, B.A., Song, L., Miller, J.J., Jeffrey, P.D., Wang, P., Chu, C., Koepp, D.M., Elledge, S.J., Pagano, M., et al. (2002b). Structure of the Cul1-Rbx1-Skp1-F boxSkp2 SCF ubiquitin ligase complex. Nature *416*, 703–709.

Materials and Methods

Materials and Methods to chapter 2.1 are extensively covered in Brand et al (2019).

Materials and Methods to chapter 2.2 can be found in Mayor-Ruiz et al (2019).

Materials and Methods to chapter 2.3 are described in the following.

Cell lines

KBM7 were obtained from T. Brummelkamp. RKO were obtained from the ATCC repository. KBM7 and RKO cells were respectively cultured in IMDM and DMEM, each supplemented with 10% FBS and 1% penicillin/streptomycin.

Chemicals and Antibodies

ARV-771 (VHL-based BET PROTAC) was obtained from MedChemExpress. dBET6 (CRBN-based BET PROTAC) was obtained form the N.S. Gray lab.

The VHL antibody (CST 2738) was obtained from Cell Signaling Technology. The GAPDH (G-9) antibody (sc-365062) was obtained from Santa Cruz Biotechnology. HRP-conjugated anti-mouse (#115-035-003) and anti-rabbit (#111-035-003) secondary antibodies were obtained from Jackson ImmunoResearch. Western Blots were performed as described in Brand et al. (2019).

Cell viability assay (Cell Titer Glo)

Cells were seeded in 96-well plates at a density of 50.000 cells/well in the presence of drug or DMSO, in triplicates. After 3 days of treatment, cell viability was assayed by CellTiter Glo (Promega) according to manufacturer's instructions. Dose-response curves were interpolated by best-fit analysis using GraphPad Prism.

Saturating mutagenesis library design and cloning

The selection of residues to be included in the saturating mutagenesis library was performed based on publicly available structures of PROTAC-induced ternary complexes CRBN (PDB: 6BOY) and VHL (PDB: 5T35) with the target protein BRD4. Residues lying within 10 Å from the ligand were determined using the *segi* command in PyMol (v2.2.3) and classified for inclusion in the library.

The saturating mutagenesis libraries were ordered from TWIST Bioscience, cloned into a XhoI-digested lentiviral pRRL-EF1α-XhoI-IRES-BlastR expression vector via Gibson Assembly using the NEBuilder HiFi DNA Assembly Mix (NEB) and electroporated into Stbl4 cells (Invitrogen) maintaining > 500-fold coverage.

Lentiviral production

293T cells seeded in 10 cm dishes were transfected with 4 µg target vector, 2 µg pMD2.G (Addgene 12259) and 1 µg psPAX2 (Addgene 12260) using PEI. Viral supernatant was harvested 60 h after transfection, filtered and stored in aliquots at -80°C.

Saturating mutagenesis screen

8 million RKO VHL and CRBN KO cells were transduced with the respective mutagenesis at low MOI of 0.2. VHL screens were performed in two infection replicates, CRBN screens in a single replicate. Transduction was performed in media containing 8 µg/ml polybrene via spininfection for 1 h at 2000 rpm at 32 °C. 48 h after spininfection, 5-day selection of transduced cells with 20 µg/ml Blasticidin was started.

2.5 million cells of the library were seeded in 15-cm culture dishes and treated with 500 nM dBET6, ARV-771 or DMSO for 7 days. Cells were split and drugs refreshed after 4 days of treatment. At harvest, cells were detached with trypsin, 2.5 million collected via centrifugation and snap-frozen in liquid nitrogen before storage at -80 °C.

For the preparation of the sequencing libraries, gDNA was extracted using the QIAamp DNA Mini Kit (QIAGEN). The mutagenized transgene was then PCR amplified in batches of 5 µg gDNA per 50 µl reaction utilizing Q5 Polymerase (NEB) according to manufacturer's instructions with the following cycling conditions: 95 °C, 30" --> n x [95 °C, 15" --> 57 °C, 30" --> 72 °C, 2'] --> 72 °C, 5' (n = 30 for VHL, 22 for CRBN). The PCR amplicon was purified using AMPure XP beads.

VHL_fwd	AGGTGTCGTGACGTACGGGATCCCAGGACCATGCCCCGGAGGGCGGAG
VHL_rev	GGGGGGGGGGCGGAATTAATTCCTACTACTCAATCTCCCATCCGTTGATGTGCAATGCG
CRBN_fwd	TGTCGTGACGTACGGGATCC
CRBN_rev	GCTTCGGCCAGTAACGTTAGGG

Prior to sequencing, the PCR amplicon was tagmented using Tn5 transposase as follows. Samples were diluted to 0.2 ng/µl with EB Buffer (Qiagen). TDE1 Enzyme (Illumina) was diluted 1:10 with Tn5 dilution buffer (50 mM Tris pH 8.0, 25 mM MgCl2, 50% v/v Dimethylformamide) on ice. Tagmentation master mix was prepared from 2 µl 5x tagmentation buffer (50 mM Tris pH7.5, 100 mM NaCl, 0.1 mM EDTA, 50% glycerol, 0.1% Triton X-100), 1 µl nuclease free water, 2 µl diluted enzyme per reaction on ice. 5 µl of tagmentation master mix was added to 5 µl of 0.2 ng/µl cDNA sample (1 ng cDNA total), mixed and incubate at 55°C for 5 minutes. 2.5 µl of 0.2% SDS was added to stop the tagmentation reaction and samples were incubated for 5 minutes at room temperature, then kept on ice. PCR amplification to include NexteraXT sequencing adapters (Illumina) was done with the program:

72 °C, 3 min → 95 °C, 30 s → 12x [95 °C, 10 s; 63 °C, 30 s; 72 °C, 30 s] → 72 °C, 5 min. Libraries purified with AMPure XP beads, pooled equimolarly based on DNA concentration (Qubit) and fragment size distribution (Bioanalyzer) and sequenced on an Illumina HiSeq3000 in 50 bp single-end.

Raw sequencing reads were converted to fastq format using samtools (v1.3.1). Trimming of adapters and low quality reads was performed using Trimmomatic (v0.32). Reads were aligned to the expression cassette using bwa (v0.7.8) aln package allowing for 5 mismatches with the -n 5 parameter followed by bwa samse. Alignment files were sorted using picard-tools (v2.9.0) SortSam function. Mutation calling was performed using the AnalyzeSaturationMutagenesis function from GenomeAnalysisTK (v4.1.2). Relative frequencies of variants were calculated for each interrogated residue. Variants covered by < 10 reads per million were considered not detected for the generation of figures and data interpretation.

Spontaneous resistance assay and hybrid capture sequencing

100 million KBM7 cells were treated with DMSO or 100 nM (10X EC50), 250 nM (25X EC50) or 500 nM (50X EC50) of dBET6 or ARV-771 for 20-25 days. In parallel, cells were seeded at 10.000 cells/well in a 384-well plate, monitored for outgrowth of resistant clones and resistance rates estimated by binomial fitting. Resistant cellular pools were harvested via Ficoll-gradient centrifugation using Lymphocyte Separation Media (Corning) according to manufacturer's protocols. gDNA was extracted (QIAamp DNA Mini, QIAGEN) and 500 ng subjected to DNA library preparation using the NEBNext Ultra II FS DNA Library Prep kit for Illumina (NEB) following manufacturer's instructions. Fragments were size-selected using AMPure XP beads for fragments of 150-350 bp.

Hybrid capture xGen Gene Capture Pools for the 29 genes of interest were purchased from IDT. Hybridization was performed for 16h following the supplier's protocols, utilizing the xGen Universal Blocker-TS Mix (IDT) blocking oligos. Post-capture PCR was performed using the NEBNext High-Fidelity 2X PCR Master Mix (NEB) for 14-20 cycles. Sequencing libraries were quantified using the Qubit dsDNA HS Kit and analyzed on an Agilent 2100 Bioanalyzer before sequencing on a MiSeq v3 lane (50 bp single-end).

Raw read files were converted to fastq format using the picard tools package (v2.9.0). Low-quality reads and sequencing adapters were trimmed using Trimmomativ (v0.36) in SE mode with standard settings. Reads were aligned to the hg38 genome assembly using bwa-mem (v0.7.8), duplicate reads filtered using the MarkDuplicates function picard tools and base quality calibration performed using the BaseRecalibrator function from the

GenomeAnalysisTK package (v3.7). Quality score recalibration was then applied to the dataset utilizing the PrintReads function with the *-BQSR* argument.

Variant calling was performed using Mutect2 function in EMIT_VARIANTS_ONLY output mode. Called variants were annotated using the Ensembl Variant Effect Predictor tool (Ensembl v98). Coding variants with > 10-fold enrichment in allele frequency (as determined by Mutect2) upon drug treatment compared to the unselected population were considered hits.

Curriculum Vitae

Personal Information

Name:	Matthias Brand
Academic Degree:	MSc
Date of birth:	Sept 4th, 1990
Nationality:	German, Italian
Email:	thias.brand@gmail.com

Education

2016-current **PhD in Molecular Medicine**
CeMM – Research Center for Molecular Medicine – Vienna (AT)
Supervisor: Georg Winter
Project: Dissecting the molecular pharmacology of targeted protein degradation

2012-2015 **Master of Science in Molecular and Cellular Medical Biotechnology**
Vita-Salute San Raffaele University – Milan (IT)
Grade: 110/110 cum laude
Thesis: An image-based screen for phosphatases regulating the formation of liquid unmixed compartments

2009-2012 **Bachelor of Science in Medical and Pharmaceutical Biotechnology**
Vita-Salute San Raffaele University – Milan (IT)
Grade: 110/110
Thesis: Use of drug-penetration promoters and peptide-based drug delivery systems as strategies to improve cancer chemotherapy

1996-2009 **German and Italian Baccalaureate**
Deutsche Schule Mailand (German School) - Milan (IT)
Grade: 100/100 cum laude

Research Experience

Sep 2019 **Visiting Scientist**
Institute for Molecular Pathology (IMP) – Vienna (AT)
Johannes Zuber Lab

2015-2016 **Research Fellowship**
Experimental Imaging Center (Centro di Imaging Sperimentale – CIS) – Milan (IT)
Carlo Tacchetti Lab

2013-2015 **Master Thesis Internship**
IMLS – Institute of Molecular Life Sciences, University of Zurich – Zurich (CH)
Lucas Pelkmans Lab

Conferences and Meetings

2019 AACR-NCI-EORTC Conference on Molecular Targets and Cancer Therapeutics, Boston (US)
Poster presentation

2019 European Targeted Protein Degradation Congress, Basel (CH)

2018 Young Scientist Retreat – joint retreat of CeMM and Institut Curie Paris (FR), Bratislava (CZ)
Organising Committee, Oral presentation

2018 CeMM Scientific Recess
Poster presentation

2017 CeMM Scientific Recess
Oral presentation

2016 Ospedale San Raffaele Scientific Retreat
Poster presentation

2014 IMLS Scientific Retreat
Poster presentation

Awards and distinctions

- Travel Grant for Keystone Meeting on Targeted Protein Degradation (2020)
- Honorary Diploma by Chapter Italy of the VDI (Association of German Engineers) for outstanding school achievements in natural sciences
- Jugend Forscht (German Youth Science Competition): 1st place at regional level in 2005 (Work environment), 2006 (Biology), 2008 (Mathematics)

List of Publications

1. Brand, M., Jiang, B., Bauer, S., Donovan, K. A., Liang, Y., Wang, E. S., Nowak, R. P., Yuan, J. C., Zhang, T., Kwiatkowski, N., Müller, A. C., Fischer, E. S., Gray, N. S., & Winter, G. E., **Homolog-Selective Degradation as a Strategy to Probe the Function of CDK6 in AML.** *Cell Chemical Biology* (2019).

2. Mayor-Ruiz, C., Jaeger, M. G., Bauer, S., Brand, M., Sin, C., Hanzl, A., Mueller, A. C., Menche, J., & Winter, G. E., **Plasticity of the Cullin-RING Ligase Repertoire Shapes Sensitivity to Ligand-Induced Protein Degradation.** *Molecular Cell* (2019).

3. Brand, M., Winter, G. E., **Locus-Specific Knock-In of a Degradable Tag for Target Validation Studies.** *Methods in Molecular Biology* (2019)

4. Brand, M., Winter, G. E., **Stick it to E3s.** *Nature Chemical Biology* (2019).

5. Ishoey, M., Chorn, S., Singh, N., Jaeger, M. G., Brand, M., Paulk, J., Bauer, S., Erb, M. A., Parapatics, K., Müller, A. C., Bennett, K. L., Ecker, G. F., Bradner, J. E., & Winter, G. E., **Translation Termination Factor GSPT1 Is a Phenotypically Relevant Off-Target of Heterobifunctional Phthalimide Degraders**. *ACS Chemical Biology* (2018).